

AMERICAN UNIVERSITY OF BEIRUT

DETERMINING THE MAIN DRIVERS OF PM AND CO
CONCENTRATION SURFACES IN THE GREATER BEIRUT
AREA USING A LANDUSE REGRESSION APPROACH

by
JAD FARES ZALZAL

A thesis
submitted in partial fulfillment of the requirements
for the degree of Master of Engineering
to the Department of Civil and Environmental Engineering
of the Maroun Semaan Faculty of Engineering and Architecture
at the American University of Beirut

Beirut, Lebanon
April 2019

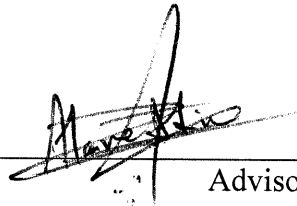
AMERICAN UNIVERSITY OF BEIRUT

DETERMINING THE MAIN DRIVERS OF PM AND CO
CONCENTRATION SURFACES IN THE GREATER BEIRUT
AREA USING A LANDUSE REGRESSION APPROACH

by
JAD FARES ZALZAL

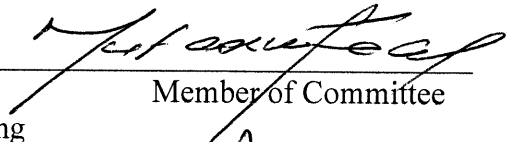
Approved by:

Dr. Ibrahim Alameddine, Assistant Professor
Department of Civil and Environmental Engineering
American University of Beirut



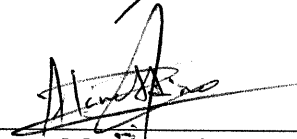
Advisor

Dr. Mutasem El-Fadel, Professor
Department of Civil and Environmental Engineering
American University of Beirut



Member of Committee

Dr. Marianne Hatzopoulou, Associate Professor
Department of Civil & Mineral Engineering
University of Toronto



Member of Committee

Signing on behalf of Dr. Hat Zopoulou.

Date of thesis defense: April 2019

AMERICAN UNIVERSITY OF BEIRUT

THESIS, DISSERTATION, PROJECT RELEASE FORM

Student Name: Zalzal Jad Fares
Last First Middle

Master's Thesis Master's Project Doctoral Dissertation

I authorize the American University of Beirut to: (a) reproduce hard or electronic copies of my thesis, dissertation, or project; (b) include such copies in the archives and digital repositories of the University; and (c) make freely available such copies to third parties for research or educational purposes.

I authorize the American University of Beirut, to: (a) reproduce hard or electronic copies of it; (b) include such copies in the archives and digital repositories of the University; and (c) make freely available such copies to third parties for research or educational purposes
after:

One ---- year from the date of submission of my thesis, dissertation, or project.

Two ---- years from the date of submission of my thesis, dissertation, or project.

Three ---- years from the date of submission of my thesis, dissertation, or project.


Signature

May 6, 2019
Date

ACKNOWLEDGMENTS

This thesis would not have been possible without the continuous guidance and support of my academic advisor and mentor, Prof. Ibrahim Alameddine, to whom I owe my deepest gratitude, for his relentless motivation, patience and encouragement throughout my graduate studies. The door to Prof. Alameddine's office was always open. With his good guidance and immense knowledge, he would put me back on the right track whenever I struggled in my research.

I would like to extend my sincere appreciation to my distinguished committee members Prof. Mutasem El-Fadel and Prof. Marianne Hatzopoulou for serving on my committee and for taking the time to pitch in with their insightful comments and valuable input.

To my father who always pushes me to be the best that I can be, and to my mother who always takes pride in everything I do, I am forever indebted to both of you.

I am also sincerely grateful to my sister for inspiring me by setting the bar high, and to my girlfriend, who always managed to lift my mood with her cheerful words and constant encouragement.

Lastly, I wish to thank the American University of Beirut's University Research Board for the fund granted to support this research project (Award Number: 103604; Project Number: 23974).

Thank you.

Jad Zalzal

AN ABSTRACT OF THE THESIS OF

Jad Fares Zalzal for Master of Engineering
Major: Environmental and Water Resources Engineering

Title: Determining the main drivers of PM and CO concentration surfaces in the Greater Beirut Area using a Landuse regression approach

The Eastern Mediterranean city of Beirut, Lebanon, suffers from poor air quality as compared to many European and North American cities. In this study, high resolution PM_{2.5} (fine particulate matter), PM₁₀ (coarse particulate matter), CO (carbon monoxide) and PM_{2.5}/PM₁₀ annual and seasonal pollution maps are generated for the Greater Beirut Area (GBA) using Land Use Regression models (LUR). The LURs were calibrated and validated on monthly data collected from 58 predefined monitoring locations within the GBA between March 2017 and March 2018. The annual mean concentrations of PM_{2.5}, PM₁₀ and CO across the monitoring stations were $68.1 \pm 15.7 \mu\text{g}/\text{m}^3$, $83.5 \pm 19.5 \mu\text{g}/\text{m}^3$ and $2.48 \pm 1.12 \text{ ppm}$ respectively. The observed spatio-temporal variability in the recorded PM concentrations was found to be larger than those typically reported in European cities. The performance of the developed LUR models was good, with R^2 ranging from 0.59 to 0.67 for the PM_{2.5} models, 0.49 to 0.63 for the PM₁₀ models, 0.50 to 0.60 for the CO models, and 0.32 to 0.51 for the PM_{2.5}/PM₁₀ ratio models. Overall, the predicted pollution surfaces were able to conserve the inter-pollution correlations that were determined from the field monitoring campaign, with the exception of the cold season. Although the model structure of the generated LUR models differed, building area, distance to main roads, and industrial area were all found to be common predictors across the majority of the annual and seasonal models. The predicted PM surfaces suggested that the entire population of the GBA was exposed to annually-averaged concentrations that exceeded the 24-hour WHO (World Health Organization) air quality standards set for PM_{2.5} and PM₁₀. Finally from a methodological point of view, the results of this study show that LURs generated using low cost purpose-designed monitoring campaigns can successfully generate air pollution surfaces for use in planning and epidemiological studies in developing countries lacking a dense fixed monitoring network.

Keywords:

Particulate Matter, Carbon Monoxide, Land-use regression models, air pollution modeling.

CONTENTS

ACKNOWLEDGMENTS.....	v
ABSTRACT.....	vi
LIST OF ILLUSTRATIONS.....	ix
LIST OF TABLES.....	xii
Chapter	
1. INTRODUCTION.....	1
2. METHODOLOGY.....	7
2.1. Study area and sampling sites	7
2.2. Air pollutants sampling	11
2.3. Analysis of measured CO, PM _{2.5} , and PM ₁₀ levels	15
2.4. Landuse regressions	17
2.4.1. Potential predictors for PM _{2.5} , PM ₁₀ and CO levels	17
2.4.2. Model development	24
2.4.2.1. Annual models	24
2.4.2.2. Seasonal models	25
2.4.2.3. PM _{2.5} /PM ₁₀ ratio models	26
2.4.2.4. LUR surfaces	26
3. RESULTS.....	28
3.1. Temporal variability.....	35
3.2. Spatial variability.....	39

3.3. Landuse regression models.....	51
3.3.1. PM _{2.5} models.....	51
3.3.2. PM10 models.....	57
3.3.3. CO models	62
3.3.4. PM _{2.5} /PM ₁₀ ratio models	67
4. DISCUSSION.....	71
4.1. Pollutant variability.....	72
4.2. LUR models.....	73
4.3. Correlations between measured and predicted concentrations	79
4.4. Exposure at schools and hospitals.....	80
4.4. Limitations	81
5. CONCLUSION AND FUTURE WORK	84
REFERENCES.....	87

ILLUSTRATIONS

Figure	Page
1. Figure 1. The landuse landcover of the GBA for the year 2005 (NCRS, 2005).....	9
2. Figure 2. Adopted monitoring sites within the GBA.....	11
3. Figure 3. Monitoring Setup (a) Site 7, (b) Site 12.....	15
4. Figure 4. PM _{2.5} histograms showing the distribution of (a) the measured PM _{2.5} concentrations across all sites and over the entire sampling campaign, and (b) the annually averaged PM _{2.5} concentrations by site. The solid vertical lines represent the mean concentrations, while the dashed lines represent the medians.....	30
5. Figure 5. PM ₁₀ histograms showing the distribution of (a) the measured PM ₁₀ concentrations across all sites and over the entire sampling campaign, and (b) the annually averaged PM ₁₀ concentrations by site. The solid vertical lines represent the mean concentrations, while the dashed lines represent the medians	32
6. Figure 6. PM _{2.5} /PM ₁₀ ratio histograms showing the distribution of (a) the actual PM _{2.5} /PM ₁₀ ratios across all sites and over the entire sampling campaign, and (b) the annually averaged PM _{2.5} /PM ₁₀ ratio by site. The solid vertical lines represent the mean ratio, while the dashed lines represent the medians.....	33
7. Figure 7. CO histograms showing the distribution of (a) the measured CO concentrations across all sites and over the entire sampling campaign, and (b) the annually averaged CO concentrations by site. The solid vertical lines represent the mean concentrations, while the dashed lines represent the medians	35
8. Figure 8. Seasonal variability of (a) PM _{2.5} , (b) PM ₁₀ , (c) PM _{2.5} /PM ₁₀ ratio and (d) CO across all monitoring sites	38
9. Figure 9. Concentrations of (a) PM _{2.5} , (b) PM ₁₀ , (c) PM _{2.5} /PM ₁₀ and (d) CO as a function of time of sampling. am = before noon; pm = afternoon	39
10. Figure 10. Variability of PM _{2.5} concentrations across sites. The blue	

	horizontal line represents the overall mean concentration of $PM_{2.5}$ across all sites	42
11.	Figure 11. Variability of PM_{10} concentrations across sites. The blue horizontal line represents the overall mean concentration of PM_{10} across all sites	43
12.	Figure 12. Variability of $PM_{2.5}/PM_{10}$ ratio across all sites. The blue horizontal line represents the overall mean $PM_{2.5}/PM_{10}$ ratio across all sites	44
13.	Figure 13. Variability of CO concentrations across all sites. The blue horizontal line represents the overall mean CO across all sites.	45
14.	Figure 14. Boxplots showing the variability of (a) $PM_{2.5}$, (b) PM_{10} , (c) $PM_{2.5}/PM_{10}$ ratio and (d) CO annual averages across different road and landuse densities	46
15.	Figure 15. Air pollution cluster categories	48
16.	Figure 16. Spatial distribution of (a) $PM_{2.5}$, (b) PM_{10} , (c) $PM_{2.5}/PM_{10}$ and (d) CO concentrations. All values are site averaged concentrations	50
17.	Figure 17. Predicted vs observed plots (a) Annual log-transformed $PM_{2.5}$ LUR Model (b) Warm season log-transformed $PM_{2.5}$ LUR model (c) Cold season log-transformed $PM_{2.5}$ LUR model. Diagonal line represents the 1:1 line	55
18.	Figure 18. $PM_{2.5}$ surfaces (a) Annual average $PM_{2.5}$ LUR (b) Warm-season $PM_{2.5}$ LUR (c) Cold-season $PM_{2.5}$ LUR	56
19.	Figure 19. Predicted vs observed plots (a) Annual log-transformed PM_{10} LUR Model (b) Warm season log-transformed PM_{10} LUR model (c) Cold season log-transformed PM_{10} LUR model. Diagonal line represents the 1:1 line	60
20.	Figure 20. PM_{10} surfaces (a) Annual average PM_{10} LUR (b) Warm-season PM_{10} LUR (c) Cold-season PM_{10} LUR	61
21.	Figure 21. Predicted vs observed plots (a) Annual log-transformed CO LUR Model (b) Warm season log-transformed CO LUR model (c) Cold season log-transformed CO LUR model. Diagonal lines represents the 1:1 lines	65
22.	Figure 22. Predicted CO surfaces (a) Annual average CO LUR (b)	

	Warm-season CO LUR (c) Cold-season CO LUR	66
23.	Figure 23. Predicted vs observed plots (a) Annual log-transformed ratio LUR Model (b) Warm season log-transformed ratio LUR model (c) Cold season log-transformed ratio LUR model. Diagonal lines represents the 1:1 lines	69
24.	Figure 24. ratio surfaces (a) Annual average ratio LUR (b) Warm-season ratio LUR (c) Cold-season ratio LUR	70
25.	Figure25. Plots showing the ECDF of (a) $PM_{2.5}$, (b) PM_{10} and (c) CO concentrations observed at schools (black dots) and hospitals (red dots), with the straight blue line showing the WHO standards and the dashed blue line showing the Lebanese standards	82

TABLES

Table	Page
1. Table 1. Monitors description	13
2. Table 2. Relevant ambient air quality standards.....	16
3. Table 3. Predictors used in previous PM _{2.5} LUR models	20
4. Table 4. Predictors used in previous PM ₁₀ LUR models	23
5. Table 5. Variability of PM _{2.5} , PM ₁₀ and CO levels across the sampling domain	28
6. Table 6. Seasonal variability in the concentrations of PM _{2.5} , PM ₁₀ and CO	37
7. Table 7. Comparison between within category and between category variability	41
8. Table 8. Cluster analysis categories and the thresholds identified for each group	48
9. Table 9. Spatial auto-correlation of the pollutants as determined through Moran's I values	49
10. Table 10. LUR models for predicting annual and seasonal log-transformed PM _{2.5} concentrations	55
11. Table 11. LUR models for predicting annual and seasonal log-transformed PM ₁₀ concentrations	59
12. Table 12. LUR models for predicting annual and seasonal log-transformed CO concentrations	64
13. Table 13. LUR models for predicting annual and seasonal log-transformed PM _{2.5} /PM ₁₀ ratios	68
14. Table 14. Table showing the correlations between the measured concentrations and between the generated prediction surfaces	80

CHAPTER 1

INTRODUCTION

The main source of air pollution in urban settings is attributed to the combustion of fossil fuels, which produces greenhouse gases and other toxic pollutants. Urban air pollution is a major cause of health problems in cities and has been attributed to the premature deaths of millions and the loss of billions of dollars in terms of medical costs and lost productivity (United Nations Environment Programme, 2014). Several studies have shown direct causal relationships between air pollution levels and the incidence of cardiovascular (Dehbi et al., 2017; Delfino et al., 2010; Franchini & Mannucci, 2012; Gan, Davies, Koehoorn, & Brauer, 2012; Vanos, Hebborn, & Cakmak, 2014) and respiratory diseases (Beelen et al., 2008; Finkelstein, Jerrett, & Sears, 2004; Iii et al., 2002; Vanos et al., 2014). According to Krzyżanowski, Kuna-Dibbert, and Schneider (2005), air pollution from the transportation sector in cities is the leading contributor towards adverse health and negative environmental impacts. As daily commutes become longer, traffic congestions become worse, and as more people reside in the vicinity of major roads with high traffic densities, traffic related air pollution is expected to increase the hazard and risk of human exposure to air pollutants.

Traffic is often the major source of air pollutants in urban areas. Traffic related emissions include Carbon Monoxide (CO), Nitrogen oxides (NO_x), sulfur dioxide (SO₂), particulate matter (PM), black carbon, and volatile organic compounds (VOCs). This study focused on assessing the concentrations of (CO) as well as particulate matter, both fine (PM_{2.5}) and coarse (PM₁₀) in the Greater Beirut Area (GBA), a densely urban area along the

eastern Mediterranean coastline. CO is an odorless, tasteless, colorless and toxic gas. It is formed by photochemical reactions in the atmosphere and by incomplete combustion of carbon containing fuels. CO has a relatively long atmospheric lifetime, ranging from 10 days in the summer to over a year in very cold regions (EPA, 2010). However, despite its long lifespan, CO ambient concentrations are found to be source specific, with background levels being unaffected by nearby sources (Jaffe, 1968). CO levels tend to have a seasonal pattern, with elevated CO concentrations in winter as compared to the summer (Jaffe, 1968). This is due to higher reactivity at elevated temperatures as well as higher emissions during the winter season. While elevated CO concentrations are a major concern in indoor environments, the occurrence of outdoor CO poisoning may take place near heavily congested major roads (Centers for Disease & Prevention, 1997). In urban areas, it has been estimated that as much as 75% of the CO emissions are caused by on-road vehicle exhausts (EPA, 2010). As such, CO is often highly correlated with other traffic related air pollutants such as NO_x, SO₂, and PM. This makes CO a good air pollution indicator. Other than traffic-related emissions, fossil fuel power generating plants are also considered a major anthropogenic source of CO in urban areas (EPA, 2010).

PM are composed of a set of physically and chemically diverse particles that are found in different sizes. Fine PM usually constitutes the majority of suspended particles; moreover, it deposits slowly, which leads to an atmospheric lifetime of around 5 to 10 days. Coarse PM on the other hand, deposit more rapidly and have an atmospheric lifetime of less than 2 days (Brook, Brook, & Rajagopalan, 2003; Rai, 2016a). As a result, PM₁₀ tends to be less homogeneously distributed and reflects more closely local pollution sources. PM usually originates from man-made stationary or mobile sources as well as from natural

sources such as fires and dust storms. The main sources of the coarse PM include the wear of tires, sea spray, erosion and dust from roads, agriculture, and construction and demolition activities (EPA, 2009). The main sources of PM_{2.5} on the other hand are fossil fuel combustion, mobile sources exhausts, dust, and wildfires. PM levels often show a seasonal pattern, with higher concentrations during the winter season. This is due to the cold-start conditions in gasoline engines, which are the main source of PM in most cities (EPA, 2009). Elevated PM levels are known to have adverse health impacts as they can penetrate deep into the lungs causing respiratory and cardiovascular diseases (Peng, Chang, Bell, & et al., 2008; Riediker et al., 2004). PM₁₀ and PM_{2.5} are the most common size fractions considered in epidemiologic studies. PM₁₀, also called “thoracic particles”, can penetrate into the lower respiratory system, whereas PM_{2.5}, or “respirable particles”, can penetrate deeper into the gas exchange regions of the lung (Wilson, Kingham, Pearce, & Sturman, 2005). PM₁₀ exposure is associated with increased ischemic heart disease among the elderly population and with higher risk of myocardial infarction. Elevated concentrations of PM have also been correlated with acute respiratory disorders such as sinusitis, bronchitis, asthma and allergy, and damage to the defensive functions of alveolar macrophages leading to an increase in respiratory infections (Rai, 2016b).

Given the gravity of exposure to elevated air pollution levels in urban centers, establishing city-wide ambient air quality fixed-station monitoring programs has been widely supported. Yet, establishing and maintaining such monitoring networks is expensive and can be prohibitive for developing countries. Moreover, these programs often lack the needed spatial coverage to capture the variability of air pollution levels within a city and/or tend to be clustered in pollution hot spots (Kanaroglou et al., 2005). Miller et al. (2007) has

shown that the spatio-temporal variability of air pollution in some cities can exceed the variability observed between cities. As such, the limited spatial coverage of fixed station monitoring networks presents a challenge towards quantifying exposure across cities given the high intra-urban spatial variability in the air pollution levels (Briggs et al., 1997). Several studies have shown that many fixed monitoring networks were unable to accurately capture variations in pollutant concentrations within transport microenvironments and failed to predict levels beyond 1 Km (J. Gulliver & Briggs, 2004; Kim, Harrad, & Harrison, 2002; Violante et al., 2006; Wright, Jewczyk, Onrot, Tomlinson, & Shephard, 1975). Given the prohibitive costs and the low spatial coverage associated with fixed air pollution monitoring programs, alternative model-based methods have been developed. These urban air pollution assessment modeling methods are often divided into four groups, namely: 1) proximity-based assessments, 2) geospatial interpolation methods, 3) dispersion models (DM), and 4) Land-Use Regression (LUR) models (Michael Jerrett et al., 2005). Proximity models are the most basic among the previously mentioned models, as they assess exposure to air pollutants based solely on the distance separating a location from a major emission source. Geostatistical interpolation models provide estimates of the pollutant concentrations as a function of the modeled spatial autocorrelations. Their skill is thus a function of the strength of the spatial behavior of the phenomena under study. DMs are mathematical simulations of pollutant dispersion in the atmosphere; they are based on emissions, meteorological conditions, and topography. DMs have the advantage of incorporating both the spatial and temporal variations in the concentrations of air pollutants; yet their adoption is often limited by the lack of needed input data, such as hourly traffic counts, hourly meteorological changes, hourly changes in emissions, and a detailed representation of the

city. Such data are seldom available at the city level or are very difficult to collect (Michael Jerrett et al., 2005), especially in developing countries. LUR models on the other hand are based on multiple linear regressions that are built to relate measured concentrations at sampling locations with a series of relevant urban predictors such as land use, building heights, weather conditions, topography, traffic counts, fleet composition, road type, point emission sources, and road density. Given the increased availability of spatial data in many cities, the use of LUR models in air pollution mapping has grown in importance.

The application of LUR models was first introduced in the SAVIAH (Small Area Variations In Air quality and Health) study to assess exposure of children to elevated NO₂ concentrations in Amsterdam, Huddersfield and Prague (Briggs et al., 1997). LURs were later successfully applied in modelling the concentrations of several pollutants including nitrogen dioxide (NO₂), PM_{2.5}, PM₁₀, volatile organic compounds (VOCs) (Hoek et al., 2008), Ozone (O₃) (Kerckhoffs et al., 2015), and Ultrafine Particles (UFP) (Abernethy, Allen, McKendry, & Brauer, 2013; Weichenthal, Van Ryswyk, Goldstein, Shekarrizfard, & Hatzopoulou, 2016) across different cities. The performance of LUR models has been well established in the literature to be robust for modeling air pollution resulting from traffic-related pollution levels.

Several studies have compared LUR to commonly used air pollution modeling methods such as geo-statistics and dispersion models. In the SAVIAH study, LUR models outperformed geo-statistical models in predicting NO₂ concentrations across three European cities (Briggs et al., 2000). Moreover, the European Study of Cohorts for Air Pollution Effects (ESCAPE) project developed and compared the skill of calibrated DM and LUR models to predict NO₂, PM_{2.5}, and PM₁₀ levels across 36 European cities. The

project concluded that the performance of the LUR models was comparable to DMs for NO₂; yet the LUR models outperformed the DM models when it came to predicting PM_{2.5} and PM₁₀ levels (de Hoogh et al., 2014). John Gulliver, de Hoogh, Fecht, Vienneau, and Briggs (2011) found that the developed LUR models outperformed the proximity analysis, kriging, and dispersion models in predicting PM₁₀ concentrations in London. In Munich, the developed LURs slightly outperformed DM in predicting NO₂ concentrations, but had similar performance in predicting PM_{2.5} concentrations (Cyrus et al., 2005).

In this study, LUR models are developed to predict annual and seasonal ambient particulate matter (PM₁₀ and PM_{2.5}) and CO concentrations, as well as the PM_{2.5}/PM₁₀ ratio across the Greater Beirut Area (GBA), Lebanon. The developed models are then used to generate pollution surfaces to map potential exposures, identify pollution hotspots, determine the strength of the spatial correlation between the pollutants, and quantify the intra-urban variations of air pollution in the study area. The models are then used to assess the compliance of the predicted air quality with relevant national and international standards across different regions of the GBA and to assess the exposure to air pollution at vulnerable locations, i.e. schools and hospitals. Finally, the study aims to identify the main air pollution drivers within the GBA and to contrast them with those that have been identified in other cities. To our knowledge this is the first attempt that such an endeavor has been initiated at the level of the Eastern Mediterranean. Additionally, this study is one of the first studies to look at assessing the skill of LURs in predicting air pollution surfaces in a highly heterogeneous city with large contrasts in land use land cover and elevation.

CHAPTER 2

METHODOLOGY

2.1 Study area and sampling sites

The study area covers the Greater Beirut Area (GBA), a mixed-use urban area that includes the capital city of Beirut along with its suburbs. The GBA is highly heterogeneous in its landuse and landcover due to poor urban planning and fast urbanization. While the city of Beirut itself is urban, highly dense, and congested, many of its suburbs are transitioning at an alarming rate from forested areas or rural low-density areas into medium to high density urban areas (Figure 1). Urban regions were found to have doubled in area in Lebanon between 1994 and 2005 (Faour, 2015). The urban growth rate was found to be equal to 3.18% per year (in terms of area) between 2010 and 2015, with a population growth rate of 0.86% in 2015 (UNHabitat, 2015). Geographically, the GBA stretches from the Mediterranean coastline up to an elevation of 800 m above mean sea level. It covers an area of 233 Km² of which 8 km² are occupied by the Rafic Hariri international airport.

The deterioration of air quality in the GBA is a growing environmental concern. While urban air quality in some industrialized countries has improved in recent decades, the problem in the GBA persists and has become a major source of concern to public health. Air pollution in Lebanon currently affects millions of people living in the mostly urban and peri-urban areas within the GBA, where smog, small particles, and toxic pollutants pose serious health concerns. Similarly to other urban areas, the air pollution problems in the GBA are mostly attributed to the transportation sector, as it accounts for 24% of carbon dioxide (CO₂), 59% of nitrogen dioxide (NO₂), 79% of non-methane volatile organic

compounds (NMVOC), and 22% of SO₂ national emissions (Ministry of Environment, 2011). Despite these problems, the GBA still lacks a dense air pollution monitoring network able to assess intra-urban variability. Several studies have been conducted to quantify the concentrations of PM and CO in the GBA. Shaka' and Saliba (2004) reported that the average concentrations of PM_{2.5} and PM₁₀ were found to be 40 µg/m³ and 76 µg/m³ respectively. Moreover, Saliba, El Jam, El Tayar, Obeid, and Roumie (2010) reported that PM_{2.5} and PM₁₀ concentrations measured at 5 urban locations in the GBA varied between 55.1 and 103.8 µg/m³ for PM₁₀ and between 27.6 and 41 µg/m³ for PM_{2.5}. CO levels measured at three busy streets in the GBA were found to vary between 1213 µg/m³ and 2709 µg/m³, with a clear seasonal pattern in the observed concentrations (Saliba, Moussa, Salame, & El-Fadel, 2006). Nevertheless, little work has been done to assess the spatial variability of these pollutants in the GBA.

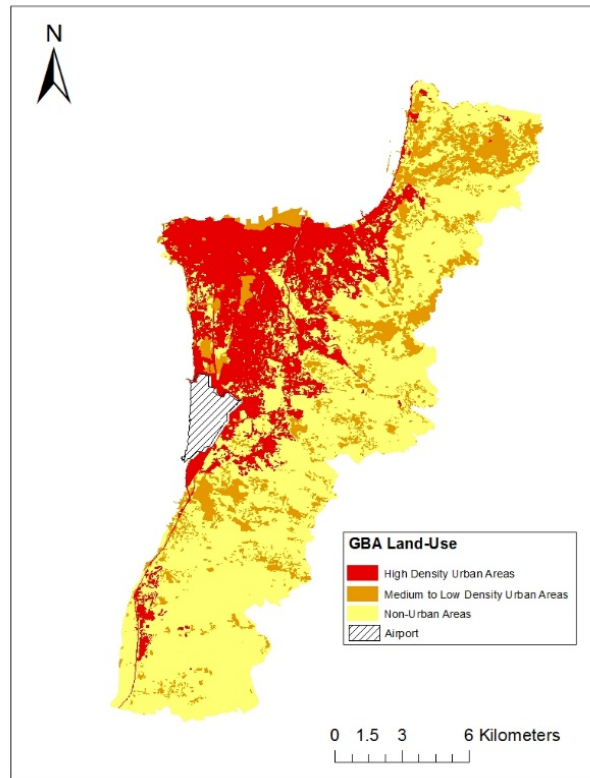


Figure 1. The landuse landcover of the GBA for the year 2005 (NCRS, 2005)

While there is no unified methodology to determine the required number of monitoring locations needed for a given area of interest, Hoek et al. (2008) found that on average, air quality-based landuse regression studies use between 20 and 100 monitoring locations. In addition, Madsen et al. (2007) reported that increasing the number of sites in Oslo, Norway from 40 to 80 didn't result in an improved model performance. M. Jerrett et al. (2007) also found that generating LUR models using a network of 94 monitoring locations instead of 65 didn't improve their model results. Given the areal extent of the GBA, this study adopted a monitoring program based on 60 monitoring sites. Note that the adopted monitoring network program is considered dense with around $0.25\text{sites}/\text{Km}^2$. The

spatial distribution of the adopted monitoring network was developed so as to provide the adequate spatial coverage needed to capture the variability in the land use types and the different road densities within the study area. Ryan and LeMasters (2007) showed the importance of refraining from adopting monitoring sites with a uniform land use. While most LUR studies use informal methods to select their monitoring site locations (Hoek et al., 2008), recent studies have started to move towards the adoption of a systematic site selection method. The most commonly used selection method was proposed by Kanaroglou et al. (2005). Their method allocates stations based on the anticipated spatial variation in air pollution and population densities. Another method identified monitoring locations based on the following criteria: population density, distance to the city center, residential or commercial type, density of the road network, and green spaces, and allocates sites in order to capture the maximum variations in these variables (Brauer et al., 2003; Saraswat et al., 2013). In the GBA, the absence of a dense air quality monitoring network and the large uncertainties in block-level population data limits the adoption of such approaches. Therefore, sites were chosen based on their LULC as well as their associated road densities. Land use can be viewed to be a surrogate of population as it identifies the intensity of urbanization, while road density can be viewed as a surrogate for air pollution, given that traffic accounts for a large portion of urban pollution in the GBA (ECODIT, 2010). As such, sites were divided into high, medium, and low density urban areas. Moreover, the road density in the GBA was divided into two categories, namely high and low road density. Finally, the 60 monitoring sites were divided equally among the 6 urban-road density categories. The adopted sampling strategy is similar to a study conducted in New York City (Matte et al., 2013). The final site selections were generated using stratified

random sampling through the use of the Spatial Analyst and the Sampling Tool Design toolboxes in ArcGIS 10.5.1 (ESRI, 2016). The locations of the air quality monitoring sites are shown in Figure 2.

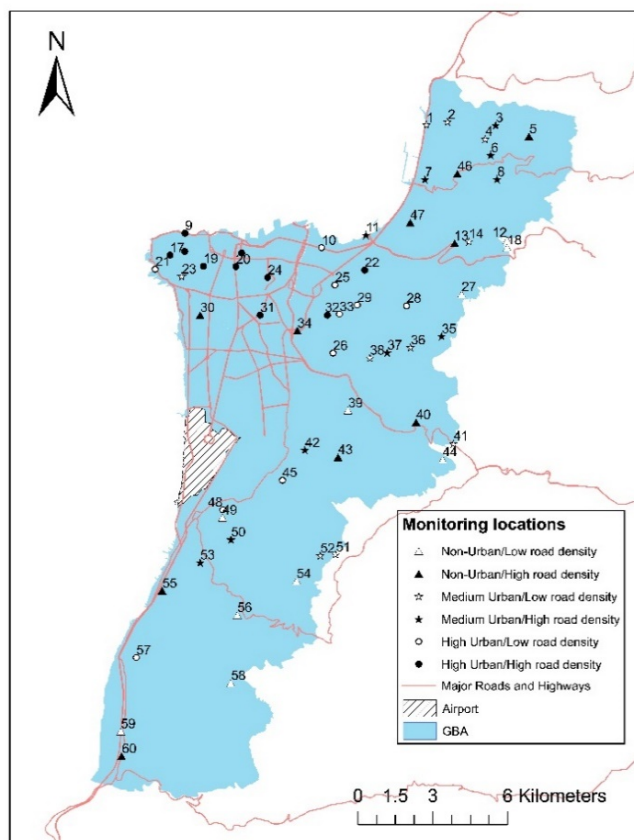


Figure 2. Adopted monitoring sites within the GBA



2.2 Air pollutants sampling

In this study, CO concentrations were monitored using the Langan CO analyzers (model L76n) (Langan Products, 2006) with a data logging interval of 1 min. The analyzers have a measurement range between 0 and 200 ppm, a resolution of 0.1 ppm, and a response

time ($t_{90\%}$) of 40 seconds (Table 1). Previous studies have successfully used the Langan L76n to measure both indoor and outdoor ambient CO concentrations (Abi Esber, El-Fadel, Nuwayhid, & Saliba, 2007; Alameddine, Abi Esber, Bou Zeid, Hatzopoulou, & El-Fadel, 2016).

PM_{2.5} and PM₁₀ were monitored using the TSI Dustrak II Model 8532 (TSI, 2014). The analyzers rely on the optical backscatter technology with a measurement range of 0.001–150 mg/m³ and an accuracy of $\pm 0.1\%$ of reading or 0.001 mg/m³, whichever is greater (Table 1). The Dustrak has been successfully tested and used in multiple studies to measure PM concentrations from several sources such as coal power generators (Lehocky & Williams, 1996), natural dust sources (X. Wang et al., 2015), and several traffic and stationary sources (Alameddine et al., 2016; X. Wang, Watson, Chow, Gronstal, & Kohl, 2012).

Table 1. Monitors description

Monitor	Manufacturer	Parameter	Detection Method	Specifications
TSI Dustrak II Model 8532 	Model 8532, TSI Corporation, Shoreview, USA	PM _{2.5} & PM ₁₀	90° light backscattering PM10 & PM2.5 impactors	Range: 0.001 to 150 mg/m ³ Resolution: ±0.1% of reading or 0.001 mg/m ³
Langan L76x 	2660 California Street, San Francisco, CA 94115 USA	CO & CO ₂	Electrochemical 3-electrode (CO)	Range: 0-200 ppm Resolution: 50 ppb Response time t₉₀: < 30 s at 20°C Repeatability: 1% of signal

Air quality data was collected through an intensive monitoring campaign, using the hand-held particulate matter (TSI DustrakII, Model 8532) and CO (Langan L76x) monitors. The monitoring campaign extended from March 2017 until March 2018, and covered a total of 64 working days (Monday to Saturday). 58 of the 60 predefined monitoring locations (Figure 2) were visited on average between 8 and 12 times throughout the year. Note that 2 of the initially proposed 60 monitoring locations were later dropped due to security reasons. The remaining 58 locations were divided into 8 routes, each encompassing between 7 to 8 sites each. On each sampling day, a route was selected and the sites within it were visited in

a random order in order to avoid any biases that might occur due to the timing of sample collection. In total 525, 30 minutes measurements were collected. Air pollution monitoring took place between 8 am and 6 pm on each sampling day. At every location, the three monitors were placed next to each other on a 1.5 m high tripod (average breathing height) for 30 minutes (Figure 3). The PM filters were cleaned, and the equipment were run in parallel before each sampling day to correct for any errors in the readings. The CO equipment were tested against a standard CO gas of 50 ppm concentration once per month. Additionally, the PM equipment were zeroed at every location before taking the measurements, and were then tested against a zero concentration after every measurement to check for any drift in the readings. All readings that showed a drift in the measurements due to equipment malfunction were discarded. Traffic counts were also recorded over the 30 minutes sampling period. Moreover, the vehicle types were also recorded. Vehicles were classified as cars, SUVs, light trucks, heavy trucks, buses, and motorcycles. Temperature and relative humidity were also measured and recorded with the Langan L76x monitors. Daily weather data (temperature, precipitation, wind speed and wind direction) were also collected from the Rafik Hariri International Airport weather station, which represented the closest meteorological station within the study area.



Figure 3. Monitoring Setup (a) Site 7, (b) Site 12

2.3 Analysis of measured CO, PM_{2.5}, and PM₁₀ levels

The correlations between the measured concentrations of the 3 pollutants were assessed using Pearson's r . These correlations were later compared to those observed between the different model predictions to check whether the models were able to conserve the observed correlations between pollutants. Cluster analysis was also conducted on the observed concentrations in order to group the 60 sites based on the measured air pollutant concentrations. Cluster analysis was done using the k-means partitioning method, which aims to partition the monitoring sites into K clusters, with each observation belonging to the cluster with the nearest mean, which serves as a prototype of the cluster. The adopted number of clusters was selected by plotting the within group sums of squares versus the

number of clusters. All analysis was conducted using the stats package in the software R (R Core Team, 2015).

Measured concentrations were also compared to the national and international air quality standards (Table 2) and percent exceedances were also reported.

Table 2. Relevant ambient air quality standards

Pollutant	Averaging time	Lebanese NAAQS ¹	EPA ²	WHO ³
CO	1 hour	30 mg/m ³	35 ppm (primary*)	30 mg/m ³
	8 hours	10 mg/m ³	9 ppm (primary)	10 mg/m ³
PM _{2.5}	24 hours	NA	35 µg/m ³ (primary)	25 µg/m ³
	1 year	NA	12 µg/m ³ (primary) 15 µg/m ³ (secondary*)	10 µg/m ³
PM ₁₀	24 hours	80 µg/m ³	150 µg/m ³ (primary and secondary)	50 µg/m ³
	1 year	NA	NA	20 µg/m ³

*: EPA identifies 2 types of ambient air quality standards: Primary and Secondary. Primary standards provide public health protection, whereas secondary standards provide public welfare protection (EPA, 2009, 2010)
1:(MOE, 2005)
2:(EPA, 2009, 2010)
3:(WHO, 2005)

Finally, average within site variability (i.e. the average of the standard deviations of the observed readings at each of the 60 sites) was compared to the between site variability (i.e. the standard deviation of the average observed readings at each of the 60 sites) for each pollutant. This allows for assessing the spatial variability of the measured air pollutants (i.e. variability between sites) in relation to their temporal variability (i.e. variability within each

site). Pollutants that show low between site variability tend to be more homogenous in space, while those with large within site variability are expected to have a temporal variance. All statistical analysis was conducted using the R software (R Core Team, 2015).

2.4 Landuse regressions

2.4.1 Potential predictors for $PM_{2.5}$, PM_{10} and CO levels

Potential predictors for the Particulate Matter and CO LUR models were identified based on previous LUR studies. Nevertheless, since only two LUR studies have been conducted on Carbon Monoxide (Hassanpour Matikolaei, Jamshidi, & Samimi, 2017; Son et al., 2018), the selection of predictors was based on previous $PM_{2.5}$ and PM_{10} studies (Table 3 and Table 4). Previous studies have reported a strong correlation between land use predictors and particulate matter concentrations (Table 3).

In addition, both road density and distance to pollution sources (industrial and airports) have been found to be strong predictors of ambient particulate matter concentrations (Table 3 and Table 4). Most LUR studies focused on 2 types of predictors, namely 1) time variant predictors, which are mainly responsible for the temporal variability of air pollutant concentrations, such as meteorological and traffic variables, and 2) time constant predictors, which are mainly responsible for the spatial variability of air pollutant concentrations. In this study, five categories of predictors were generated for the study region.

- a. **Meteorological predictors:** These included wind speed (m/sec), wind direction, temperature ($^{\circ}\text{C}$), relative humidity (%) and precipitation (mm/day). Temperature and relative humidity were measured simultaneously with air pollution monitoring using the Langan L76x. The remaining variables were collected for each sampling day from the Rafic Hariri International Airport weather station. The square of the wind speed was also included as a potential predictor in an attempt to account for the non-linear effect that wind might have on pollution levels.
- b. **Land Use predictors:** These included total building area (Km^2), high density urban area (Km^2), medium density urban area (Km^2), low density urban area (Km^2), industrial area (Km^2), park area (Km^2), waterbody area (Km^2), agricultural area (Km^2) and forest area (Km^2). All land-use variables were reported in terms of their occurrence within a predefined buffer. Buffers were generated for each of the predefined monitoring locations using ArcGIS 10.5.1 (ESRI, 2017). The radii of the generated buffers ranged from 50 meters up to 3000 meters. In an attempt to remove potential problems caused by autocorrelation, the correlations between all buffers of the same predictor were assessed using Pearson correlation. Given the potential for high correlations between several of the different buffer distances, only the buffered predictor that had the highest correlation with the measured pollutant concentrations was kept along with all buffers that showed low levels of correlation. The most recent landuse data for the GBA were generated for the year 2005 and were obtained from the Lebanese National Center for Remote Sensing (NCRS, 2005).
- c. **Traffic predictors:** These included distance to major roads and highways (Km), length of roads within a certain buffer (Km), and length of major roads within a

certain buffer (Km). The buffers used to calculate the length of roads were also generated using ArcGIS 10.5.1 (ESRI, 2017). In addition, traffic predictors included the 30 min traffic counts that were recorded simultaneously with air pollution measurements on the nearest road to each of the sampled sites. These predictors include the total number of vehicles, the number of passenger cars, the number of SUVs, the number of buses, the number of light trucks, the number of heavy trucks, and the number of motorcycles. Note that due to the lack of traffic data in the GBA, traffic counts were not included in the final LUR models in order to ensure that the generated models can be used for predicting pollution surfaces over the entire GBA.

- d. Predictors specific to the GBA:** These included distance to the Rafik Hariri International Airport (Km) which is located in the middle of the study area and distance to the Zouk power plant (Km) which is located 2 Km north of the GBA, and considered to be one of the largest air pollution sources along the Lebanese coastline.
- e. Other predictors:** These included variables such as elevation from sea level (m) and the Aerosol Optical depth (AOD). Elevation can play a role with regards to modulating the concentrations of air pollutants in the GBA given that changes in elevation can affect pollution dispersion. Unlike many other urban areas that tend to be flat, elevation in the study region varies between 0 and 800 m. Elevation was found to be a good predictor of particulate matter in several previous studies (Tables 3 and 4). It had a negative effect in all of these studies since most of the air pollution sources (i.e. traffic and population density) were located at lower elevations. However, particulate matter and carbon monoxide emissions from

combustion engines are expected to increase with altitude, since the efficiency of these engines decreases with elevation due to lower available oxygen (EPA, 2009, 2010). Moreover, AOD has been successfully used in previous LUR studies as a predictor of particulate matter concentrations (Y. Liu, Paciorek, & Koutrakis, 2009; Zhang et al., 2018). Daily AOD readings were downloaded from the MODIS aqua satellite, using the 550 nm dark target aerosol product (MYD08_D3 v6) at a temporal resolution of 1 day, and a spatial resolution of 10km (Rob Levy, 2015).

Table 3. Predictors used in previous PM_{2.5} LUR models

Source	Location	Meteorological predictors	Land-use predictors	Traffic predictors	Other predictors
(Henderson, Beckerman, Jerrett, & Brauer, 2007)	Vancouver, Canada	-	Commercial area, Residential area, Industrial area	Traffic density	Elevation
(Sanchez et al., 2018)	Hyderabad, India	-	Number of trees, NDVI, Household density	-	Night-time light intensity, elevation, longitude
(Ross, Jerrett, Ito, Tempalski, & Thurston, 2007)	New York, USA	-	Industrial area, Vegetative area	Traffic density	Population
(Saraswat et al., 2013)	New Delhi, India	-	-	Distance to major road, Length of roads	Population
(Shi, Lau, & Ng, 2016)	Hong Kong	-	-	Public transport vehicles density, road density	Frontal area index
(Hankey & Marshall, 2015)	Minneapolis, USA	-	Industrial area, Retail area, Open area	Railway length, Nus route length, Traffic intensity, Length of major roads, Intersections	Population density, House density, household income
(Eeftens et al., 2012)	20 European study areas	-	Industrial area, Green area, Natural area, Residential area, Port	Road length, Traffic density, Distance to major road, Length	Population, Elevation

Source	Location	Meteorological predictors	Land-use predictors	Traffic predictors	Other predictors
			area	of major roads	
(Y. Liu et al., 2009)	Massachusetts, USA	Temperature, Relative humidity	-	-	Population, AOD, Day of the year, Planetary boundary layer height
(Ho et al., 2015)	Taipei, Taiwan	-	Industrial area	Road length, Major road length	-
(Yang, Wu, Chen, Lin, & Lu, 2018)	Zhejiang, China	Relative humidity	Residential area, Water area	-	Latitude
(Clougherty, Wright, Baxter, & Levy, 2008)	Boston, USA	-	-	Road length	Population
(de Hoogh et al., 2016)	19 countries in Europe	-	Urban green area, Natural area, Residential area, Industrial/Commercial area	Major roads length, Road length	Y coordinate, Elevation
(Wolf et al., 2017)	Augsburg, Germany	-	Semi natural area, number of buildings, Industrial area	-	Elevation
(Dirgawati et al., 2016)	Perth, Australia	-	Open area, Water area	Traffic intensity	Distance to coast, Population density
(Li, Ma, Xu, & Song, 2018)	Beijing, China	-	NDVI	-	Terrain slope, Distance to Beijing south boundary, Population
(C. Liu, Henderson, Wang, Yang, & Peng, 2016)	Shanghai, China	-	Water area, Industrial area	Length of highways	Longitude, Distance to coast
(Zhang et al., 2018)	China	Temperature, Relative humidity, Wind speed	Artificial land area, Forest area, Grass and arable area	Distance to road	Latitude and Longitude, Population density, Elevation, Distance to power plants, Year and month, AOD
(Merbitz, Fritz, & Schneider,	Aachen, Germany	-	Building area, Green area	-	-

Source	Location	Meteorological predictors	Land-use predictors	Traffic predictors	Other predictors
2012)					
(Huang, Zhang, & Bi, 2017)	Nanjing, China	Wind index	Residential area	Road length	-
(Brauer et al., 2003)	3 European cities	-	Address density	Traffic intensity, Length of roads	Population
(Hochadel et al., 2006)	North Rhine-Westphalia, Germany	-	Building density	Traffic, Distance to major road	-
(Moore, Jerrett, Mack, & Künzli, 2007)	Los Angeles, USA	-	Industrial area, Governmental area	Traffic density	-
(Saucy et al., 2018)	Western Cape Province, South Africa	-	Construction sites	Length of railway,	Distance to grill, Number of grills, Population, Distance to nearest refuse transfer station, Waste burning sites
(Morgenstern et al., 2007)	Munich, Germany	-	Land cover factor	Length of rural roads, Distance to motorway	Population density

Table 4. Predictors used in previous PM₁₀ LUR models

Source	Location	Meteorological predictors	Land-use predictors	Traffic predictors	Other predictors
(Shi et al., 2016)	Hong Kong	-	Governmental area	Public transport vehicles density, road density	Frontal area index
(Eeftens et al., 2012)	20 European study areas	-	Industrial area, Green area, Natural area, Residential area, Port area	Road length, Traffic density, Distance to major road, Length of major roads	Population, Elevation
(Vienneau et al., 2010)	UK and Netherlands	-	Urban influence, Residential area, Industrial area	Major road length	Elevation, Y coordinate
(Chen, Baili, et al., 2010)	Tianjin, China	Wind speed	Residential area	Length of major roads	Population density
(Wolf et al., 2017)	Augsburg, Germany	-	Industrial area, Urban green area, building area	Road length, traffic density	-
(Dirgawati et al., 2016)	Perth, Australia	-	Open area, Building area	Heavy traffic	-
(Zhang et al., 2018)	China	Temperature, Relative humidity, Wind speed	Artificial land area, Forest area, Grass and arable area	Distance to road	Latitude and Longitude, Population density, Elevation, Year and month, AOD
(Amini et al., 2014)	Tehran, Iran	-	Other land use area	Road distance, Distance to major road	Distance to airport, Distance to bus terminal, Distance to military base
(Merbitz et al., 2012)	Aachen, Germany	-	Building area, Green area	-	-

2.4.2 *Model development*

2.4.2.1 Annual models

Four annual multiple linear regression models were developed to predict PM_{2.5}, PM₁₀ and CO concentrations, as well as the PM_{2.5}/PM₁₀ ratios. The multiple linear regression models can be presented by equation 1.

$$Y = X_{(k+1,n)}B + \varepsilon \quad (\text{Equation 1})$$

Where Y represents a vector of n observations of the response variable; X is a model matrix with columns for k + 1 predictors with an initial column of 1 to allow for model intercepts; B is a vector of regression coefficients, with one column for each response variable; and finally ε is a vector of the model errors (Fox & Weisberg, 2011). The multiple linear regression models were generated using a supervised forward selection procedure. The final models were selected based on their Akaike's Information Criteria (AIC) (Akaike, 1974). At each step, the predictor resulting in the model with the lowest AIC value (i.e. the most parsimonious model) was added. Each selected predictor was plotted alone against the concentration of each pollutant to ensure that the sign of the model variable coefficient matched the univariate relationship. A change in the sign of the relationship could be an indication of multi-collinearity issues. Any predictor that resulted in a change in the sign of a previously added predictor once included in the model was discarded to avoid overfitting or the introduction of significant interactions between the predictors. Finally, predictors that resulted in other predictors becoming insignificant (with p-value > 0.1) were also excluded. Some predictors with p-values slightly larger than 0.1 were kept in the model if their removal resulted in a large drop in the model performance and if the sign

of their coefficient was plausible. Problems associated with collinearity were continuously assessed through tracking the variance inflation factors (VIF). Predictors with VIF values greater than 5 were removed from the final model, except for predictors with quadratic terms (i.e. Wind speed). Final residual diagnostic tests were applied to check for linearity, influential observations (Cook's D), heteroskedasticity, and non-normality. Additionally, the spatial autocorrelation of the residuals was assessed using Moran's I. Moran's I values vary between -1 and 1, with a value of 0 signifying no spatial autocorrelation, values close to -1 signifying dispersion in the residuals, and values close to 1 signifying clustering in the residuals. The percent bias (PBIAS) was also calculated as a measure of the tendency of the models to overpredict or underpredict. All statistical analyses were performed using the R software (R Core Team, 2015). A 10-fold (k-fold) cross-validation was also performed on the developed models, using the DAAG package (Maindonald & Braun, 2014) in the software R (R Core Team, 2015). Cross validation assesses the predictive power and internal robustness of the generated models. Model performance was evaluated using the R^2 , the adjusted R^2 , the cross validation R^2 and the root mean squared errors (RMSE).

2.4.2.2 Seasonal models

Additionally, seasonal LUR models were generated for each of the 3 pollutants using the same approach adopted for the generation of the annual models. The structure of these models was compared to that of the annual models in order to better understand if the impact of some predictors varied seasonally and to assess the temporal variation of pollutant concentrations. The monitoring campaign was divided into two seasons (the warm

and the cold) based on the temperatures and precipitation values observed during the sampling campaign. The warm season extended from April to October; it is also mostly dry. The cold season extended between November and March and is relatively a very wet period given the Mediterranean climate of the GBA.

2.4.2.3 PM_{2.5}/PM₁₀ ratio models

Little has been done on modeling the PM_{2.5}/PM₁₀ ratio through an LUR. Similarly to the other 3 pollutants, 1 annual and 2 seasonal models were generated for the ratio of PM_{2.5}/PM₁₀. This method is one way of modeling fine and coarse particulate matter together. This method is expected to generate better results as compared to generating PM_{2.5}/PM₁₀ ratio surfaces by dividing the predictions of the PM_{2.5} models by the predictions of the PM₁₀ models, as it accounts for the correlations between the two pollutants. Prediction surfaces were generated for all 3 ratio models and those were compared to the surfaces generated by dividing the PM_{2.5} surfaces by the PM₁₀ surfaces. Correlations as well as percent differences between these surfaces were calculated to assess any disagreement.

2.4.2.4 LUR surfaces

LUR prediction surfaces were generated for both the annual and seasonal models for each pollutant using the ArcGIS 10.5.1 (ESRI, 2017). The GBA was divided into a grid of 100x100m cells. All relevant predictions were calculated for each cell. Correlations

between the different pollutant generated surfaces were then quantified and checked against the sampling-based inter-pollutant correlations. Note that the production of all prediction surfaces assumed mean values for the windspeed, relative humidity, and AOD for each site across the monitoring campaign. The generated surfaces were then used to assess exposures at vulnerable locations (i.e. schools and hospitals) to the modeled $PM_{2.5}$, PM_{10} and CO ambient levels.

CHAPTER 3

RESULTS

The measured ambient concentrations of PM_{2.5}, PM₁₀ and CO ranged from 8 µg/m³ (Site 12) to 192 µg/m³ (Site 32) for PM_{2.5}, 9 µg/m³ (Site 12) to 313 µg/m³ for PM₁₀ (Site 32), and 0.91 ppm (Site 59) to 12.4 ppm (Site 24) for CO (Table 5).

Table 5. Variability of PM_{2.5}, PM₁₀ and CO levels across the sampling domain

Pollutant	Number of readings	Min	Max	Mean	median	Sd	IQR
PM _{2.5} (µg/m ³)	525	8 µg/m ³	192 µg/m ³	68.1 µg/m ³	62 µg/m ³	35.9 µg/m ³	49 µg/m ³
Annual averaged PM _{2.5} (µg/m ³)	58	28.5 µg/m ³	104.7 µg/m ³	66.8 µg/m ³	67.4 µg/m ³	15.7 µg/m ³	19.3 µg/m ³
PM ₁₀ (µg/m ³)	520	9 µg/m ³	313 µg/m ³	83.5 µg/m ³	76.5 µg/m ³	42.9 µg/m ³	57.2 µg/m ³
Annual averaged PM ₁₀ (µg/m ³)	58	35.5 µg/m ³	129.8 µg/m ³	82.1 µg/m ³	81 µg/m ³	19.5 µg/m ³	23.1 µg/m ³
PM _{2.5} / PM ₁₀ (%)	520	32.4 %	99 %	80.9 %	81.7 %	9.67 %	10.06 %
Annual averaged PM _{2.5} / PM ₁₀ (%)	58	55.7 %	87.7 %	81.3 %	81.9 %	4.89 %	3.82 %
CO (ppm)	466	0.91 ppm	12.4 ppm	2.48 ppm	2.06 ppm	1.42 ppm	1.24 ppm
Annual averaged CO (ppm)	58	1.08 ppm	5.61 ppm	2.45 ppm	2.06 ppm	1.12 ppm	1.2 ppm

With respect to PM_{2.5}, the measured concentrations were found to show a large variability both in space and time, with a standard deviation of 35.9 µg/m³. This is expected given the long span of the monitoring campaign (1 year) and the adopted monitoring program. When the readings were averaged annually by site, the standard deviation between sites dropped to 15.7 µg/m³. It should be noted that the within site variability (standard deviation=32.15 µg/m³) was larger than the between site variability. This indicates that the temporal variability of PM_{2.5} was more pronounced than its spatial variability. As expected, the collected data across all sites and over the entire sampling

campaign was found to follow a lognormal distribution, whereas the site averaged annual data followed a normal distribution (Figure 4). With regards to the measured ambient PM_{2.5} levels, 82% of the samples were found to exceed the 24-hour standard set by EPA, whereas the 1-year standard was exceeded 99.5% of the time. Annual site averaged data were found to exceed the 24-hour EPA standards at 57 of the 58 sites, and the 1-year standard was exceeded across all sites.

The 3 sites that had the largest annually averaged PM_{2.5} levels were sites 41 (104.67 $\mu\text{g}/\text{m}^3$), 34 (99.92 $\mu\text{g}/\text{m}^3$) and 42 (95.67 $\mu\text{g}/\text{m}^3$). Site 41 is located on the Beirut-Damascus highway, which is one of the busiest highways in Lebanon; it connects the capital Beirut to the Bekaa Governorate and Syria. The highway serves as the main route for thousands of trucks and busses every day. During the monitoring campaign, Site 41 was found to have one of the highest numbers of heavy trucks and busses recorded in half an hour (on average 50 heavy trucks, 26 busses and 1553 total vehicles in 30 minutes). Site 34 is located on a very busy main road in the Mkalles region of Beirut, next to a major intersection surrounded by high rise buildings. This region is densely populated and was found to have an average of 2,046 vehicles per half hour (4th highest following the 3 sites located on the main Beirut-Jounieh highway). Site 42 is located next to the Kfarchima industrial and military areas. The site is along a major road that is used by heavy trucks and busses as well as diesel operated military vehicles. On the other hand, the 3 sites with the lowest annual averages were sites 55 (43.5 $\mu\text{g}/\text{m}^3$), 20 (45 $\mu\text{g}/\text{m}^3$) and 52 (45.5 $\mu\text{g}/\text{m}^3$). Sites 55 and 52 are located in the southern, less densely populated part of the GBA, with an average observed traffic of 15 and 188 vehicles per half hour respectively. Site 20 however, is

located on a local road in Beirut that is surrounded by several major roads (with an average traffic of 891 vehicles per 30 minutes). The low annually averaged concentration at that site might be due to it being located close to the coast and surrounded by open areas that promote dispersion.

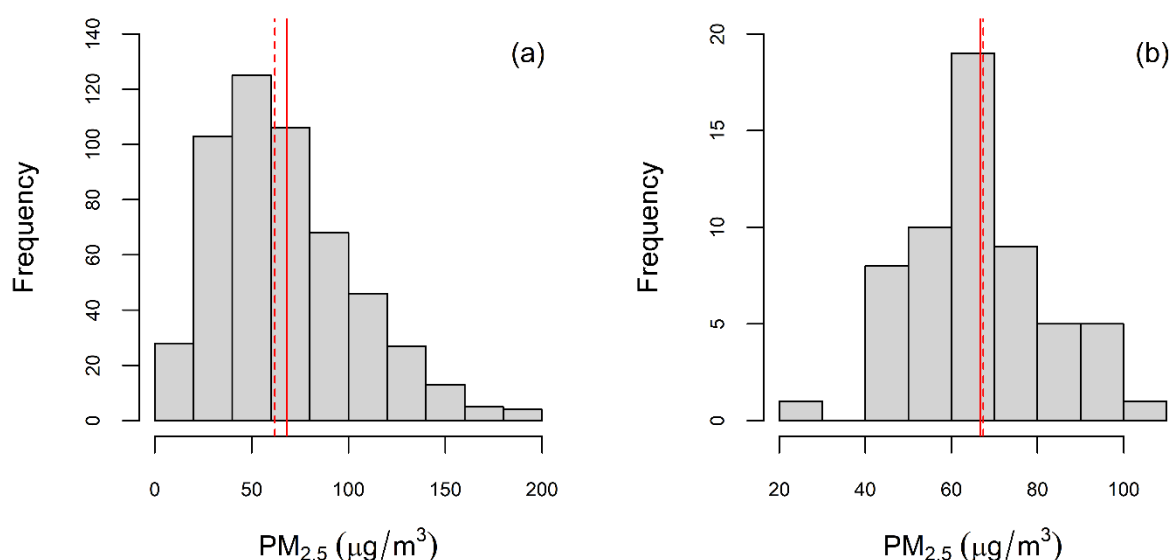


Figure 4. PM_{2.5} histograms showing the distribution of (a) the measured PM_{2.5} concentrations across all sites and over the entire sampling campaign, and (b) the annually averaged PM_{2.5} concentrations by site. The solid vertical lines represent the mean concentrations, while the dashed lines represent the medians

The measured PM₁₀ concentrations showed a large variability with a standard deviation of 42.9 µg/m³. When the readings were averaged over the entire year for each site, the standard deviation dropped to 19.5 µg/m³. Similar to PM_{2.5} the within site variability (standard deviation=38.02 µg/m³) was found to be larger than the variation observed between sites. This indicates that the temporal variability of PM₁₀ is more

pronounced than the observed spatial variation. The measured PM_{10} concentrations were found to follow a lognormal distribution, whereas the annually averaged concentrations followed a normal distribution (Figure 5). The PM_{10} Lebanese standard was exceeded more than 45 % of the time, whereas the USEPA standard was exceeded less than 10 % of the time. Site averaged PM_{10} concentrations were found to exceed the national standards at 25 of the 58 monitoring locations, however all sites were within the USEPA standard. The 3 sites that had the worst annual averages of PM_{10} concentrations were the same as those that had the highest $PM_{2.5}$ annual averages. The annually averaged concentrations were found to be $129.8 \mu\text{g}/\text{m}^3$ at Site 42, $121 \mu\text{g}/\text{m}^3$ at Site 41, and $119.2 \mu\text{g}/\text{m}^3$ at Site 34. Similarly, the sites with the lowest PM_{10} were found to be collocated with those with the lowest annually averaged $PM_{2.5}$ levels. Annually averaged fraction of fine particulate matter ($PM_{2.5}$) to coarse particulate matter (PM_{10}) was found to vary between 55.7 % and 87.7 % between the 60 sites, with an overall average of 80.1% (Figure 6); this indicates that the majority of the particulate matter across the study area is fine by mass.

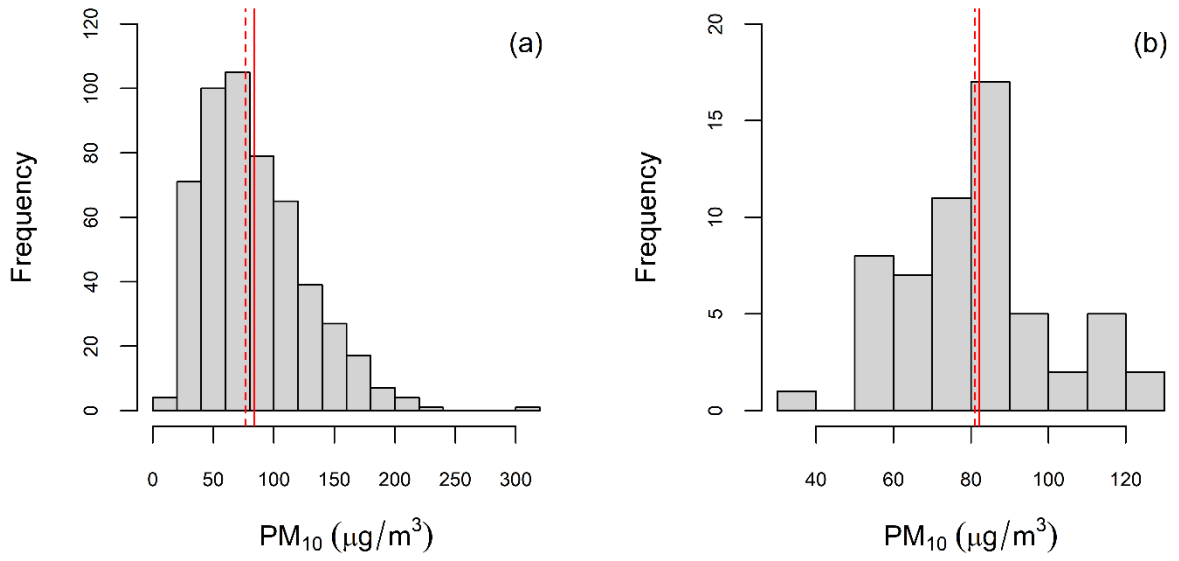


Figure 5. PM₁₀ histograms showing the distribution of (a) the measured PM₁₀ concentrations across all sites and over the entire sampling campaign, and (b) the annually averaged PM₁₀ concentrations by site. The solid vertical lines represent the mean concentrations, while the dashed lines represent the medians

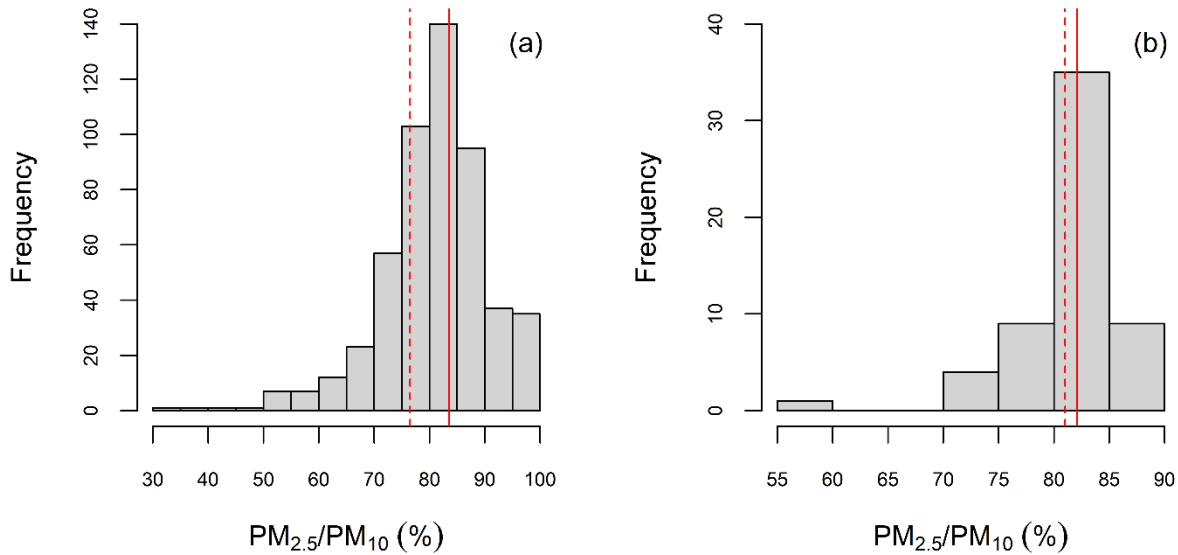


Figure 6. PM_{2.5}/PM₁₀ ratio histograms showing the distribution of (a) the actual PM_{2.5}/PM₁₀ ratios across all sites and over the entire sampling campaign, and (b) the annually averaged PM_{2.5}/PM₁₀ ratio by site. The solid vertical lines represent the mean ratio, while the dashed lines represent the medians

The CO concentrations measured across all sites over the entire sampling period showed a large variability, with a standard deviation of 1.42 ppm. The annually averaged CO concentrations by site showed slightly less variability with a standard deviation of 1.12 ppm. The within site variability of CO (standard deviation=0.7ppm) was found to be smaller than the variability seen between sites. This indicates that, contrary to particulate matter, CO concentrations seem to be more stable temporally and more affected by the spatial heterogeneity of the study region. Both the measured as well as the site averaged annual CO data were found to be lognormally distributed (Figure 7). The annual averaged CO concentration across all sites was found to be 2.5 ppm, which didn't exceed the 1 hour or the 8 hour NAAQS and EPA standards (35 ppm and 9 ppm respectively). The 8 hour

standard was only exceeded 3 times out of the 466 readings, whereas the 1 hour standard was never exceeded. Moreover, none of the annually averaged CO concentrations at the sampling sites exceeded the 1 and 8 hour standards.

The highest annually averaged concentrations of CO were observed at sites 10 (5.38 ppm), 24 (5.08 ppm) and 19 (5.02 ppm). Site 10 is located in the Dora region on the Beirut-Jounieh highway, which is the busiest and most congested highway in the country. Sites 24 (Achrafieh) and 19 (Algeria Street) are both located inside the city of Beirut in busy urban canyons. On the other hand, the lowest annually averaged concentrations of CO were observed at sites 59 (1.08 ppm), 58 (1.09 ppm) and 52 (1.28 ppm). All 3 sites are located in the southern less densely populated area of the GBA, with sites 58 and 52 located in mountainous villages at an elevation of around 700 m above sea level (Aramoun and Sarhmoul respectively). Site 59 on the other hand is located on the Damour highway which has significantly less traffic than the previously mentioned highways and is surrounded by agricultural and open areas from all sides. This result is interesting given that several other sites with significantly less traffic than site 59 and located in more remote areas of the GBA had higher concentrations of CO.

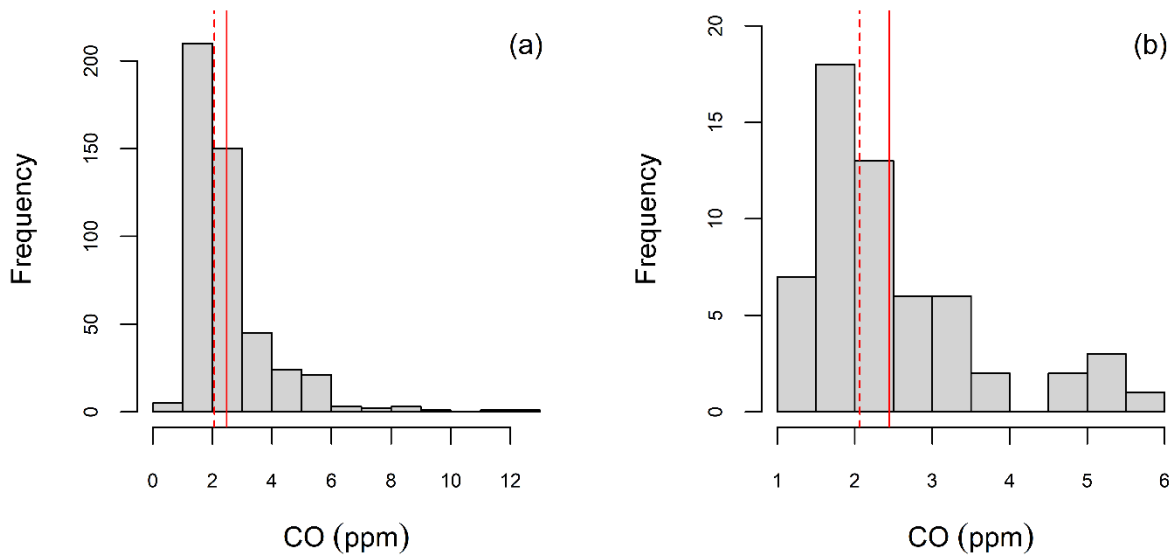


Figure 7. CO histograms showing the distribution of (a) the measured CO concentrations across all sites and over the entire sampling campaign, and (b) the annually averaged CO concentrations by site. The solid vertical lines represent the mean concentrations, while the dashed lines represent the medians

3.1 Temporal variability

In total, 230 measurements were taken during the cold season versus 295 measurements during the warm season. Table 6 summarizes the observed variability in measured pollutant concentrations across the two seasons. As can be seen in Table 6, the cold season was associated with higher concentrations for the 3 pollutants whereas its $PM_{2.5}/PM_{10}$ ratio was smaller as compared to the warm season. The cold season was also associated with slightly higher within-site variability for all three pollutants. Statistically, there was no difference between the means and standard deviations of PM_{10} (F-value = 1.22; t-value = -1.56) and $PM_{2.5}$ (F-value = 1.26; t-value = -0.88) across the two seasons (p-

values > 0.1). On the other hand, the means of both CO (t-value = -2.95; p-value = 0.005) and the $PM_{2.5}/PM_{10}$ ratio (t-value = 3.84; p-value = 0.0003) were found to be statistically different across the 2 seasons (p-values < 0.1), with higher concentrations of CO and lower ratios in the cold-wet season (Figure 8). With regards to the variability of the measured concentrations by season, only CO was found to have statistically different variance in the concentrations between the two seasons (F-value = 0.61; p-value = 0.07) (Figure 8). On the other hand, it should be noted that there were no statistically significant differences in the measured $PM_{2.5}$, PM_{10} and CO levels in samples collected before noon (from 8 am till noon) versus those collected in the afternoon (1 pm until 6 pm) on a given day (Figure 9). This ensures that no biases might have been introduced due to differences in the sampling times.

Table 6. Seasonal variability in the concentrations of PM_{2.5}, PM₁₀ and CO

<i>Pollutant</i>	<i>Season</i>	<i>Number of readings (sampled sites)</i>	<i>Mean (site averaged mean)</i>	<i>SD¹ (site averaged sd)</i>
<i>PM_{2.5}</i>	Warm	295 (58)	66.42 µg/m ³ (66.21 µg/m ³)	31.49 µg/m ³ (19.46 µg/m ³)
	Cold	230 (56)	70.31 µg/m ³ (69.64 µg/m ³)	40.77 µg/m ³ (17.46 µg/m ³)
<i>PM₁₀</i>	Warm	294 (58)	80.33 µg/m ³ (80.18 µg/m ³)	36.80 µg/m ³ (22.92 µg/m ³)
	Cold	226 (56)	87.76 µg/m ³ (86.94 µg/m ³)	49.68 µg/m ³ (22.02 µg/m ³)
<i>CO</i>	Warm	260 (58)	2.29 ppm (2.28 ppm)	1.08 ppm (0.91 ppm)
	Cold	206 (56)	2.71 ppm (2.67 ppm)	1.75 ppm (1.49 ppm)
<i>PM_{2.5}/PM₁₀</i>	Warm	294 (58)	82.5 % (82.4 %)	9.8 % (5.9 %)
	Cold	226 (56)	78.7 % (78.7 %)	9.1 % (5.7 %)

¹: SD = standard deviation

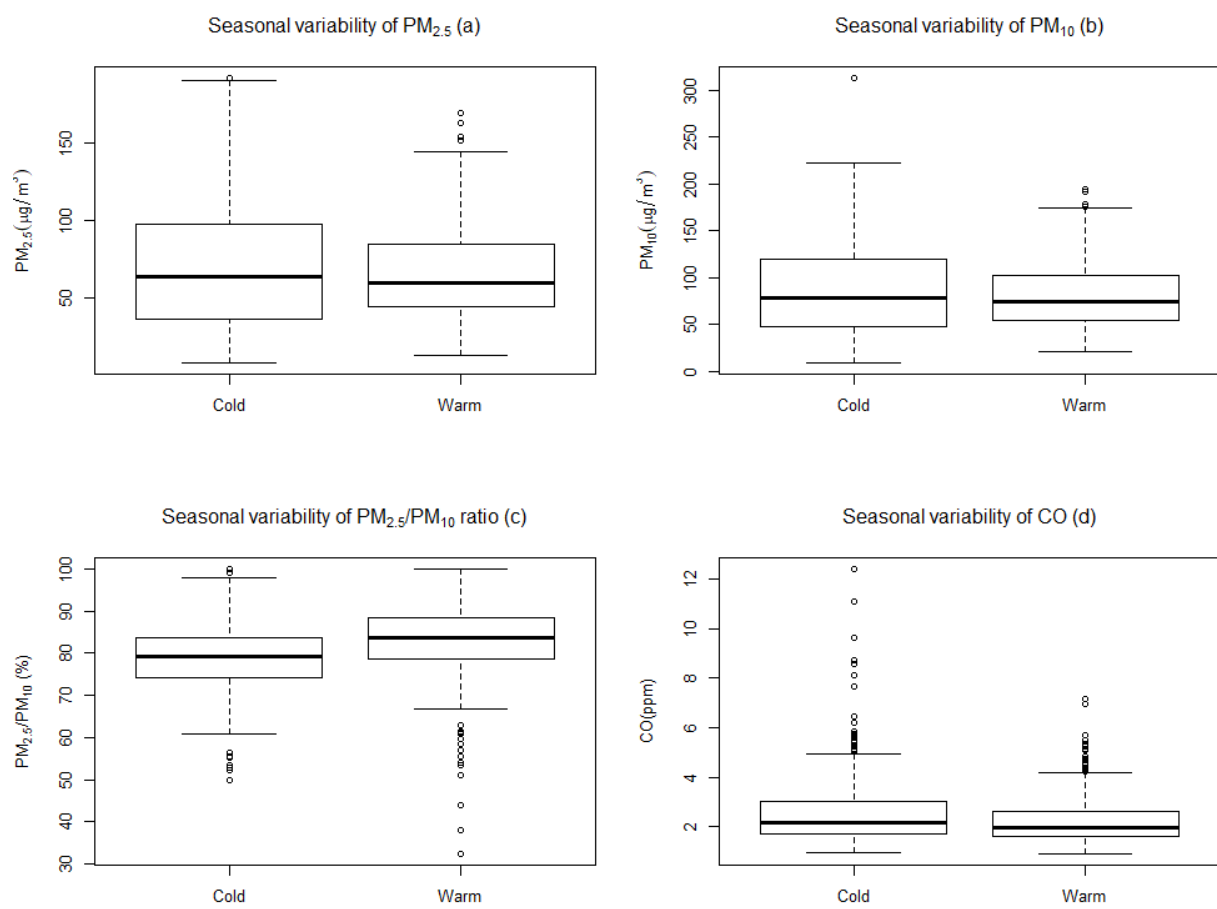


Figure 8. Seasonal variability of (a) $PM_{2.5}$, (b) PM_{10} , (c) $PM_{2.5}/PM_{10}$ ratio and (d) CO across all monitoring sites

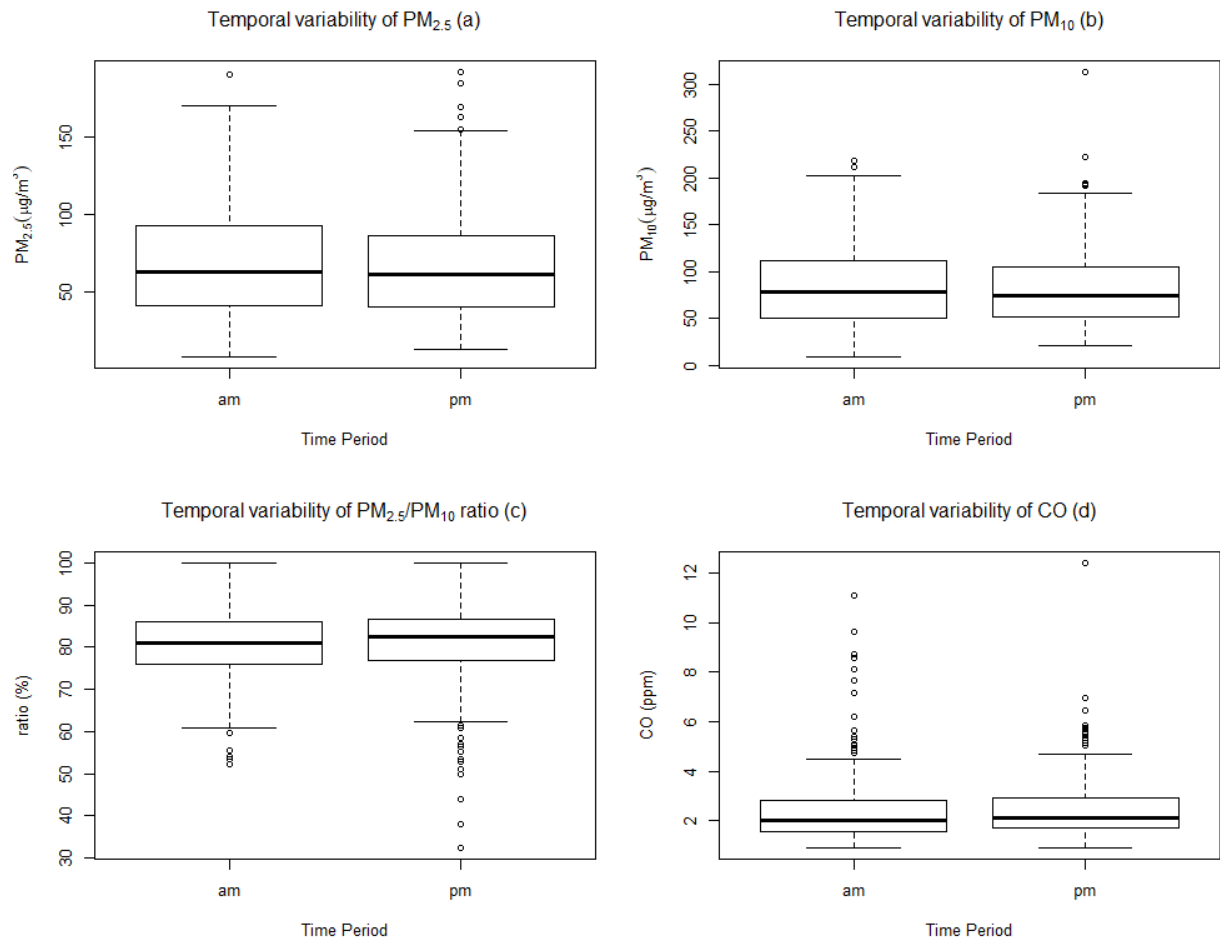


Figure 9. Concentrations of (a) $PM_{2.5}$, (b) PM_{10} , (c) $PM_{2.5}/PM_{10}$ and (d) CO as a function of time of sampling. am = before noon; pm = afternoon

3.2 Spatial variability

While pollutants concentrations showed large variabilities between the 58 sites (Figure 10, 11, 12, and 13), the variability of the pollutants across the six predefined classes of different urbanization rates and road densities was found to be low, with the exception of CO. A two-way ANOVA was conducted to test for any statistical difference between averaged pollutant concentrations across these categories, while accounting for a potential

interaction between level of urbanization and road densities. The results showed no statistical difference in $PM_{2.5}$ and PM_{10} concentrations across the 6 categories and the interaction between the two factors was also not statistically significant. However, there was a statistical difference between these groupings with regards to the measured CO concentrations. The High urban/Low road category was found to have statistically higher concentrations of CO (mean = 2.98 ppm) as compared to the remaining categories, whereas the Low urban/High road category had statistically lower concentrations than the remaining categories (mean = 1.59 ppm) (Figure 14). The High Urban/Low road category mainly comprises locations near industrial areas with a lot of heavy truck traffic, whereas the Low urban/High road category mainly comprises sites located in villages with high road densities with low traffic or nearby highways. However, having high road densities doesn't signify having high traffic density, since several sites within the high road density categories are located next to minor roads with low traffic. Similarly, sites within the low road density category can be located next to highly congested highways.

The variance in the measured pollutant concentrations across the adopted 6 groupings was also found to be statistically not significant, except for CO (Fligner-Killen test). For CO, the High urban/High road category had the largest variability (standard deviation = 1.53 ppm), whereas the Low urban/High road category had the smallest variability between its sites (0.41 ppm). The large variability in the High urban/High road category is due to some of the sites being located in busy urban canyons within Beirut, leading for CO to be trapped at the street level, whereas the remaining sites were located close to the sea where dispersion was favorable. The Low urban/High road category however, had the smallest

variability due to the similarities between its sites, and due to the sites having similar CO sources, thus leading to almost similar CO concentrations.

Overall, the lack of clear variability across the 6 adopted LULC-road density groupings indicates that using such broad-scale groupings fails to capture an accurate picture of the different sources and sinks associated with each site. This is evident by the large inter-site variability observed across the adopted 6 broad spatial clusters (Figure 10, Figure 11, Figure 12 and Figure 13), which was significantly larger than the between group variability (Table 7). This reinforces the need to develop LURs in order to better capture the spatial variabilities of air pollutant concentrations in an urban area.

Table 7. Comparison between within category and between category variability

Pollutant/Parameter	Average within category standard deviation	Between category standard deviation
PM _{2.5}	15.56 µg/m ³	4.33 µg/m ³
PM ₁₀	19.49 µg/m ³	4.27 µg/m ³
PM _{2.5} / PM ₁₀	4.46 %	1.2 %
CO	0.99 ppm	0.50 ppm

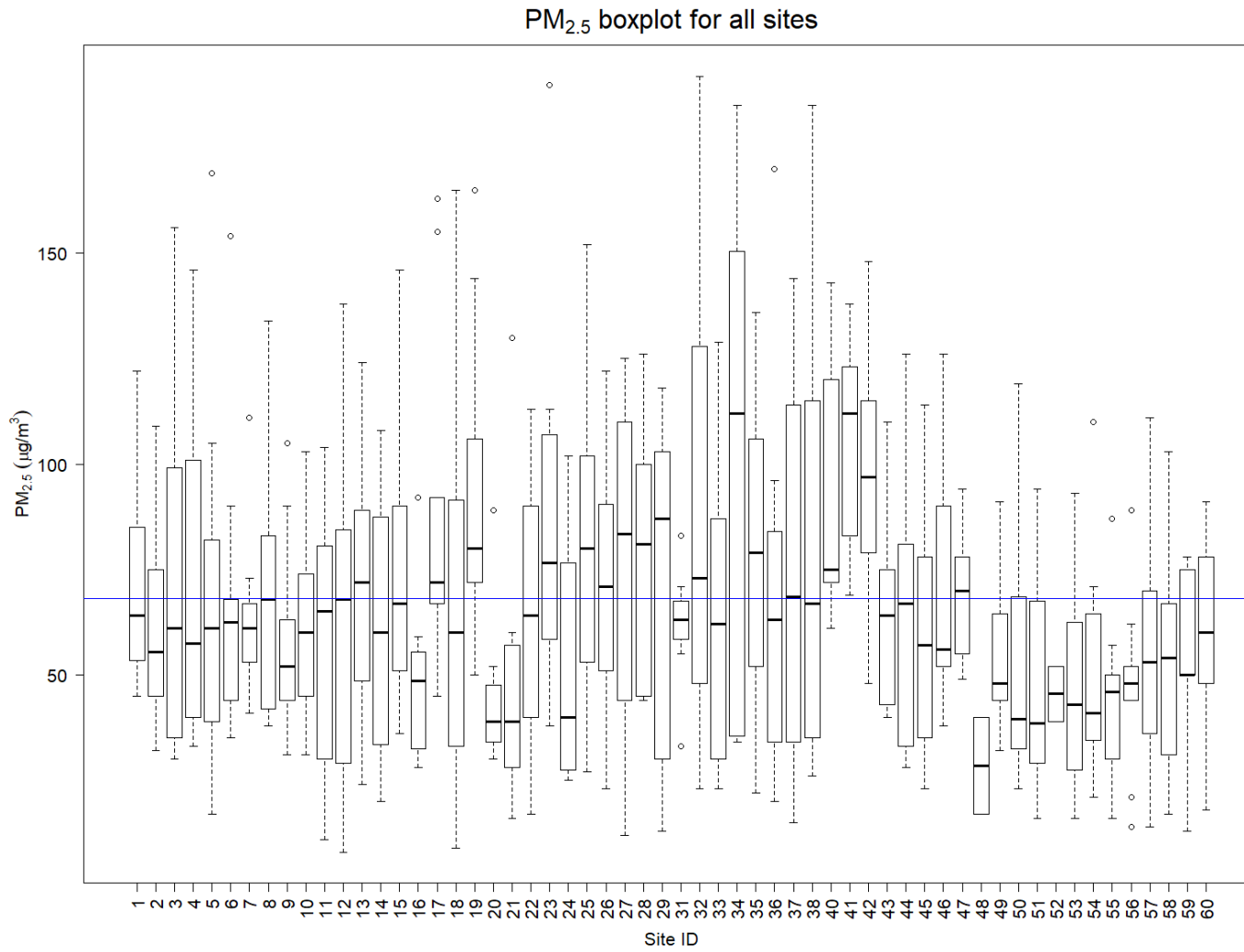


Figure 10. Variability of PM_{2.5} concentrations across sites. The blue horizontal line represents the overall mean concentration of PM_{2.5} across all sites

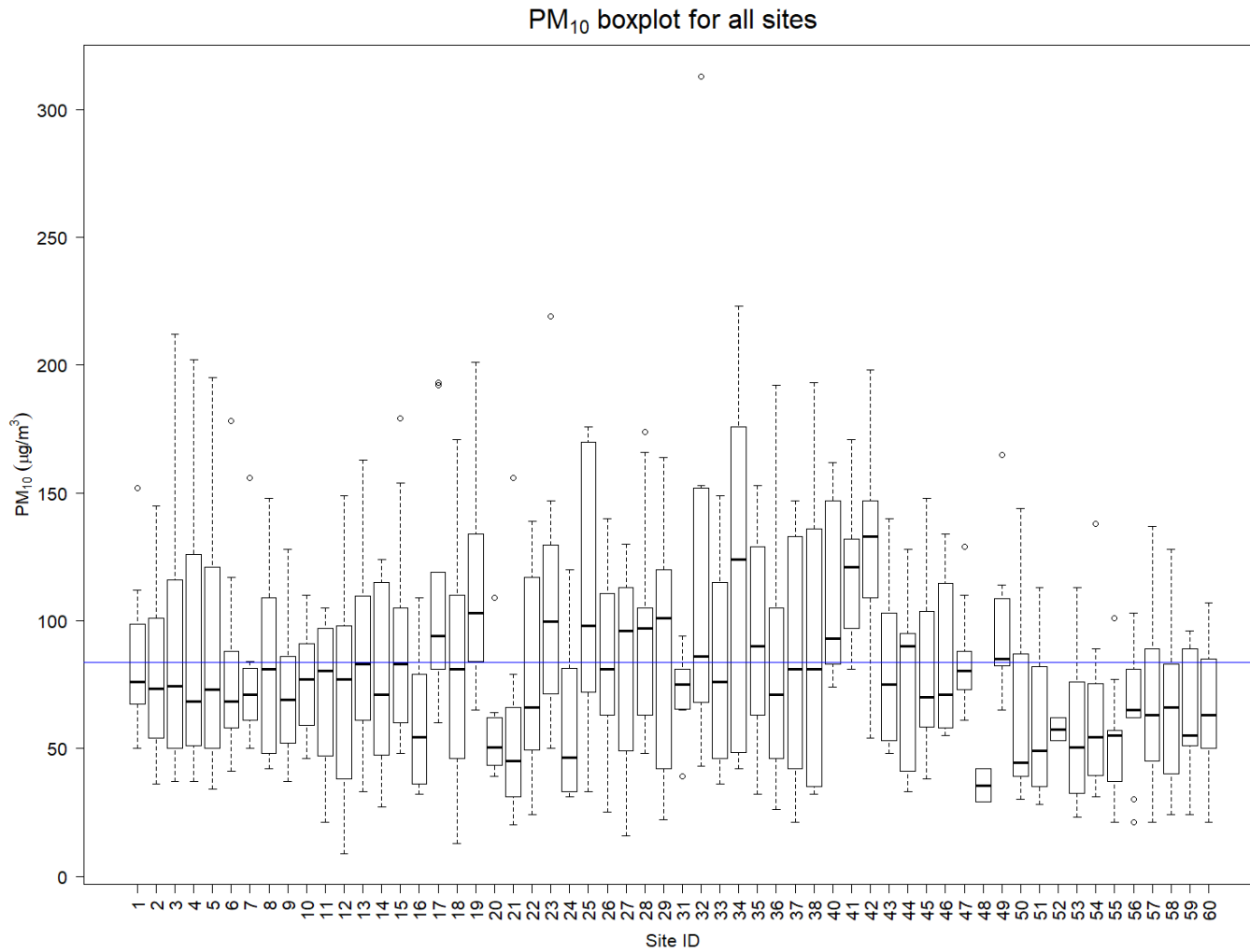


Figure 11. Variability of PM₁₀ concentrations across sites. The blue horizontal line represents the overall mean concentration of PM₁₀ across all sites

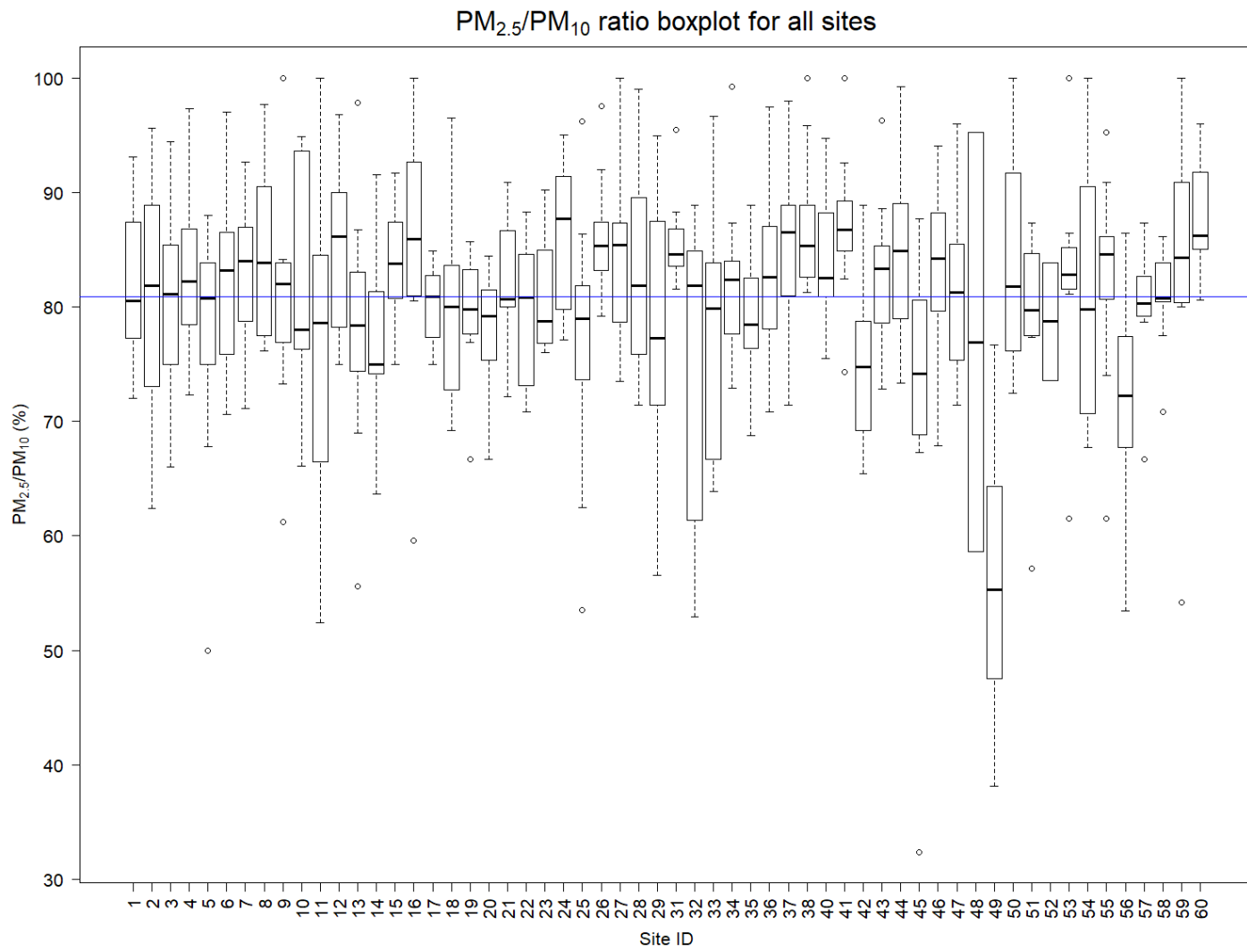


Figure 12. Variability of PM_{2.5}/PM₁₀ ratio across all sites. The blue horizontal line represents the overall mean PM_{2.5}/PM₁₀ ratio across all sites

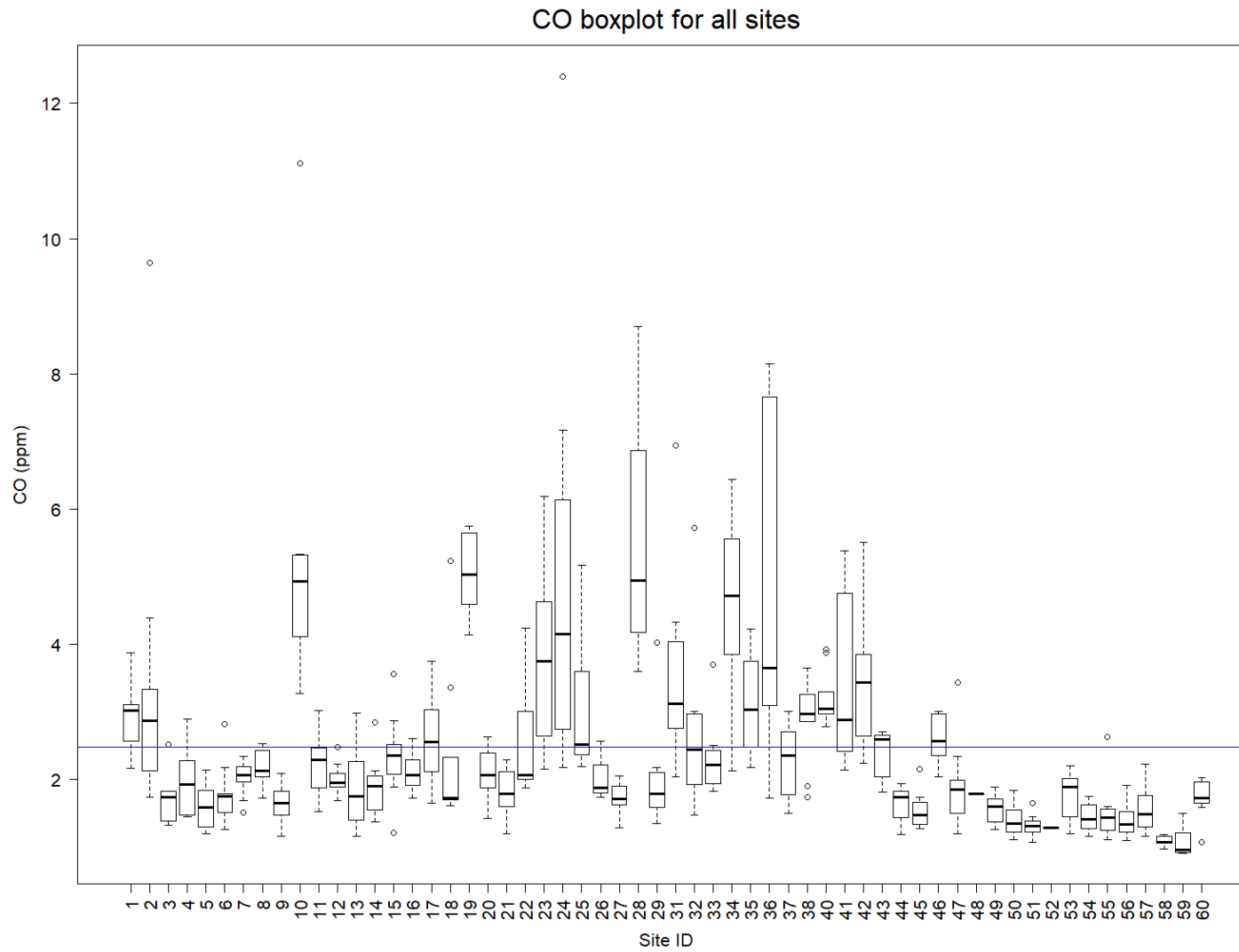


Figure 13. Variability of CO concentrations across all sites. The blue horizontal line represents the overall mean CO across all sites.

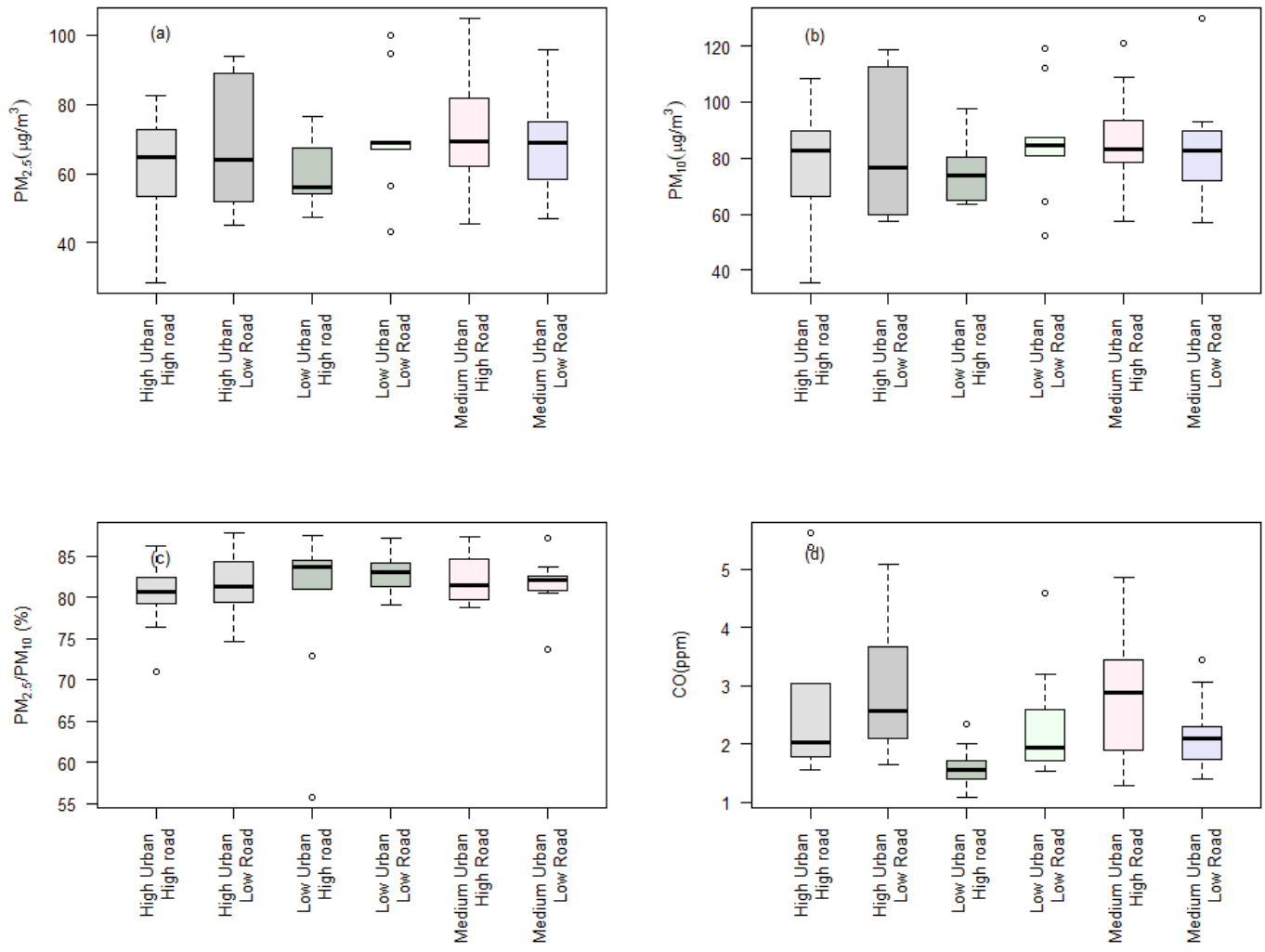


Figure 14. Boxplots showing the variability of (a) $PM_{2.5}$, (b) PM_{10} , (c) $PM_{2.5}/PM_{10}$ ratio and (d) CO annual averages across different road and landuse densities

The cluster analysis, using the K-means partitioning method, was conducted on the 3 measured pollutant concentrations concurrently at each of the 60 sites. The adequate number of clusters was found to be 3 after plotting the within groups sum of squares versus the number of clusters extracted. Clustering based on the 3 pollutants simultaneously generated sort of an air pollution index, whereby sites were segregated into 3 air pollution categories: high, medium and low pollution (Table 8). The results of the cluster analysis showed different grouping of stations as compared to the initially defined landuse and road density categories. This further reinforces that the original predefined categories weren't adequate to explain the air pollution levels observed in the study area. Highly polluted sites were mainly clustered near the Beirut-Damascus highway, near industrial areas and within urban canyons within the limits of Beirut proper. Sites categorized with medium air pollution levels were mainly clustered in the Northern part of the GBA, whereas the sites with low air pollution were clustered in the Southern less populated sections of the GBA as expected (Figure 15). In addition, the Moran's I was calculated for the three pollutants to assess for any spatial clustering or dispersion of pollution levels as a function of Euclidean distance. As shown in Table 9, significant spatial autocorrelation between the sites was only observed for CO, where weak clustering was found. These findings are also reflected in the site averaged pollutant concentration mapping shown in Figure 16.

Table 8. Cluster analysis categories and the thresholds identified for each group

Category	PM _{2.5} average	PM ₁₀ average	CO average
1 (High pollution levels)	93.3 µg/m ³	116.3 µg/m ³	3.54 ppm
2 (Medium pollution levels)	68.7 µg/m ³	84.0 µg/m ³	2.49 ppm
3 (Low pollution levels)	49.2 µg/m ³	60.3 µg/m ³	1.80 ppm

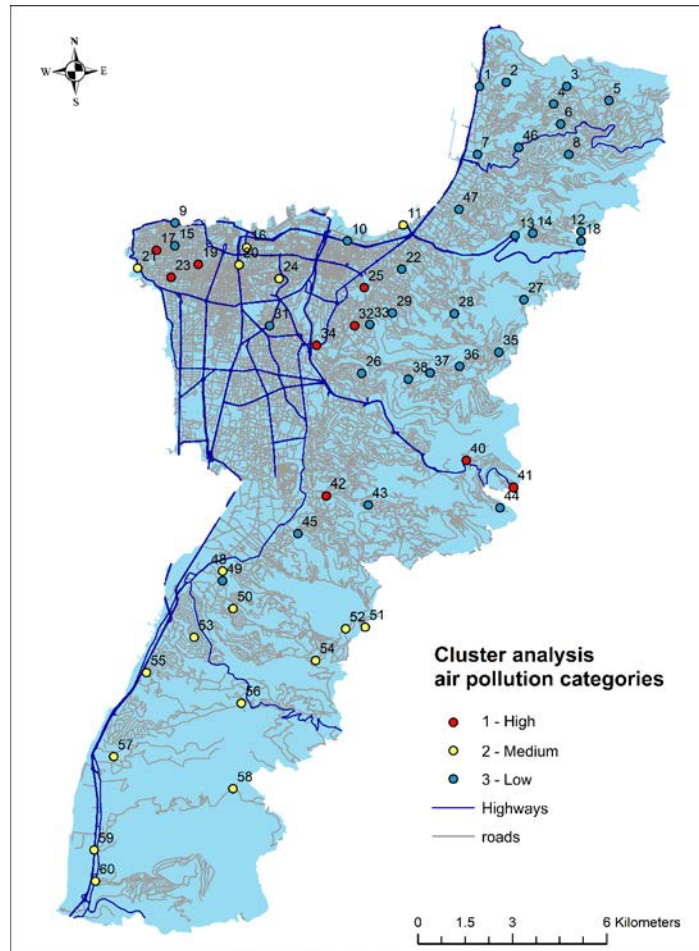


Figure 15. Air pollution cluster categories

Table 9. Spatial auto-correlation of the pollutants as determined through Moran's I values

Pollutant	Moran's I	p-value
PM _{2.5}	0.11	0.129 (>0.05)
PM ₁₀	0.015	0.7 (>0.05)
PM _{2.5} / PM ₁₀	-0.03	0.82 (>0.05)
CO	0.15	0.05

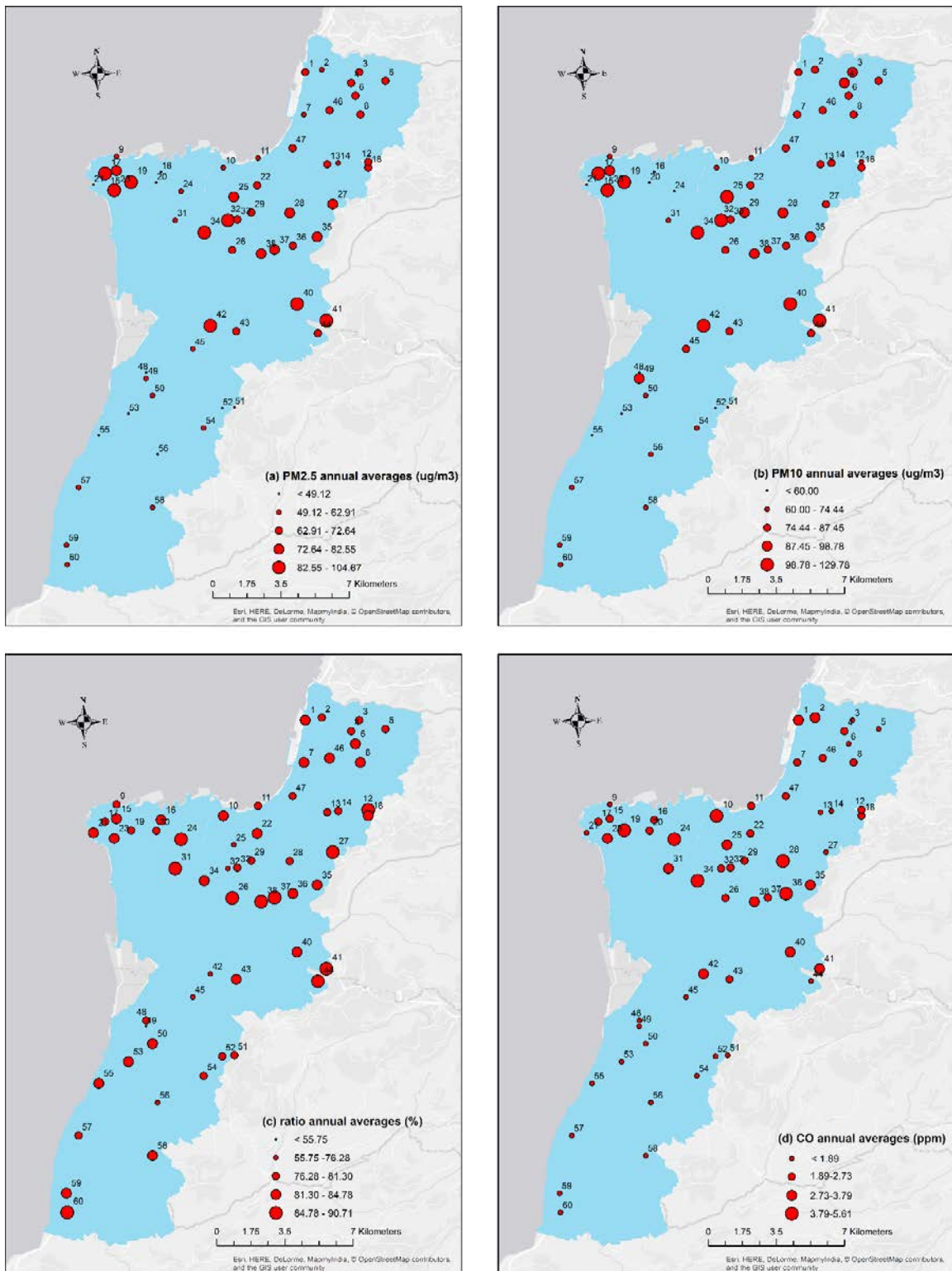


Figure 16. Spatial distribution of (a)PM_{2.5}, (b) PM₁₀, (c)PM_{2.5}/PM₁₀ and (d) CO concentrations. All values are site averaged concentrations

3.3 Landuse regression models

3.3.1 *PM_{2.5} models*

The landuse regression model developed for predicting annual $PM_{2.5}$ levels within the study area was able to explain 66.8% of the observed variability. The significant predictors included building area within a 3000 m buffer, wind speed, wind speed squared, elevation, relative humidity and inverse distance to the Zouk power plant (Table 10). The building area within a 3000 m buffer had a positive effect on the predicted concentrations of $PM_{2.5}$, whereby a 1 Km^2 increase in building area resulted in a 1.75 percent increase in $PM_{2.5}$ concentrations on average. Wind speed was found to have a quadratic relationship with the measured $PM_{2.5}$ concentrations; concentrations tended to drop with increased annually averaged site-specific wind speeds up to a threshold of (30 m/s), all averaged windspeeds across sites had windspeeds below that threshold. This is probably due to the dual role that wind speed has with respect to the concentration of particulate matter, whereby at low wind speeds pollution dispersion is favored, whereas at higher wind speeds particle resuspension dominates (Nicholson, 1993). In the case of the GBA, the role of wind speed as a promoter of dispersion was more dominant as compared to promoting resuspension since most wind speed values at the 58 sites were below the model defined threshold. In addition, increases in the relative humidity levels, elevation, and the inverse of the distance to the Zouk power plant were all found to increase the $PM_{2.5}$ concentrations. A 10-fold cross-validation was conducted to check the internal stability and robustness of the model; the results showed a minor drop in the cross-validated R^2 (0.55). Moreover, the model didn't show any significant biases with a PBIAS value of 0 (Figure 17); yet the model residuals showed minor spatial clustering with a Moran's I value of 0.22 and a p-value < 0.05.

The warm season PM_{2.5} model performed as well as the annual model and explained around 66% of the variability in the observed PM_{2.5} concentrations. On the other hand, the cold season model was only able to explain 59% of the observed variability. Percentage of open areas within a 2000 m buffer, distance to Zouk, relative humidity, water area within a 750 m buffer, industrial area within a 100 m buffer and wind speed were all significant predictors for the warm season, whereas AOD, distance to airport, water area within a 750 m buffer, industrial area within a 1500 m area, distance to major roads and agricultural area within a 500 m buffer were significant predictors for the cold season. As shown in Table 10, the annual model had 3 predictors in common with the warm season model (relative humidity, wind speed and distance to Zouk), whereas it didn't share any predictor with the cold season model. The seasonal models only had 1 predictor in common (water area within a 750 m buffer). The cross-validation R² for both models were acceptable but lower than that achieved for the annual-based model, the values were 0.47 and 0.44 for the warm and cold season respectively. Both seasonal models didn't show any significant bias (PBIAS = 0). Moreover, the residuals of the warm season model did show slightly more pronounced spatial clustering as compared to the annual model, with a Moran's I value of 0.36 and a p-value <0.05, whereas the cold season model didn't show any spatial autocorrelation (p-value = 0.11).

PM_{2.5} prediction surfaces (100 m × 100 m) were generated for the GBA for each of the 3 PM_{2.5} models (annual and seasonal) (Figure 18). Note that the production of the prediction surfaces assumed mean values for wind speed, relative humidity and AOD as observed during the monitoring campaign. The generated PM_{2.5} prediction results showed

that the annual model resulted in the smoothest pollution surface; it also predicted the lowest GBA averaged concentration among the 3 models (mean for the GBA = 52.27 $\mu\text{g}/\text{m}^3$). It also shows the smallest spatial variability in the predicted concentrations among the 3 models, with a standard deviation of 5.14 $\mu\text{g}/\text{m}^3$. Warm and cold season model predictions on the other hand showed larger spatial variabilities (standard deviation of 14.3 $\mu\text{g}/\text{m}^3$ and 10.7 $\mu\text{g}/\text{m}^3$ respectively). The highest GBA-wide spatially-averaged predicted $\text{PM}_{2.5}$ concentration was predicted by the cold season model, where the predicted mean value was 67.9 $\mu\text{g}/\text{m}^3$. The predictions from the annual and warm season models were highly correlated, with a Pearson's r of 0.73; however, they were weakly correlated with the cold season model predictions, with a Pearson's r of -0.02 and -0.35 respectively.

Interestingly, the effects of traffic-related sources were not apparent in both the annual and summer models due to the lack of any of the traffic predictors in both models. However, in the case of the annual model, the length of roads within a 2000 m buffer was found to be highly correlated with the building area within a 3000 m buffer and as such its inclusion in the model instead of the building area would have resulted in a slight drop in the model's R^2 . On the other hand, the winter model had a strong traffic related predictor, which was the distance to major roads. As a matter of fact, for every increase of 1 km in the distance between a site and the closest major road, the winter $\text{PM}_{2.5}$ concentrations were expected to drop by 15% on average. This is probably due to increased congestion during the morning and afternoon rush hours in the winter season as compared to the summer season and to increased vehicular emissions due to lower ambient temperatures. In the winter, the model identified pollution hotspots in the vicinity of major roads and in the

southern parts of the GBA, which are adjacent to the airport. Note that the airport in the winter season was a significant source of $PM_{2.5}$. In the annual model, major hotspots were observed in the center of Beirut, which is the most densely populated region of the GBA, and in the Northern parts of the GBA which are affected by the emissions of the Zouk power plant. In addition, predicted concentrations tended to increase with elevation, which is positively correlated with distance to the sea. This is explained by the fact that areas close to the sea tend to have better dispersion potential in addition to the dominant westerly winds that carry the pollutants from their initial sources (i.e. the densely populated coastal areas) to the less densely populated mountainous regions of the GBA, where pollutants get trapped due to the valley effect created by the mountains. This effect is apparent in both the annual and winter models surfaces. The effect of the Zouk power plant was very prominent in the summer model, as we can see an apparent decrease in predicted concentrations as we move away from the Zouk power plant.

All predictors in the three models behaved as expected with respect to the modulating the $PM_{2.5}$ concentrations, except for the coverage of industrial areas within a 1500 m buffer in the winter model, which had a negative coefficient. This might be explained by the fact that all the industrial areas in the GBA, excluding the ones surrounding the port and airport, are small and are surrounded by forested regions, which tends to decrease the measured $PM_{2.5}$ concentrations. Moreover, removing this predictor from the model resulted in a significant decrease in the performance of the model, therefore it was kept.

Table 10. LUR models for predicting annual and seasonal log-transformed PM_{2.5} concentrations

Model	Model equation (^a Variable key given below)	R ²	Adj R ²	CV R ²	RMSE
Annual PM _{2.5}	$4.954 + 0.0175 \times \text{BUILD.3000} - 0.18 \times \text{WS} + 0.004 \times \text{WS}^2 + 0.0004 \times \text{ELEV} + 0.009 \times \text{RH} + 0.672 \times \text{INVZ}$	0.67	0.63	0.55	0.149
Warm season PM _{2.5}	$3.982 + 0.12 \times \text{OPEN.2000} - 0.027 \times \text{DISTZ} + 0.018 \times \text{RH} - 0.42 \times \text{WAT.750} + 13.3 \times \text{IND.100} - 0.027 \times \text{WS}$	0.66	0.62	0.47	0.194
Cold season PM _{2.5}	$3.877 + 3.36 \times \text{AOD} - 0.025 \times \text{DISTA} - 0.3 \times \text{WAT.750} - 0.24 \times \text{IND.1500} - 0.16 \times \text{DISTMJR} + 0.47 \times \text{AGRI.500}$	0.59	0.54	0.44	0.179

^aLeft-hand side of period denotes variable type and right-hand side denotes buffer size so that **BUILD.3000** = building area within 3000 m buffer (in Km²). Variable types are: **WS** = wind speed (m/s); **WS2** = wind speed squared; **ELEV** = elevation (m); **RH** = relative humidity (%); **INVZ** = inverse distance to Zouk power plant (1/km); **OPEN** = open area (Km²); **DISTZ** = distance to Zouk power plant (Km); **WAT** = water area (Km²); **IND** = industrial area (Km²); **AOD** = aerosol optical depth; **DISTA** = distance to airport (Km); **DISTMJR** = distance to major road (Km); **AGRI** = agricultural area (Km²)

^bCross-validated R²

^cRoot Mean Square Error

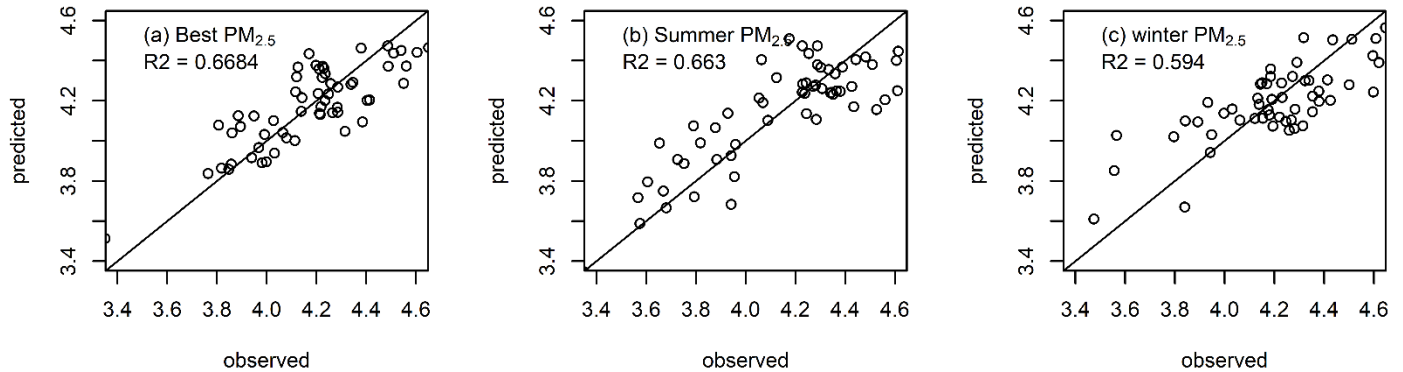


Figure 17. Predicted vs observed plots (a) Annual log-transformed PM_{2.5} LUR Model (b) Warm season log-transformed PM_{2.5} LUR model (c) Cold season log-transformed PM_{2.5} LUR model. Diagonal line represents the 1:1 line

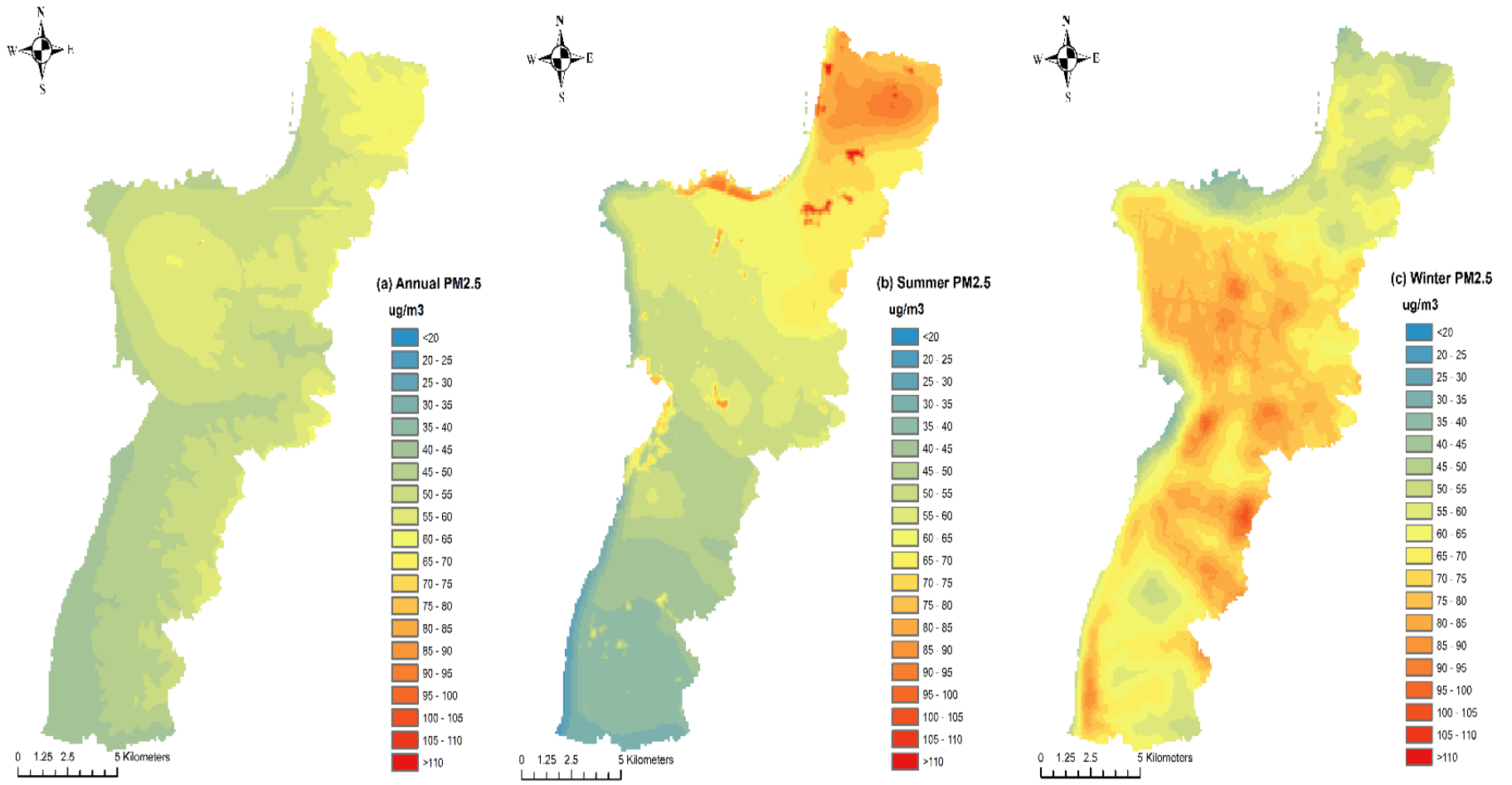


Figure 18. PM_{2.5} surfaces (a) Annual average PM_{2.5} LUR (b) Warm-season PM_{2.5} LUR (c) Cold-season PM_{2.5} LUR

3.3.2 *PM10 models*

The annual PM_{10} model performed equally well as the $PM_{2.5}$ annual model and was able to explain 63% of the PM_{10} variability in the GBA. Significant predictors included relative humidity, industrial area within a 100 m buffer, water area within a 1500 m buffer, wind speed, wind speed squared, building area within a 3000 m buffer and the medium urban area within a 3000 m buffer. Similarly to the $PM_{2.5}$ model, wind speed had a quadratic effect on the concentrations of PM_{10} . In addition, increases in relative humidity, industrial area within a 100 m buffer, building area within a 3000 m buffer, and medium urban area within a 3000 m buffer all resulted in increased predictions of the PM_{10} concentrations. Only the water area within a 750 m buffer of a site acted as a PM_{10} sink. The only present waterbody in or near the GBA is the Mediterranean Sea, which enhances the dispersion of air pollutants, leading to lower concentrations along the coastline. The cross validation R^2 was 0.51; the model also didn't show any significant biases with a PBIAS value of 0 (Figure 19). In addition, the model didn't show any spatial autocorrelation in the residuals with a Moran's I value of 0.07 and a p-value of 0.29.

The performance of PM_{10} seasonal models was lower than the PM_{10} annual model, with the warm season model explaining 57% of the observed seasonal PM_{10} variability and the cold season model explaining only 49% of the variability in PM_{10} . Relative humidity, water area within a 1500 m buffer, wind speed, industrial area within a 100 m buffer, building area within a 3000 m buffer, and medium urban area within a 3000 m buffer were all significant predictors in the warm season model. On the other hand, AOD, distance to airport, medium urban area within a 1000 m buffer, open area within a 1000 m buffer and

water area within a 750 m buffer were significant predictors for the cold season model. The structure of the warm season model was very similar to that of the annual model, as it had 5 predictors in common, namely, water area, wind speed, industrial area, building area and medium urban area. On the other hand, the cold season model only had 2 predictors in common with the annual model (water area and medium urban area) but with different buffer sizes. The cold season model had a cross validation R^2 of 0.31, whereas the warm season model fared better with a cross validation R^2 of 0.48. Both models didn't show any significant bias (PBIAS=0). In addition, the residuals of the warm season model showed some clustering, with a Moran's I value of 0.30 and a p-value <0.05, whereas the cold season model didn't show any spatial autocorrelation (p-value = 0.91). The structural form of all 3 PM₁₀ models are summarized in Table 11.

PM₁₀ prediction surfaces (100 m × 100 m) were generated for the GBA for each of the 3 PM₁₀ models (annual and seasonal) (Figure 20). Similarly to the PM_{2.5} surfaces, the production of the PM₁₀ prediction surfaces assumed mean values for wind speed, relative humidity and AOD as observed during the monitoring campaign. The annual PM₁₀ model generated the smoothest surface; yet it predicted the lowest study-area averaged concentrations among the 3 models (mean = 67.9 $\mu\text{g}/\text{m}^3$). It also had a significantly lower spatial variability (standard deviation of 5.93 $\mu\text{g}/\text{m}$) as compared to the seasonal surfaces with standard deviation of 12.3 $\mu\text{g}/\text{m}^3$ and 12.1 $\mu\text{g}/\text{m}^3$ for the warm and cold season models respectively. The largest GBA-wide predicted concentration was predicted by the cold season model, with a study-area averaged concentration of 87.9 $\mu\text{g}/\text{m}^3$.

The direct effect of traffic was not apparent for the 3 PM₁₀ models, yet it was represented in the 3 models through the building area and the coverage of medium urban areas, which witness high traffic densities. PM₁₀ concentrations were found to be directly affected by industrial point sources, as is clearly represented by hotspots next to industrial areas in the annual and warm season models. The Northern part of the GBA was found to have high PM₁₀ concentrations in the annual and warm season models. whereas hotspots were observed in the southern, less populated, region of the GBA in the vicinity of the airport for the cold season model. The annual and warm season model surfaces were highly correlated with a Pearson's r of 0.86, whereas the cold season model was poorly correlated with the other PM₁₀ models with Pearson's r values of -0.11 and 0.01 for the annual and warm season models respectively.

Table 11. LUR models for predicting annual and seasonal log-transformed PM₁₀ concentrations

Model	Model equation (^a Variable key given below)	R ²	Adj R ²	^b CV R ²	^c RMSE
Annual PM ₁₀	4.801 + 0.016×RH + 7.72×IND.100 – 0.051×WAT.1500 – 0.16×WS + 0.003×WS2 + 0.009×BUILD.3000 + 0.02×MED.3000	0.63	0.58	0.51	0.158
Warm season PM ₁₀	3.688 + 0.024×RH – 0.084×WAT.1500 – 0.048×WS + 17.6×IND.100 + 0.024×BUILD.3000 + 0.021×MED.3000	0.57	0.52	0.48	0.211
Cold season PM ₁₀	4.02 + 3.11×AOD – 0.031×DISTA + 0.12×MED.1000 + 0.23×OPEN.1000 – 0.22×WAT.750	0.49	0.43	0.31	0.198
^a Left-hand side of period denotes variable type and right-hand side denotes buffer size so that BUILD.3000 = building area within 3000 m buffer (in Km ²). Variable types are: WS = wind speed (m/s); WS2 = wind speed squared; RH = relative humidity (%); OPEN = open area (Km ²); WAT = water area (Km ²); IND = industrial area (Km ²); AOD = aerosol optical depth; DISTA = distance to airport (Km); MED = Urban area of medium building density (Km ²) ^b Cross-validated R ² ^c Root Mean Square Error					

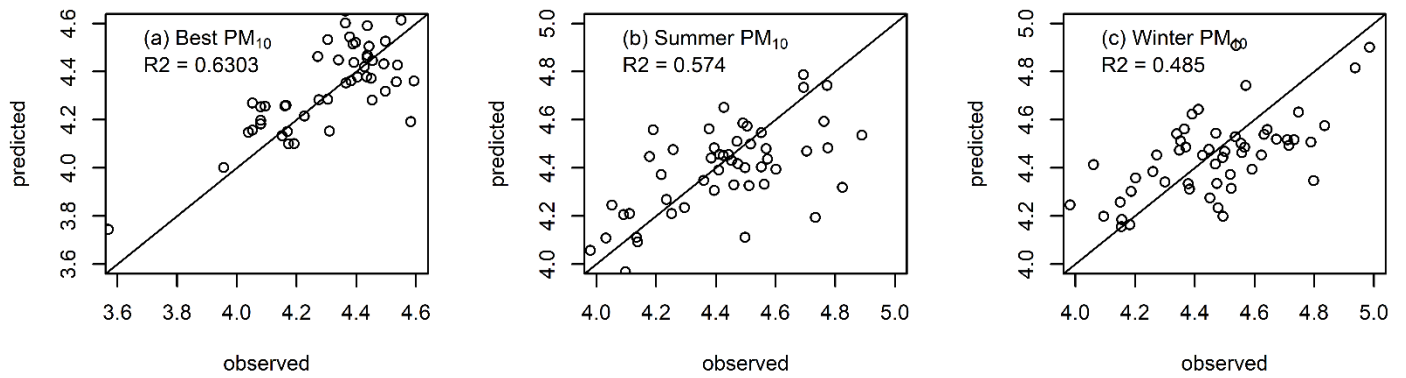


Figure 19. Predicted vs observed plots (a) Annual log-transformed PM₁₀ LUR Model (b) Warm season log-transformed PM₁₀ LUR model (c) Cold season log-transformed PM₁₀ LUR model. Diagonal line represents the 1:1 line

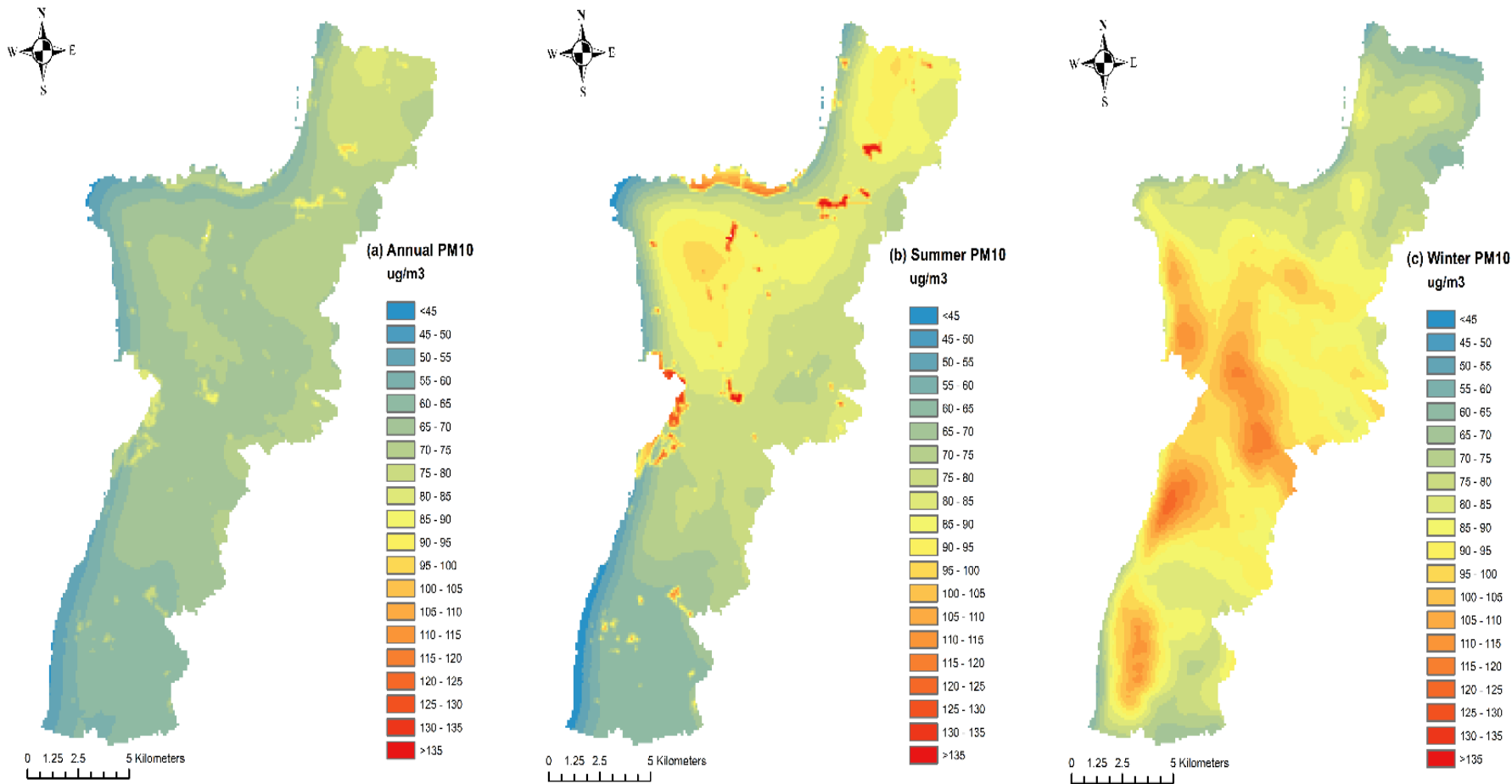


Figure 20. PM₁₀ surfaces (a) Annual average PM₁₀ LUR (b) Warm-season PM₁₀ LUR (c) Cold-season PM₁₀ LUR

3.3.3 CO models

The annual CO model was able to explain 60% of the CO variability observed in the GBA. Significant predictors included building area within a 3000 m buffer, forest area within a 100 m buffer, industrial area within a 500 m buffer, distance to major road, water area within a 1000 m buffer and wind speed. Building area and industrial area were found to have a significant positive effect on the observed CO concentrations, whereas distance to major roads, water area, and wind speed were found to have a negative effect on the concentrations. Increases in the coverage of forested areas were also found to have a positive effect on the concentrations of CO. We believe that this counterintuitive result was due to the fact that many of the monitoring sites on major highways leading out of Beirut were located in non-urbanized areas with a high vegetative cover. The latent effect of forest cover on CO concentrations was partially resolved by allowing for interactions between forest area and other predictors. Only the interaction between forest area and industrial area proved to be negative and significant. The cross validation R^2 was found to be 0.44; the model also didn't have any significant biases (PBIAS=0) (Figure 21). There was also no sign of spatial autocorrelation of the residuals, with a p-value of 0.09.

The performance of the CO seasonal models was comparable to that of the annual model, with the warm season model explaining 58% of the CO variability; on the other hand the cold season model explaining only 50% of the variability. Road length within a 1500 m buffer, forest area within a 100 m buffer, industrial area within a 200 m buffer, distance to major road and AOD were significant predictors in the warm season, whereas, road length within a 2000 m buffer, wind speed, water area within a 1000 m buffer,

industrial area within a 500 m buffer and distance to major roads were significant predictors in the cold season model. The 3 generated CO models had very similar model structures. The annual model had 3 predictors in common with each of the seasonal models although they had different buffer sizes. Both seasonal models also had 3 predictors in common. The seasonal models had a cross-validation R^2 of 0.46 and 0.38 for the warm and cold seasons respectively, while their predictions did not show any significant biases (PBIAS=0). In addition, the warm season model didn't show any spatial autocorrelation (p-value = 0.8), whereas the cold season model showed some spatial clustering in its residuals, with a Moran's I of 0.26 and a p-value < 0.05. All 3 CO models are summarized in Table 12.

CO prediction surfaces (100 m × 100 m) were generated for the GBA for each of the 3 CO models (annual and seasonal) (Figure 22). Similar to the $PM_{2.5}$ and PM_{10} surfaces, the prediction of the CO surfaces assumed mean values for wind speed, relative humidity and AOD as observed during the monitoring campaign. The 3 generated CO prediction surfaces showed large variabilities, with standard deviations of 0.68 ppm, 0.61 ppm and 0.75 ppm for the annual, warm season and cold season models respectively. The highest predicted CO surface for the GBA was associated with the annual model, with a predicted mean GBA-wide CO concentration of 2.41 ppm, whereas the lowest predicted surface was associated with the warm season model, which predicted a GBA-wide mean concentration of 2.1 ppm. The 3 prediction surfaces were highly correlated with Pearson's r correlations ranging from 0.78 (annual model and warm season model) to 0.82 (warm season model and cold season model).

The effect of traffic on CO concentrations was very strongly apparent in all 3 models that included distance to major road as a predictor. As such, hotspots were observed near roads and the CO concentrations decays rapidly as the distance to roads increased. In addition, the positive relationship between industrial areas and CO levels was found to be very strong and was captured by all 3 models. As a matter of fact, the highest predicted concentrations were observed in the vicinity of the industrial areas, especially next to the Beirut port and airport. Overall, the high CO concentrations were observed within the limits of Beirut proper, with lower concentrations observed in the Northern and Southern suburbs of Beirut.

Table 12. LUR models for predicting annual and seasonal log-transformed CO concentrations

Model	Model equation (^a Variable key given below)	R ²	Adj R ²	^b CV R ²	^c RMSE
Annual CO	$0.7397 + 0.055 \times \text{BUILD.3000} + 18.85 \times \text{FOREST.100} + 1.79 \times \text{IND.500} - 0.53 \times \text{DISTMJR} - 0.22 \times \text{WAT.1000} - 0.031 \times \text{WS} - 425.6 \times \text{FOREST.100} \times \text{IND.500}$	0.60	0.54	0.44	0.275
Warm season CO	$0.066 + 0.004 \times \text{RD.1500} + 9.32 \times \text{FOREST.100} + 7.72 \times \text{IND.200} - 0.41 \times \text{DISTMJR} + 1.524 \times \text{AOD}$	0.58	0.53	0.46	0.250
Cold season CO	$0.945 + 0.003 \times \text{RD.2000} - 0.03 \times \text{WS} - 0.4 \times \text{WAT.1000} + 1.28 \times \text{IND.500} - 0.33 \times \text{DISTMJR}$	0.50	0.45	0.38	0.345

^aLeft-hand side of period denotes variable type and right-hand side denotes buffer size so that **BUILD.3000** = building area within 3000 m buffer (in Km²). Variable types are: **WS** = wind speed (m/s); **WAT** = water area (Km²); **IND** = industrial area (Km²); **AOD** = aerosol optical depth; **DISTMJR** = distance to major road (Km); **FOREST** = forest area (Km²); **RD** = length of roads (Km)

^bCross-validated R²

^cRoot Mean Square Error

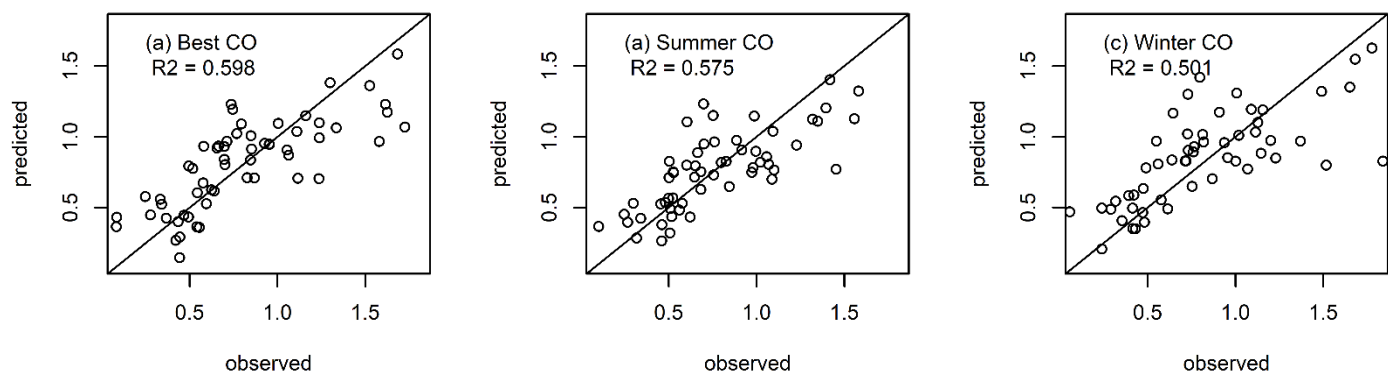


Figure 21. Predicted vs observed plots (a) Annual log-transformed CO LUR Model (b) Warm season log-transformed CO LUR model (c) Cold season log-transformed CO LUR model. Diagonal lines represents the 1:1 lines

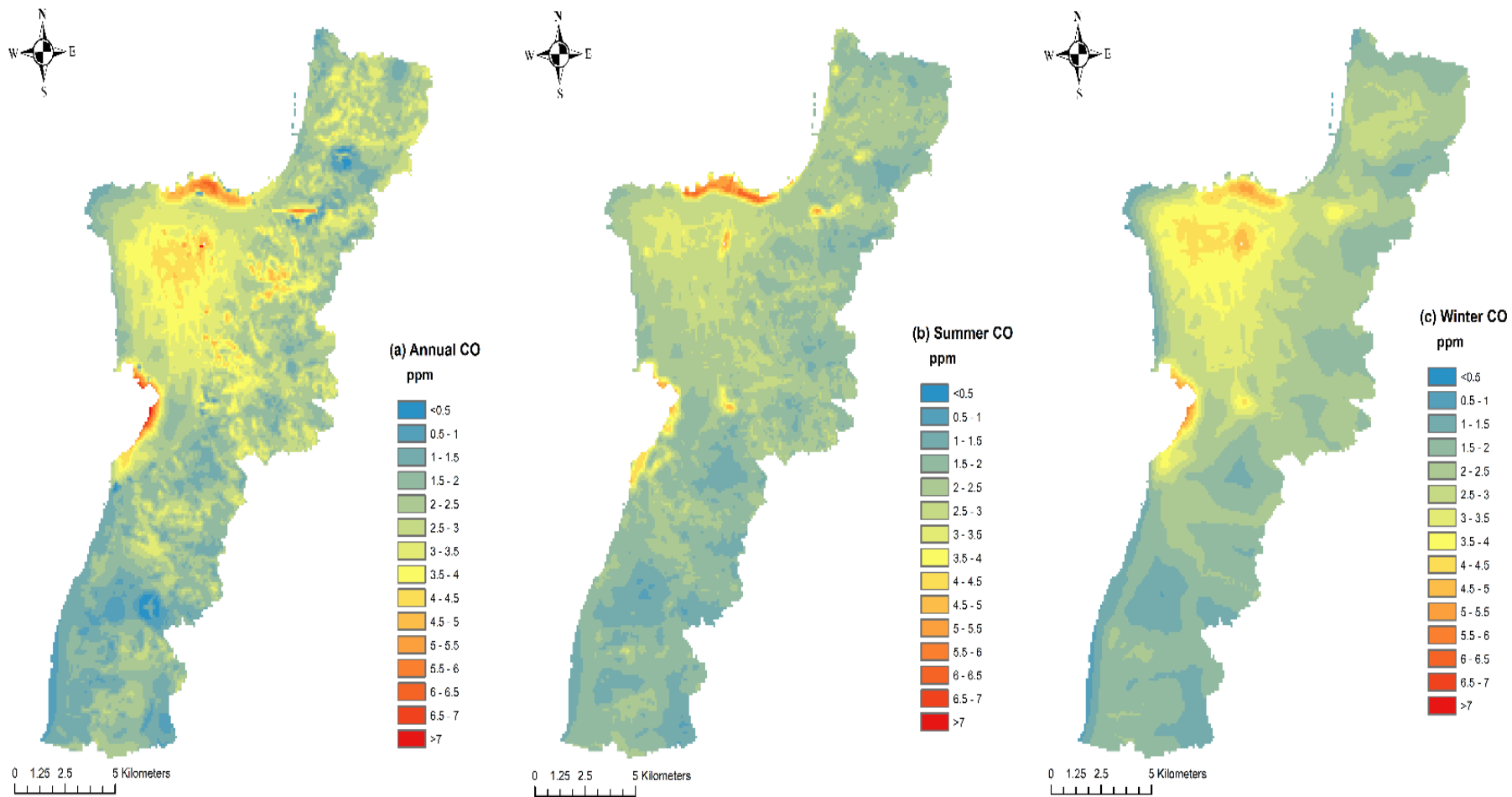


Figure 22. Predicted CO surfaces (a) Annual average CO LUR (b) Warm-season CO LUR (c) Cold-season CO LUR

3.3.4 *PM_{2.5}/PM₁₀ ratio models*

The annual PM_{2.5}/PM₁₀ ratio model was able to explain 51% of the observed annual variability in the PM ratio. Significant predictors included industrial area within a 3000 m buffer, industrial area within a 100 m buffer, length of major roads within a 300 m buffer, open area within a 200 m buffer, low density urban areas within a 300 m buffer, relative humidity, and forest area within a 100 m area. Only the length of major roads within a 300 m buffer and forest areas within a 100 m buffer had a positive effect on the ratio, this reinforces that traffic on major roads contribute a higher percentage of PM_{2.5} as compared to PM₁₀ while forest areas tend to reduce more the airborne coarse particles as compared to the finer PM_{2.5}. On the other hand, an increase in the rest of the predictors caused a drop in the percentage of fine particles by mass. The model had a cross validation R² of 0.3 and it didn't show any significant biases or any spatial autocorrelation.

The warm season model was able to explain only 32% of the observed seasonal variability in the PM_{2.5}/PM₁₀ ratio. The strongest promoter of a high PM_{2.5}/PM₁₀ ratio was the percent coverage of high urban areas within a 50 m buffer. The cold season model was largely similar to the annual model; it also was able to explain 45% of the observed ratio variability. The seasonal ratio models had a cross validation R² of 0.18 and 0.28 for the warm and cold seasons respectively. Both models didn't show any biases (PBIAS = 0) (Figure 23 and Figure 24) or any residual spatial autocorrelations. The three PM_{2.5}/PM₁₀ ratio models are summarized in Table 13.

Prediction surfaces were generated for the 3 models similarly to the other pollutants. Both the annual and warm season models showed low spatial variability in the median

predicted PM ratio, with standard deviations of 3.65 % and 4.57 % respectively, whereas the cold season model showed larger variabilities with a standard deviation of 28.5 %. No clear spatial patterns in the PM_{2.5}/ PM₁₀ ratio were observed in both the cold season and the annual prediction surfaces. However, cold spots were observed next to the airport and port, signifying that PM emissions in these areas were largely coarse. The warm season model on the other hand, showed very high ratios across the study area, with ratios rarely dropping below 85 %. The highest ratios were observed inside the limits of Beirut proper, where the dense urban fabric appears to retard the settling out of the fine particulate matter.

Table 13. LUR models for predicting annual and seasonal log-transformed PM_{2.5}/PM₁₀ ratios

Model	Model equation (^a Variable key given below)	R ²	Adj R ²	^b CV R ²	^c RMSE
Annual ratio	4.515 – 0.017×IND.3000 – 2.42×IND.100 + 0.018×RD2.300 – 0.79×OPEN.200 – 1.68×LOW.300 – 0.003×RH + 1.64×FOREST.100	0.51	0.44	0.30	0.035
Warm season ratio	4.424 – 0.017×OPEN.200 – 0.002×RD2.300 + 18.3×HIGH.50 – 0.79×LOW.300	0.32	0.27	0.18	0.044
Cold season ratio	4.677 – 0.45×IND.500 – 0.008×RH – 14.7×OPEN.50 + 0.02×RD2.300 + 0.58×FOREST.200	0.45	0.4	0.28	0.056
^a Left-hand side of period denotes variable type and right-hand side denotes buffer size so that LOW.300 = low density urban area within 300 m buffer (in Km ²). Variable types are: RH = relative humidity (%); HIGH = high density urban area (Km ²); IND = industrial area (Km ²); OPEN = open area (Km ²); FOREST = forest area (Km ²); RD2 = length of major roads (Km) ^b Cross-validated R ² ^c Root Mean Square Error					

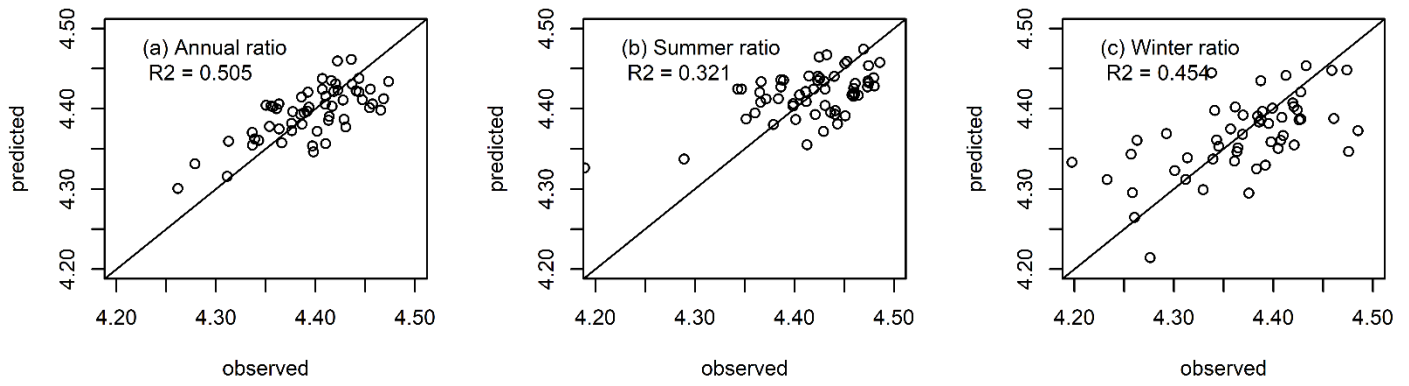


Figure 23. Predicted vs observed plots (a) Annual log-transformed ratio LUR Model (b) Warm season log-transformed ratio LUR model (c) Cold season log-transformed ratio LUR model. Diagonal lines represents the 1:1 lines

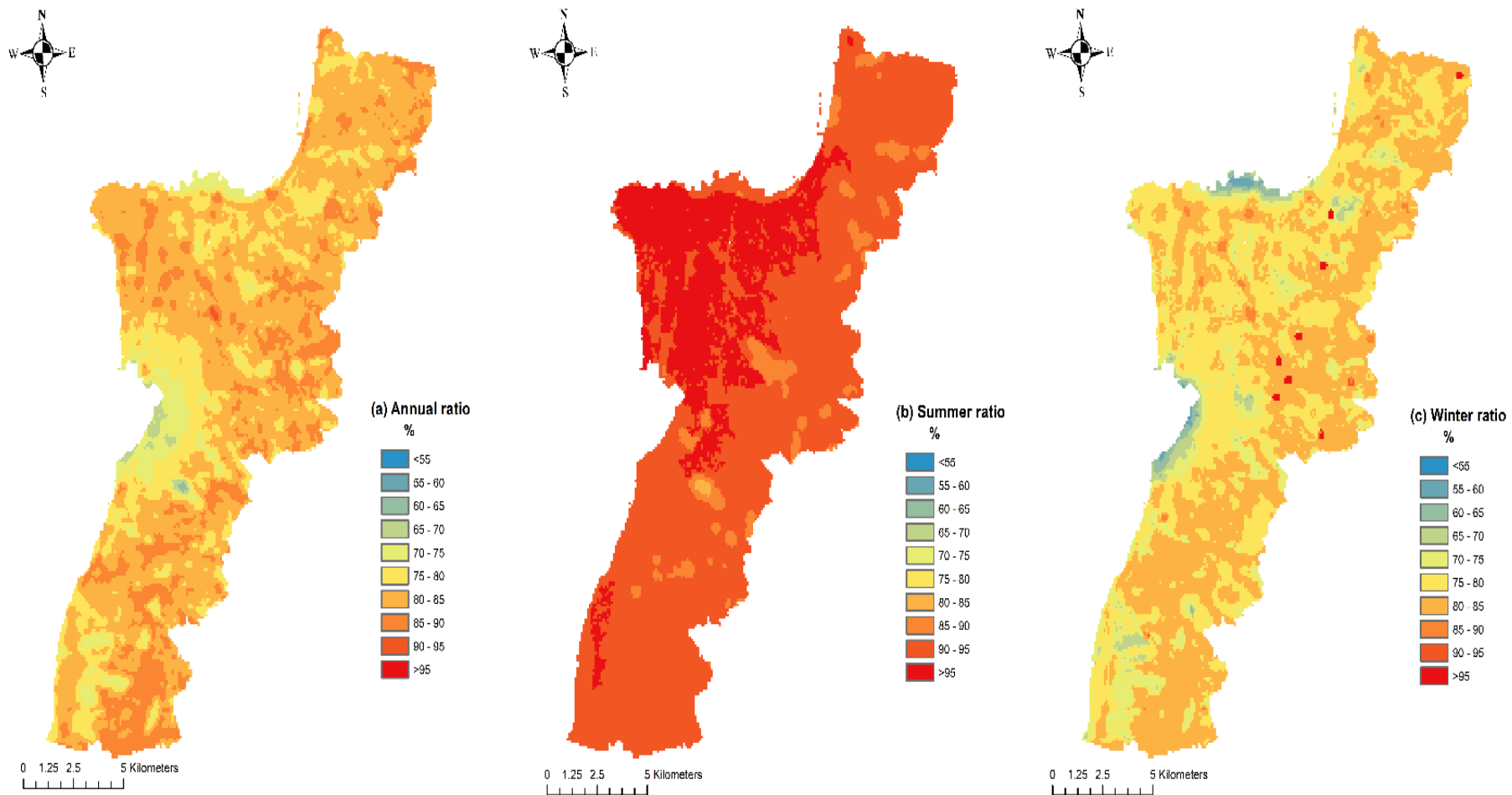


Figure 24. ratio surfaces (a) Annual average ratio LUR (b) Warm-season ratio LUR (c) Cold-season ratio LUR

CHAPTER 4

DISCUSSION

4.1 Pollutant variability

The current study is the first detailed assessment of the spatio-temporal variability in PM_{2.5}, PM₁₀ and CO levels at the level of the GBA. While previous studies have attempted to assess PM and CO variability in the study area, they were either limited by the number of monitored sites (all studies had less than 10 sampling sites) and/or by the short period over which the sampling campaign was implemented (Daher et al., 2013; Kouyoumdjian & Saliba, 2006; Massoud et al., 2011; Saliba, Atallah, & Al-Kadamany, 2009; Saliba et al., 2010; Saliba et al., 2006; Shaka' & Saliba, 2004). The annually averaged PM_{2.5} and PM₁₀ levels across the study area (68.1 µg/m³ and 83.5 µg/m³ respectively) were found to be slightly higher than those reported in previous studies (ranging from 27.6 to 41 µg/m³ for PM_{2.5}, and from 55.1 and 103.8 µg/m³ for PM₁₀) conducted in Beirut city proper. This could indicate a worsening in the pollution levels within the GBA and/or could be due to differences between the sampling campaigns (e.g. sampling times, averaging period, and sampling locations).

Seasonally, the measured cold season PM pollution levels were found to be higher than those of the warm season concurring with what was previously reported by Saliba et al. (2006). However, this seasonal effect contrasts with the findings of several other studies that reported that PM and CO concentrations were lower during the cold season due to the scrubbing effect of rain (Kouyoumdjian & Saliba, 2006; Saliba et al., 2009; Saliba et al., 2010). The observed range over which the PM_{2.5}/PM₁₀ ratio varied over was between 0.56

and 0.88, which is significantly higher than what has been previously reported in other studies within the GBA (between 0.32 and 0.57) (Kouyoumdjian & Saliba, 2006; Saliba et al., 2009; Saliba et al., 2010). Moreover, the ratio showed a seasonal pattern, with the hot season having a higher ratio (mean of 82.43 %) as compared to the cold season (mean of 78.68 %). Data from other urban regions have reported ratios between 0.45 and 0.85, with near road locations having lower ratios as compared to urban background locations (Chaloulakou, Kassomenos, Spyrellis, Demokritou, & Koutrakis, 2003; Eeftens et al., 2012; Gehrig & Buchmann, 2003; Hueglin et al., 2005; Marcazzan, Vaccaro, Valli, & Vecchi, 2001; Xavier Querol et al., 2001; X. Querol et al., 2004; Sahanavin, Prueksasit, & Tantrakarnapa, 2018).

The observed correlations between CO and PM₁₀ (r=0.46), and CO and PM_{2.5} (r=0.50) were similar to those previously reported in Lebanon by Saliba et al. (2006) and Alameddine et al. (2016) respectively. Lower correlations between PM_{2.5} and CO (r=0.20), and PM₁₀ and CO (r=0.33) were observed in London (Kaur, Nieuwenhuijsen, & Colvile, 2005) and Australia (Morawska, Thomas, Bofinger, Wainwright, & Neale, 1998) respectively, whereas similar correlations between PM₁₀ and CO (r=0.42-0.51) were observed in Hong Kong (Tian et al., 2013). In addition, the strength of these correlations was found to be seasonal, with stronger associations in the warm season (r=0.48 and 0.46 for PM_{2.5} and PM₁₀ respectively) as compared to the cold season (0.28 and 0.25 for PM_{2.5} and PM₁₀ respectively).

4.2 LUR models

This study developed, calibrated, and validated annual and seasonal LUR models for PM_{2.5}, PM₁₀ and CO using data collected from 58 predefined sites through a monitoring campaign that extended over a year. This work is the first attempt at generating high resolution air pollution maps in Lebanon that are based on calibrated pollution-based land use regression models. The developed models were used to generate air pollution maps for the entire GBA, which allowed us to assess the intra-city variations of air pollutant concentrations. Overall, the PM model results highlight the potential for significant public health concerns in the GBA. This study showed that the entire population of the GBA is exposed to annually-averaged concentrations that exceeded the 24-hour WHO Air Quality Standards set for PM_{2.5} and PM₁₀ during the sampling period (2017-2018).

With respect to model performance, the annual models outperformed their seasonal counterparts for all 3 pollutants as well as for the PM_{2.5}/PM₁₀ ratio, with an R² ranging between 0.67 for the annual PM_{2.5} model and 0.51 for the annual PM_{2.5}/PM₁₀ ratio model. The performance of the GBA annual models was found to compare favorably with other LULC models developed for predicting PM_{2.5} levels in several European and North American cities (R² between 0.17-0.73) (Hoek et al., 2008), PM₁₀ levels in Tehran, Iran; Perth, Australia; 20 European cities; Hong Kong; Augsburg, Germany and China (Amini et al., 2014; Dirgawati et al., 2016; Eeftens et al., 2012; Shi et al., 2016; Wolf et al., 2017; Zhang et al., 2018) (R² between 0.25-0.72), and CO concentrations in Tehran, Iran and Mexico city, Mexico (Hassanpour Matikolaei et al., 2017; Son et al., 2018) (R² between 0.38-0.53).

The seasonal $PM_{2.5}$ models for the GBA were found to outperform their seasonal counterparts in other cities. The R^2 values for the hot season model was 0.66, while that for the cold season was 0.59. In comparison, seasonal models developed for Hyderabad, India and the Western Cape province, South Africa (Sanchez et al., 2018; Saucy et al., 2018) had R^2 values ranging between 0.34 and 0.58. For the seasonal PM_{10} models, the GBA models (R^2 values of 0.57 and 0.49 for the hot and cold season respectively) performed as well as the seasonal PM_{10} models that were developed for Tehran, Iran and Tianjin, China (Amini et al., 2014; Chen, Bai, et al., 2010) (R^2 ranging between 0.49 and 0.72). With respect to CO, no seasonal models have been previously generated.

The model structure of the developed LUR models were found to vary by season, especially for $PM_{2.5}$ and PM_{10} . For both PM models, the cold and warm seasonal models only shared 3 predictors in total. This was reflected in the poor correlation between the generated warm and cold season pollution surfaces ($r = -0.35$ for $PM_{2.5}$ and $r = 0.01$ for PM_{10}). This indicates that important sources and sinks of PM in the GBA are seasonal in nature. As a matter of fact, our results show that the impact of traffic related emissions are much more pronounced in the cold season when it comes to $PM_{2.5}$ pollution levels. These results were consistent with the findings of Chen, Bai, et al. (2010) and Sanchez et al. (2018) who also reported that their seasonal PM_{10} and $PM_{2.5}$ models, developed for Tianjin, China and Hyderabad, India respectively, had very different model structures. Nevertheless, Amini et al. (2014) and Saucy et al. (2018) reported stable model structures for their PM_{10} and $PM_{2.5}$ models that were developed for Tehran, Iran and Western Cape province, South Africa respectively, irrespective of season. Additionally, we found that in the case of the

GBA the warm season models for both $PM_{2.5}$ and PM_{10} were closer in structure to the annual models and their generated surfaces were also found to be highly correlated (r values of 0.73 and 0.86 for $PM_{2.5}$ and PM_{10} respectively).

As for CO, we found that the model structures for the annual as well as the seasonal models were to a large extent similar. Additionally, the 3 generated prediction surfaces had a high correlation (r values of 0.78, 0.80 and 0.82 for the warm-cold season, annual-cold, and annual-warm respectively). These findings point to the absence of significant seasonal differences in the CO sources and sinks within the GBA. As compared to the PM predicted surfaces, the generated CO surfaces showed higher spatial variabilities across the study domain with clear peaks next to major roads and industrial areas. This is expected given that CO is mainly emitted from anthropogenic sources and is rarely affected by natural events (EPA, 2010). Despite its long atmospheric life, CO is known to be source specific and as such background sites tend to have much lower concentrations as compared to sites near sources; these characteristics lead to large spatial variability in CO concentrations (Jaffe, 1968).

The main common predictor across the LURs developed for the 3 pollutants was the building area within a 3000 m buffer. This predictor was found to be highly correlated with the lengths of roads and the length of major roads within the same buffer. As such, the parameter acts as a surrogate for traffic-related emissions in dense urban areas. Moreover, it indirectly accounts for the emissions from private diesel generators operating in the study area, as their numbers are expected to be directly proportional to the building density. Explicit traffic predictors were only featured in the CO models, whereby distance to main

roads was found to be a significant predictor alongside building area. This further reinforces the tight relationship between traffic and CO concentrations as compared to a weaker link with PM levels. It should be noted that the inclusion of traffic counts as model predictors resulted in better models for both the annual and seasonal models of PM_{2.5} and CO. As a matter of fact, the R² of the annual PM_{2.5} model improved from 0.67 to 0.75, while the annual CO model improved from 0.60 to 0.64. Nevertheless, traffic counts were excluded from the final models due to absence of spatially explicit traffic information for the GBA that are needed to generate reliable pollution prediction surfaces. Another major pollution source that was consistently significant across all 3 pollutants was the presence of industrial areas; their negative effects on air quality were very apparent in most of the generated prediction surfaces. On the other hand, the role that the heavy-fuel burning Zouk power plant, which is the main point source emitter in the GBA, has on the pollution levels in the GBA was very evident when it came to the PM_{2.5} and PM₁₀ models but was absent in the CO models. Fuel burning power plants have been known for emitting pollutants such as NO_x, SO_x, CO₂, CO, PM, organic gases and polycyclic aromatic hydrocarbons. They were found to account for 24% of PM₁₀ emissions nationwide in Mexico (Conzelmann et al., 2006) and 11% of PM₁₀ emissions in Beijing, China (He, Yu, Lu, Hao, & Fu, 2003). In addition, fossil fueled power plants were found to increase the ambient PM_{2.5} concentrations in Illinois, USA by 0.04 µg/m³ (Levy, Spengler, Hlinka, Sullivan, & Moon, 2002).

Interestingly, the developed LUR models were able to capture some of local geospatial characteristic of the GBA, which play a role in transporting and dispersing air

pollution. The impact of the sea, captured by the area covered by water, was found to have a major effect in attenuating concentrations across all the models, with the exception for the CO warm season model. The sea-breeze is known to disperse pollutants and as such the coastal areas were predicted to have lower concentrations as compared to similar regions further inland. Additionally, the GBA LUR models captured the effect of elevation on the concentrations of particulate matter. Contrary to previous studies (de Hoogh et al., 2016; Henderson et al., 2007; Vienneau et al., 2010; Wolf et al., 2017), increases in elevation were found to increase the levels of $PM_{2.5}$ and PM_{10} . This is probably due to the transport of pollutants generated from the city and the highly urban coastal zone by the sea-breeze to locations further inland. The fact that these inland areas are elevated and overlook the city causes them to suffer from thermal inversion events that trap and concentrate pollutants. Our results mirror what has been observed in Los Angeles, USA, where sea breeze, strong thermal inversion, and the presence of a mountain range result in elevated pollution levels in the mountainous regions overlooking the densely populated coastal regions of the city (Lu & Turco, 1994). In Freiburg, Germany, the mountain-valley breeze was also found to transport air pollutants to the neighboring mountain range during thermal inversion events (Baumbach & Vogt, 1999). Similar observations were also reported for the Santiago valley in Chile with regards to $PM_{2.5}$ and Black Carbon (Gramsch et al., 2014).

Spatially, all the generated surfaces, except for the warm season $PM_{2.5}$ surface, showed high pollution concentrations within the limits of Beirut city proper, which is the most densely populated and congested region of the GBA. Moreover, concentrations were found to decrease near the coast. The Northern part of the GBA was found to have high

levels of $PM_{2.5}$ and PM_{10} due to the emissions from the Zouk power plant and the predominant southwesterly winds that appear to transport PM generated in the highly congested regions of Beirut towards its northern suburbs. On the other hand, the southern parts of the GBA were found to have the lowest concentrations across all models with the exception of the PM levels in the cold season. These low concentrations are due to the fact that the southern parts of the GBA are less populated and not as congested as the rest of GBA. As for the CO prediction surfaces, the Northern and Southern parts of the GBA were found to have lower concentrations as compared to Beirut proper. Elevated CO levels were also predicted to occur next to traffic sources.

In addition to the $PM_{2.5}$, PM_{10} , and CO LUR models that were generated for the GBA, this work also developed annual and seasonal LUR models for predicting the $PM_{2.5}/PM_{10}$ ratios across the GBA. This is the first study to our knowledge that has looked at generating an LUR model that predicts the covariance of the two PM pollutants concurrently in the same model. The performance of the annual ratio model ($R^2=0.51$) was found to be comparable to that of the $PM_{2.5}$, PM_{10} and CO models and to previous LUR models in general. However, the seasonal ratio models performed poorly as compared to the other seasonal models with R^2 of 0.32 and 0.45 for the warm and cold season models respectively. The poor performance of these models could be due to constraining the model predictors to concurrently and proportionately affect the $PM_{2.5}$ and PM_{10} levels.

4.3 Correlations between measured and predicted concentrations

The measured concentrations of PM_{2.5} and PM₁₀ had large within site variability as compared to the between site variability, whereas CO concentrations had large between site variability. This indicates that the temporal variability in CO concentrations at a given site was relatively low, whereas PM concentrations had large temporal variability in each of the sites. These patterns were also captured in the LUR results, where the annual and seasonal CO models had similar structures and resulted in highly correlated prediction surfaces, whereas the annual and seasonal PM_{2.5} and PM₁₀ models had different model structures and resulted in poorly correlated prediction surfaces that tended to be more spatially homogeneous by comparison to the CO generated surfaces. The large temporal variability associated with the PM_{2.5} and PM₁₀ concentrations is partially due to the effect of large-scale natural PM emission sources in arid and semi-arid regions, such as the Eastern Mediterranean basin (Kattenberg et al., 1996; Xavier Querol et al., 2001). PM_{2.5} and PM₁₀ concentrations in Mediterranean cities have been known to show large temporal variability as a result of the long range transport of dust from North Africa and the Arabian Desert (Bergametti, Dutot, Buat-MéNard, Losno, & Remoudaki, 1989; Chester et al., 1993; Kubilay & Saydam, 1995; Xavier Querol et al., 1998; Rodriguez, Querol, Alastuey, Kallos, & Kakaliagou, 2001; Saliba et al., 2010). Overall, the generated prediction surfaces for the annually averaged and warm season models were found to be able to conserve the inter-pollutant correlations seen with the field-measured PM_{2.5}, PM₁₀ and CO levels (Table 14). However, inter-pollutant correlations differed between the field-measured and the modeled surfaces in the cold season.

Table 14. Table showing the correlations between the measured concentrations and between the generated prediction surfaces

Pollutant		CO			PM _{2.5}			PM ₁₀			PM _{2.5} /PM ₁₀ ratio		
		Annual	Warm	Cold	Annual	Warm	Cold	Annual	Warm	Cold	Annual	Warm	Cold
CO	Annual	^a 1.00 (^b 1.00)			0.50* (0.43*)			0.46* (0.42*)			0.13 (0.03*)		
	Warm	-	1.00 (1.00)			0.48* (0.42*)			0.46* (0.62*)			0.16 (0.29*)	
	Cold	-	-	1.00 (1.00)			0.28* (0.11*)			0.25* (0.15*)			0.09 (-0.04*)
PM _{2.5}	Annual	-	-	-	1.00 (1.00)			0.96* (0.73*)			0.03 (0.18*)		
	Warm	-	-	-	-	1.00 (1.00)			0.96* (0.71*)			0.19 (-0.007)	
	Cold	-	-	-	-	-	1.00 (1.00)			0.94* (0.57*)			0.29* (0.02*)
PM ₁₀	Annual	-	-	-	-	-	-	1.00 (1.00)			-0.14 (-0.06*)		
	Warm	-	-	-	-	-	-	-	1.00 (1.00)			0.04 (0.14*)	
	Cold	-	-	-	-	-	-	-	-	1.00 (1.00)			0.025 (-0.07*)
PM _{2.5} /PM ₁₀ ratio	Annual	-	-	-	-	-	-	-	-	-	1.00 (1.00)		
	Warm	-	-	-	-	-	-	-	-	-	-	1.00 (1.00)	
	Cold	-	-	-	-	-	-	-	-	-	-	-	1.00 (1.00)

^a Correlation between observed measurements

^b Correlation between prediction surfaces

* Significant correlation

4.4 Exposure at schools and hospitals

Schools and hospitals within the GBA were superimposed on the generated annual prediction air pollution surfaces (Figure 25). The results show that 100% of the schools and hospitals in the GBA are exposed to annual average $PM_{2.5}$ concentrations that exceed the WHO standards ($25 \mu\text{g}/\text{m}^3$ for 24hr standard and $10 \mu\text{g}/\text{m}^3$ for 1-year standard). Moreover, we found that 50% of the schools were located in regions where the concentrations exceeded the $55 \mu\text{g}/\text{m}^3$, while 50% of hospitals were in locations with concentrations greater than $50 \mu\text{g}/\text{m}^3$. With regards to the PM_{10} concentrations, all schools and hospitals were found to be located in regions with levels exceeding the WHO standards ($50 \mu\text{g}/\text{m}^3$ for 24hr standard and $20 \mu\text{g}/\text{m}^3$ for 1-year standard); yet lower than the current Lebanese standard ($80 \mu\text{g}/\text{m}^3$ for the 24hr standard). More than 50% of the hospitals were found to be located in regions where the PM_{10} concentrations exceeded $64 \mu\text{g}/\text{m}^3$, while 50% of the schools were found in areas where the predicted concentrations exceeded $68 \mu\text{g}/\text{m}^3$. As for CO, all the predicted concentrations were found to be lower than both the WHO and Lebanese standards (8.73 ppm for 24hr standard and 26.19 ppm for 1-year standard).

These results show that children and hospital patients in the GBA are exposed to elevated concentrations of $PM_{2.5}$ and PM_{10} , which may lead to adverse health effects. These preliminary results highlight the importance of using the generated air pollution surfaces for the GBA to further investigate the health and economic impacts that air pollution has on the residing population. Nevertheless, this assessment has been limited to assessing exposure only as a function of ambient outdoor concentrations. Future efforts should look more

closely at the correlations between outdoor concentrations and indoor concentrations, especially at vulnerable receptors such as schools and hospitals.

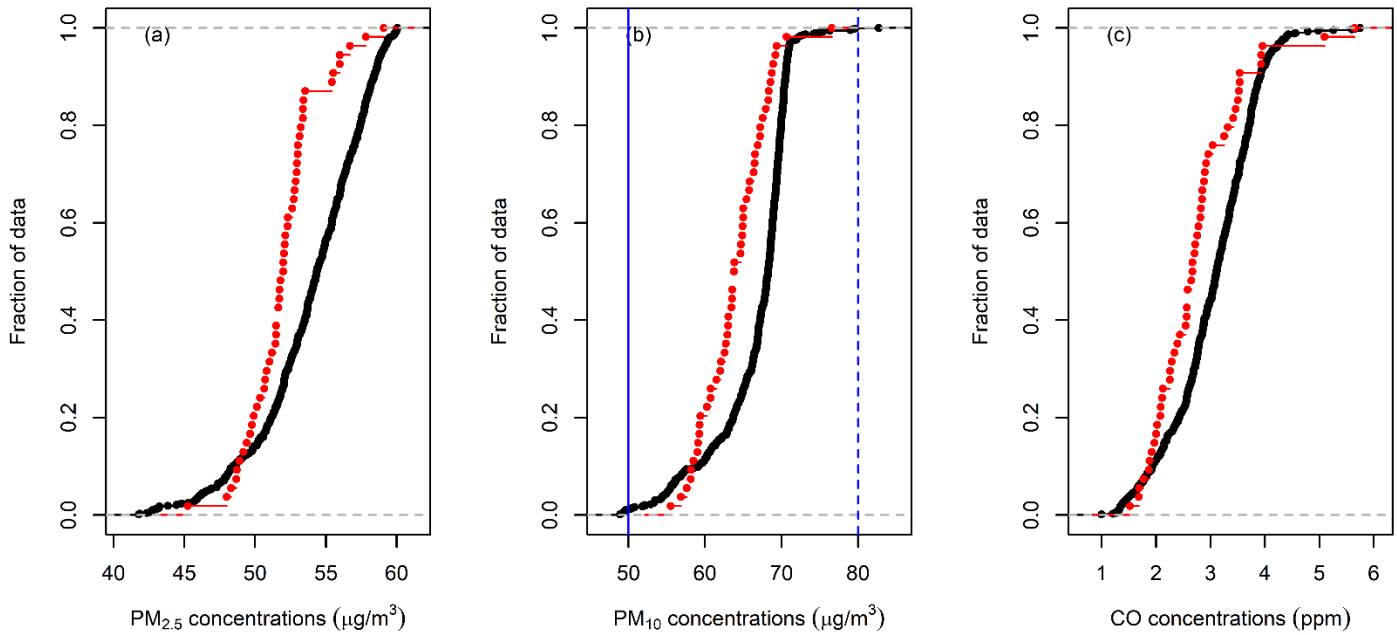


Figure 25. Plots showing the empirical cumulative density function (ECDF) of (a) $PM_{2.5}$, (b) PM_{10} and (c) CO concentrations observed at schools (black dots) and hospitals (red dots), with the straight blue line showing the WHO standards and the dashed blue line showing the Lebanese standards

4.5 Limitations

Despite the good performance of the generated LUR models, the current study faced several limitations. One major limitation was the lack of reference or background sites that can be used to standardize the daily readings. Standardization could have reduced the large variabilities observed at each site, especially during the cold season where rain plays an important role in precipitating out the PM from the atmosphere. Another limitation of this study was the lack of data on several potentially important predictors, such as traffic data,

industrial emissions, and data on the location, capacities, types, and operational schedule of private power generators. Another limitation of this study was the relatively short sampling time adopted in the monitoring campaign (average of 30 min readings). Short sampling periods may impede the capture of the true temporal variability of the measured air pollutant (Hoek et al., 2008).

CHAPTER 5

CONCLUSION AND FUTURE WORK

The LUR approach was first developed in Europe (Briggs et al., 1997) and has since been applied across several European and North American cities (Hoek et al., 2008). More recently, LURs have been successfully tested in several developing countries in Asia (Amini et al., 2014; Chen, Baili, et al., 2010; Sanchez et al., 2018; Saraswat et al., 2013; M. Wang et al., 2014; Zhang et al., 2018; Zou et al., 2015), South America (Habermann & Gouveia, 2012; Sangrador et al., 2008) and Africa (Saucy et al., 2018). The current study further reinforces the strength of LURs, as a modeling technique, in providing informative pollution exposure maps in data-scarce regions that show high heterogeneity in both their landuse/landcover fabric and their geospatial settings. In addition, the results of the current study suggest that the existing monitoring network established by the Ministry of the Environment and that consists of 5 monitoring stations will not be able to accurately reflect the variability of air pollution levels across the whole GBA region despite the relatively small area of the study region (233 Km²). We hope that the results of this study can guide future monitoring initiatives in the GBA as well as drive policies that aim to improve its air quality, particularly with regards to urban planning, school and healthcare siting, traffic management, environmental monitoring, and public awareness. Moreover, the results of this work has great potential to be used by epidemiologists to better quantify the direct and indirect effects of air pollution on health, a topic that has only recently been studied in Lebanon (Nakhlé et al., 2015; Nasser et al., 2015).

In addition, future studies should make use of the generated air pollution concentration maps to quantify the socio-economic impacts associated with exposure to the predicted $PM_{2.5}$, PM_{10} and CO levels. This is typically achieved by overlaying the pollution maps on geo-referenced health data to assign exposure to individuals at their place of residence, work or some combination of both. These prediction surfaces can also be cross-validated against personal exposure measurements that target individuals with specific health conditions in order to ensure the validity of these predictions for use in epidemiological studies. Additionally, these surfaces can be used to assess the economic impacts of the measured air pollutants in the GBA. This can be done by looking at the cost and the number of hospital visits that might be attributed to air pollution related conditions, in addition to the loss in labor income resulting from these conditions. Finally, it is hoped that these these prediction surfaces can reduce the current uncertainties in exposure levels resulting from the lack of spatially explicit air pollution data so as to promote policy intervention that aim towards protecting public health and reducing air pollution related costs.

Despite the good performance of the generated models, much research remains to be done in assessing exposure to air pollution in the GBA. Thus, future studies should expand on this study to better assess the variability in the pollution levels of finer PM, i.e. Ultrafine particles (UFPs) and Black Carbon (BC). The effects of these pollutants on human health are a growing concern and are thought to have worse effects than $PM_{2.5}$ and PM_{10} (EPA, 2009). Unfortunately, very little work has been done to measure these pollutants in Lebanon.

Another area for future research, would be to generate LUR models using mobile monitoring campaigns. Several LUR studies have highlighted the usefulness of mobile monitoring given the large spatial coverage associated with these campaigns as compared to stationary monitoring. Additionally, the current study was limited to curbside measurements. However, for a better use of these results in epidemiological studies, future studies will have to look at the correlations between the predicted outdoor ambient concentrations and indoor concentrations. Finally, several recent LUR studies have successfully incorporated remote sensing data into their models. This was attempted in this study by including AOD data from the MODIS sensor, however, the resolution of the product was low compared to the resolution of the generated surfaces. Future LUR studies in the GBA should try to incorporate several aerosol and meteorological satellite data with finer spatial resolution.

REFERENCES

- Abernethy, R. C., Allen, R. W., McKendry, I. G., & Brauer, M. (2013). A Land Use Regression Model for Ultrafine Particles in Vancouver, Canada. *Environmental Science & Technology*, 47(10), 5217-5225. doi:10.1021/es304495s
- Abi Esber, L., El-Fadel, M., Nuwayhid, I., & Saliba, N. (2007). The effect of different ventilation modes on in-vehicle carbon monoxide exposure. *Atmospheric Environment*, 41(17), 3644-3657. doi:https://doi.org/10.1016/j.atmosenv.2006.12.036
- Akaike, H. (1974). A new look at the statistical model identification. *IEEE Transactions on Automatic Control*, 19, 716-723.
- Alameddine, I., Abi Esber, L., Bou Zeid, E., Hatzopoulou, M., & El-Fadel, M. (2016). Operational and environmental determinants of in-vehicle CO and PM2.5 exposure. *Science of The Total Environment*, 551-552, 42-50. doi:<https://doi.org/10.1016/j.scitotenv.2016.01.030>
- Amini, H., Taghavi-Shahri, S. M., Henderson, S. B., Naddafi, K., Nabizadeh, R., & Yunesian, M. (2014). Land use regression models to estimate the annual and seasonal spatial variability of sulfur dioxide and particulate matter in Tehran, Iran. *Science of The Total Environment*, 488-489, 343-353. doi:<https://doi.org/10.1016/j.scitotenv.2014.04.106>
- Baumbach, G., & Vogt, U. (1999). Experimental determination of the effect of mountain-valley breeze circulation on air pollution in the vicinity of Freiburg. *Atmospheric Environment*, 33(24), 4019-4027. doi:[https://doi.org/10.1016/S1352-2310\(99\)00143-0](https://doi.org/10.1016/S1352-2310(99)00143-0)
- Beelen, R., Hoek, G., van den Brandt, P. A., Goldbohm, R. A., Fischer, P., Schouten, L. J., . . . Brunekreef, B. (2008). Long-Term Exposure to Traffic-Related Air Pollution and Lung Cancer Risk. *Epidemiology*, 19(5), 702-710. doi:10.1097/EDE.0b013e318181b3ca
- Bergametti, G., Dutot, A.-L., Buat-MéNard, P., Losno, R., & Remoudaki, E. (1989). Seasonal variability of the elemental composition of atmospheric aerosol particles over the northwestern Mediterranean. *Tellus B: Chemical and Physical Meteorology*, 41(3), 353-361.
- Brauer, M., Hoek, G., van Vliet, P., Meliefste, K., Fischer, P., Gehring, U., . . . Brunekreef, B. (2003). Estimating Long-Term Average Particulate Air Pollution Concentrations: Application of Traffic Indicators and Geographic Information Systems. *Epidemiology*, 14(2), 228-239.
- Briggs, D. J., Collins, S., Elliott, P., Fischer, P., Kingham, S., Lebet, E., . . . Van Der Veen, A. (1997). Mapping urban air pollution using GIS: a regression-based approach. *International Journal of Geographical Information Science*, 11(7), 699-718. doi:10.1080/136588197242158
- Briggs, D. J., de Hoogh, C., Gulliver, J., Wills, J., Elliott, P., Kingham, S., & Smallbone, K. (2000). A regression-based method for mapping traffic-related air pollution: application and testing in four contrasting urban environments. *Science of The Total Environment*, 253(1), 151-167. doi:10.1016/S0048-9697(00)00429-0
- Brook, R. D., Brook, J. R., & Rajagopalan, S. (2003). Air pollution: The "heart" of the problem. *Current Hypertension Reports*, 5(1), 32-39. doi:10.1007/s11906-003-0008-y
- Centers for Disease, C., & Prevention, U. S. A. (1997). Outdoor carbon monoxide poisoning attributed to tractor exhaust--Kentucky, 1997. *MMWR: Morbidity and mortality weekly report*, 46(51), 1224-1227.
- Chaloulakou, A., Kassomenos, P., Spyrellis, N., Demokritou, P., & Koutrakis, P. (2003). Measurements of PM10 and PM2.5 particle concentrations in Athens, Greece.

- Atmospheric Environment*, 37(5), 649-660. doi:[https://doi.org/10.1016/S1352-2310\(02\)00898-1](https://doi.org/10.1016/S1352-2310(02)00898-1)
- Chen, L., Bai, Z., Kong, S., Han, B., You, Y., Ding, X., . . . Liu, A. (2010). A land use regression for predicting NO₂ and PM₁₀ concentrations in different seasons in Tianjin region, China. *Journal of Environmental Sciences*, 22(9), 1364-1373. doi:[https://doi.org/10.1016/S1001-0742\(09\)60263-1](https://doi.org/10.1016/S1001-0742(09)60263-1)
- Chen, L., Baili, Z., Kong, S., Han, B., You, Y., Ding, X., . . . Liu, A. (2010). A land use regression for predicting NO₂ and PM₁₀ concentrations in different seasons in Tianjin region, China. *Journal of environmental sciences (China)*, 22(9), 1364-1373. doi:10.1016/s1001-0742(09)60263-1
- Chester, R., Nimmo, M., Alarcon, M., Saydam, C., Murphy, K., Sanders, G., & Corcoran, P. (1993). Defining the chemical character of aerosols from the atmosphere of the Mediterranean Sea and surrounding regions. *Oceanologica Acta*, 16(3), 231-246.
- Clougherty, J. E., Wright, R. J., Baxter, L. K., & Levy, J. I. (2008). Land use regression modeling of intra-urban residential variability in multiple traffic-related air pollutants. *Environmental Health*, 7(1), 17. doi:10.1186/1476-069x-7-17
- Conzelmann, G., Quintanilla, J., Aguilar, V., Conde, L. A., Fernández, J., Mar, E., . . . Ortega, R. (2006). Mexico's long-term energy outlook: results of a detailed energy supply and demand simulation. *Energy Studies Review*, 14(1), 80.
- Cyrus, J., Hochadel, M., Gehring, U., Hoek, G., Diegmann, V., Brunekreef, B., & Heinrich, J. (2005). GIS-based estimation of exposure to particulate matter and NO₂ in an urban area: stochastic versus dispersion modeling. *Environmental Health Perspectives*, 113(8), 987-992. doi:10.1289/ehp.7662
- Daher, N., Saliba, N. A., Shihadeh, A. L., Jaafar, M., Baalbaki, R., & Sioutas, C. (2013). Chemical composition of size-resolved particulate matter at near-freeway and urban background sites in the greater Beirut area. *Atmospheric Environment*, 80, 96-106. doi:<https://doi.org/10.1016/j.atmosenv.2013.08.004>
- de Hoogh, K., Gulliver, J., Donkelaar, A. v., Martin, R. V., Marshall, J. D., Bechle, M. J., . . . Hoek, G. (2016). Development of West-European PM_{2.5} and NO₂ land use regression models incorporating satellite-derived and chemical transport modelling data. *Environmental Research*, 151(Supplement C), 1-10. doi:10.1016/j.envres.2016.07.005
- de Hoogh, K., Korek, M., Vienneau, D., Keuken, M., Kukkonen, J., Nieuwenhuijsen, M. J., . . . Bellander, T. (2014). Comparing land use regression and dispersion modelling to assess residential exposure to ambient air pollution for epidemiological studies. *Environment International*, 73, 382-392. doi:10.1016/j.envint.2014.08.011
- Dehbi, H.-M., Blangiardo, M., Gulliver, J., Fecht, D., de Hoogh, K., Al-Kanaani, Z., . . . Hansell, A. L. (2017). Air pollution and cardiovascular mortality with over 25 years follow-up: A combined analysis of two British cohorts. *Environment International*, 99, 275-281. doi:10.1016/j.envint.2016.12.004
- Delfino, R. J., Tjoa, T., Gillen, D. L., Staimer, N., Polidori, A., Arhami, M., . . . Longhurst, J. (2010). Traffic-related Air Pollution and Blood Pressure in Elderly Subjects With Coronary Artery Disease. *Epidemiology (Cambridge, Mass.)*, 21(3). doi:10.1097/EDE.0b013e3181d5e19b
- Dirgawati, M., Heyworth, J. S., Wheeler, A. J., McCaul, K. A., Blake, D., Boeyen, J., . . . Hinwood, A. (2016). Development of Land Use Regression models for particulate matter and associated components in a low air pollutant concentration airshed. *Atmospheric Environment*, 144, 69-78. doi:<https://doi.org/10.1016/j.atmosenv.2016.08.013>

- ECODIT. (2010). *State & Trends of the Lebanese Environment, Chapter 4: Air Quality*. Retrieved from Lebanon:
- Eeftens, M., Beelen, R., de Hoogh, K., Bellander, T., Cesaroni, G., Cirach, M., . . . Hoek, G. (2012). Development of Land Use Regression Models for PM2.5, PM2.5 Absorbance, PM10 and PMcoarse in 20 European Study Areas; Results of the ESCAPE Project. *Environmental Science & Technology*, 46(20), 11195-11205. doi:10.1021/es301948k
- EPA. (2009). *Integrated Science Assessment for Particulate Matter* Retrieved from Research Triangle Park, NC:
- EPA. (2010). *Integrated Science Assessment for Carbon Monoxide*. Research Triangle Park, NC.
- ESRI. (2016). ArcGIS Desktop: Release 10.4. Redlands, CA: Environmental Systems Research Institute.
- ESRI. (2017). ArcGIS Desktop. Redlands, CA: Environmental Systems Research Institute.
- Faour, G. H. (2015). Evaluating urban expansion using remotely-sensed data in Lebanon. *Lebanese Science Journal*(16,1), 23-31.
- Finkelstein, M. M., Jerrett, M., & Sears, M. R. (2004). Traffic Air Pollution and Mortality Rate Advancement Periods. *American Journal of Epidemiology*, 160(2), 173-177. doi:10.1093/aje/kwh181
- Fox, J., & Weisberg, S. (2011). *An R Companion to Applied Regression* (2nd ed.). Thousands Oak, CA: SAGE Publications.
- Franchini, M., & Mannucci, P. M. (2012). Air pollution and cardiovascular disease. *Thrombosis Research*, 129(3), 230-234. doi:10.1016/j.thromres.2011.10.030
- Gan, W. Q., Davies, H. W., Koehoorn, M., & Brauer, M. (2012). Association of Long-term Exposure to Community Noise and Traffic-related Air Pollution With Coronary Heart Disease Mortality. *American Journal of Epidemiology*, 175(9), 898-906. doi:10.1093/aje/kwr424
- Gehrig, R., & Buchmann, B. (2003). Characterising seasonal variations and spatial distribution of ambient PM10 and PM2.5 concentrations based on long-term Swiss monitoring data. *Atmospheric Environment*, 37(19), 2571-2580. doi:[https://doi.org/10.1016/S1352-2310\(03\)00221-8](https://doi.org/10.1016/S1352-2310(03)00221-8)
- Gramsch, E., Cáceres, D., Oyola, P., Reyes, F., Vásquez, Y., Rubio, M. A., & Sánchez, G. (2014). Influence of surface and subsidence thermal inversion on PM2.5 and black carbon concentration. *Atmospheric Environment*, 98, 290-298. doi:<https://doi.org/10.1016/j.atmosenv.2014.08.066>
- Gulliver, J., & Briggs, D. J. (2004). Personal exposure to particulate air pollution in transport microenvironments. *Atmospheric Environment*, 38(1), 1-8. doi:10.1016/j.atmosenv.2003.09.036
- Gulliver, J., de Hoogh, K., Fecht, D., Vienneau, D., & Briggs, D. (2011). Comparative assessment of GIS-based methods and metrics for estimating long-term exposures to air pollution. *Atmospheric Environment*, 45(39), 7072-7080. doi:<https://doi.org/10.1016/j.atmosenv.2011.09.042>
- Habermann, M., & Gouveia, N. (2012). Aplicação de regressão baseada no uso do solo para prever a concentração de material particulado inalável no município de São Paulo, Brasil. *Engenharia Sanitaria e Ambiental*, 17, 155-162.
- Hankey, S., & Marshall, J. D. (2015). Land Use Regression Models of On-Road Particulate Air Pollution (Particle Number, Black Carbon, PM2.5, Particle Size) Using Mobile Monitoring. *Environmental Science & Technology*, 49(15), 9194-9202. doi:10.1021/acs.est.5b01209

- Hassanpour Matikolaie, S. A. H., Jamshidi, H., & Samimi, A. (2017). Characterizing the effect of traffic density on ambient CO, NO₂, and PM_{2.5} in Tehran, Iran: an hourly land-use regression model. *Transportation Letters*, 1-11. doi:10.1080/19427867.2017.1385201
- He, K.-B., Yu, X.-C., Lu, Y.-Q., Hao, J.-M., & Fu, L.-X. (2003). Characterization of urban air pollution sources. *Urban Environment & Urban Ecology*, 16(6), 269-271.
- Henderson, S. B., Beckerman, B., Jerrett, M., & Brauer, M. (2007). Application of Land Use Regression to Estimate Long-Term Concentrations of Traffic-Related Nitrogen Oxides and Fine Particulate Matter. *Environmental Science & Technology*, 41(7), 2422-2428. doi:10.1021/es0606780
- Ho, C.-C., Chan, C.-C., Cho, C.-W., Lin, H.-I., Lee, J.-H., & Wu, C.-F. (2015). Land use regression modeling with vertical distribution measurements for fine particulate matter and elements in an urban area. *Atmospheric Environment*, 104, 256-263. doi:<https://doi.org/10.1016/j.atmosenv.2015.01.024>
- Hochadel, M., Heinrich, J., Gehring, U., Morgenstern, V., Kuhlbusch, T., Link, E., . . . Krämer, U. (2006). Predicting long-term average concentrations of traffic-related air pollutants using GIS-based information. *Atmospheric Environment*, 40(3), 542-553. doi:<https://doi.org/10.1016/j.atmosenv.2005.09.067>
- Hoek, G., Beelen, R., de Hoogh, K., Vienneau, D., Gulliver, J., Fischer, P., & Briggs, D. (2008). A review of land-use regression models to assess spatial variation of outdoor air pollution. *Atmospheric Environment*, 42(33), 7561-7578. doi:<https://doi.org/10.1016/j.atmosenv.2008.05.057>
- Huang, L., Zhang, C., & Bi, J. (2017). Development of land use regression models for PM_{2.5}, SO₂, NO₂ and O₃ in Nanjing, China. *Environmental Research*, 158, 542-552. doi:<https://doi.org/10.1016/j.envres.2017.07.010>
- Hueglin, C., Gehrig, R., Baltensperger, U., Gysel, M., Monn, C., & Vonmont, H. (2005). Chemical characterisation of PM_{2.5}, PM₁₀ and coarse particles at urban, near-city and rural sites in Switzerland. *Atmospheric Environment*, 39(4), 637-651. doi:<https://doi.org/10.1016/j.atmosenv.2004.10.027>
- Iii, C. A. P., Burnett, R. T., Thun, M. J., Calle, E. E., Krewski, D., Ito, K., & Thurston, G. D. (2002). Lung Cancer, Cardiopulmonary Mortality, and Long-term Exposure to Fine Particulate Air Pollution. *JAMA*, 287(9), 1132-1141. doi:10.1001/jama.287.9.1132
- Jaffe, L. S. (1968). Ambient Carbon Monoxide And Its Fate in the Atmosphere. *Journal of the Air Pollution Control Association*, 18(8), 534-540. doi:10.1080/00022470.1968.10469168
- Jerrett, M., Arain, A., Kanaroglou, P., Beckerman, B., Potoglou, D., Sahsuvaroglu, T., . . . Giovis, C. (2005). A review and evaluation of intraurban air pollution exposure models. *Journal of exposure analysis and environmental epidemiology*, 15(2), 185-204. doi:10.1038/sj.jea.7500388
- Jerrett, M., Arain, M. A., Kanaroglou, P., Beckerman, B., Crouse, D., Gilbert, N. L., . . . Finkelstein, M. M. (2007). Modeling the Intraurban Variability of Ambient Traffic Pollution in Toronto, Canada. *Journal of Toxicology and Environmental Health, Part A*, 70(3-4), 200-212. doi:10.1080/15287390600883018
- Kanaroglou, P. S., Jerrett, M., Morrison, J., Beckerman, B., Arain, M. A., Gilbert, N. L., & Brook, J. R. (2005). Establishing an air pollution monitoring network for intra-urban population exposure assessment: A location-allocation approach. *Atmospheric Environment*, 39(13), 2399-2409. doi:<https://doi.org/10.1016/j.atmosenv.2004.06.049>

- Kattenberg, A., Giorgi, F., Grassl, H., Meehl, G., Mitchell, J., Stouffer, R., . . . Wigley, T. M. (1996). Climate models—projections of future climate. *Climate Change 1995: The Science of Climate Change. Contribution of Working Group I to the Second Assessment Report of the Intergovernmental Panel on Climate Change*, 285-357.
- Kaur, S., Nieuwenhuijsen, M., & Colvile, R. (2005). Personal exposure of street canyon intersection users to PM_{2.5}, ultrafine particle counts and carbon monoxide in Central London, UK. *Atmospheric Environment*, 39(20), 3629-3641. doi:<https://doi.org/10.1016/j.atmosenv.2005.02.046>
- Kerckhoffs, J., Wang, M., Meliefste, K., Malmqvist, E., Fischer, P., Janssen, N. A. H., . . . Hoek, G. (2015). A national fine spatial scale land-use regression model for ozone. *Environmental Research*, 140, 440-448. doi:<https://doi.org/10.1016/j.envres.2015.04.014>
- Kim, Y. M., Harrad, S., & Harrison, R. M. (2002). Levels and Sources of Personal Inhalation Exposure to Volatile Organic Compounds. *Environmental Science & Technology*, 36(24), 5405-5410. doi:10.1021/es010148y
- Kouyoumdjian, H., & Saliba, N. A. (2006). Mass concentration and ion composition of coarse and fine particles in an urban area in Beirut: effect of calcium carbonate on the absorption of nitric and sulfuric acids and the depletion of chloride. *Atmospheric Chemistry and Physics*, 6(7), 1865-1877. doi:<https://doi.org/10.5194/acp-6-1865-2006>
- Krzyżanowski, M., Kuna-Dibbert, B., & Schneider, J. (2005). *Health effects of transport-related air pollution*. Copenhagen, Denmark: World Health Organization Europe.
- Kubilay, N., & Saydam, A. (1995). Trace elements in atmospheric particulates over the Eastern Mediterranean; concentrations, sources, and temporal variability. *Atmospheric Environment*, 29(17), 2289-2300.
- Langan Products, I. (2006). Model L76n Indoor Air Quality Measurer.
- Lehocky, A. H., & Williams, P. L. (1996). Comparison of Respirable Samplers to Direct-Reading Real-Time Aerosol Monitors for Measuring Coal Dust. *American Industrial Hygiene Association Journal*, 57(11), 1013-1018. doi:10.1080/15428119691014341
- Levy, J. I., Spengler, J. D., Hlinka, D., Sullivan, D., & Moon, D. (2002). Using CALPUFF to evaluate the impacts of power plant emissions in Illinois: model sensitivity and implications. *Atmospheric Environment*, 36(6), 1063-1075. doi:[https://doi.org/10.1016/S1352-2310\(01\)00493-9](https://doi.org/10.1016/S1352-2310(01)00493-9)
- Li, R., Ma, T., Xu, Q., & Song, X. (2018). Using MAIAC AOD to verify the PM_{2.5} spatial patterns of a land use regression model. *Environmental Pollution*, 243, 501-509. doi:<https://doi.org/10.1016/j.envpol.2018.09.026>
- Liu, C., Henderson, B. H., Wang, D., Yang, X., & Peng, Z.-r. (2016). A land use regression application into assessing spatial variation of intra-urban fine particulate matter (PM_{2.5}) and nitrogen dioxide (NO₂) concentrations in City of Shanghai, China. *Science of The Total Environment*, 565, 607-615. doi:<https://doi.org/10.1016/j.scitotenv.2016.03.189>
- Liu, Y., Paciorek, C. J., & Koutrakis, P. (2009). Estimating Regional Spatial and Temporal Variability of PM(2.5) Concentrations Using Satellite Data, Meteorology, and Land Use Information. *Environmental Health Perspectives*, 117(6), 886-892. doi:10.1289/ehp.0800123
- Lu, R., & Turco, R. P. (1994). Air Pollutant Transport in a Coastal Environment. Part I: Two-Dimensional Simulations of Sea-Breeze and Mountain Effects. *Journal of the Atmospheric Sciences*, 51(15), 2285-2308. doi:10.1175/1520-0469(1994)051<2285:APTIAC>2.0.CO;2
- Madsen, C., Carlsen, K. C. L., Hoek, G., Oftedal, B., Nafstad, P., Meliefste, K., . . . Brunekreef, B. (2007). Modeling the intra-urban variability of outdoor traffic pollution in Oslo, Norway—A

- GA2LEN project. *Atmospheric Environment*, 41(35), 7500-7511.
doi:<https://doi.org/10.1016/j.atmosenv.2007.05.039>
- Maindonald, J., & Braun, W. J. (2014). DAAG: Data Analysis And Graphics data and functions: R. Retrieved from <http://CRAN.R-project.org/package=DAAG>
- Marcazzan, G. M., Vaccaro, S., Valli, G., & Vecchi, R. (2001). Characterisation of PM10 and PM2.5 particulate matter in the ambient air of Milan (Italy). *Atmospheric Environment*, 35(27), 4639-4650. doi:[https://doi.org/10.1016/S1352-2310\(01\)00124-8](https://doi.org/10.1016/S1352-2310(01)00124-8)
- Massoud, R., Shihadeh, A. L., Roumié, M., Youness, M., Gerard, J., Saliba, N., . . . Saliba, N. A. (2011). Intraurban variability of PM10 and PM2.5 in an Eastern Mediterranean city. *Atmospheric Research*, 101(4), 893-901.
doi:<https://doi.org/10.1016/j.atmosres.2011.05.019>
- Matte, T. D., Ross, Z., Kheirbek, I., Eisl, H., Johnson, S., Gorczynski, J. E., . . . Clougherty, J. E. (2013). Monitoring intraurban spatial patterns of multiple combustion air pollutants in New York City: Design and implementation. *Journal of Exposure Science and Environmental Epidemiology*, 23, 223. doi:10.1038/jes.2012.126
- Merbitz, H., Fritz, S., & Schneider, C. (2012). Mobile measurements and regression modeling of the spatial particulate matter variability in an urban area. *Science of The Total Environment*, 438, 389-403. doi:<https://doi.org/10.1016/j.scitotenv.2012.08.049>
- Miller, K. A., Siscovick, D. S., Sheppard, L., Shepherd, K., Sullivan, J. H., Anderson, G. L., & Kaufman, J. D. (2007). Long-term exposure to air pollution and incidence of cardiovascular events in women. *New England Journal of Medicine*, 356(5), 447-458.
- Ministry of Environment. (2011). *State and Trends of the Lebanese Environment*. Retrieved from Beirut, Lebanon:
- Draft Law on Air Quality Protection, (2005).
- Moore, D. K., Jerrett, M., Mack, W. J., & Künzli, N. (2007). A land use regression model for predicting ambient fine particulate matter across Los Angeles, CA. *Journal of Environmental Monitoring*, 9(3), 246-252. doi:10.1039/B615795E
- Morawska, L., Thomas, S., Bofinger, N., Wainwright, D., & Neale, D. (1998). Comprehensive characterization of aerosols in a subtropical urban atmosphere: particle size distribution and correlation with gaseous pollutants. *Atmospheric Environment*, 32(14), 2467-2478. doi:[https://doi.org/10.1016/S1352-2310\(98\)00023-5](https://doi.org/10.1016/S1352-2310(98)00023-5)
- Morgenstern, V., Zutavern, A., Cyrus, J., Brockow, I., Gehring, U., Koletzko, S., . . . Heinrich, J. (2007). Respiratory health and individual estimated exposure to traffic-related air pollutants in a cohort of young children. *Occup Environ Med*, 64(1), 8-16. doi:10.1136/oem.2006.028241
- Nakhlé, M. M., Farah, W., Ziadé, N., Abboud, M., Salameh, D., & Annesi-Maesano, I. (2015). Short-term relationships between emergency hospital admissions for respiratory and cardiovascular diseases and fine particulate air pollution in Beirut, Lebanon. *Environmental Monitoring and Assessment*, 187(4), 196. doi:10.1007/s10661-015-4409-6
- Nasser, Z., Salameh, P., Dakik, H., Elias, E., Abou Abbas, L., Lev, . . . que, A. (2015). Outdoor Air Pollution and Cardiovascular Diseases in Lebanon: A Case-Control Study. *Journal of Environmental and Public Health*, 2015, 6. doi:10.1155/2015/810846
- NCRS. (2005). *GBA LULC map*.
- Nicholson, K. W. (1993). Wind tunnel experiments on the resuspension of particulate material. *Atmospheric Environment. Part A. General Topics*, 27(2), 181-188. doi:[https://doi.org/10.1016/0960-1686\(93\)90349-4](https://doi.org/10.1016/0960-1686(93)90349-4)

- Pace, T. G. (2005, April, 2005). *Examination of the multiplier used to estimate PM2.5 fugitive dust emissions from PM10*. Paper presented at the EPA Emission Inventory Conference, Las Vegas NV.
- Peng, R. D., Chang, H. H., Bell, M. L., & et al. (2008). Coarse particulate matter air pollution and hospital admissions for cardiovascular and respiratory diseases among medicare patients. *JAMA*, 299(18), 2172-2179. doi:10.1001/jama.299.18.2172
- Querol, X., Alastuey, A., Puigercus, J. A., Mantilla, E., Miro, J. V., Lopez-Soler, A., . . . Artiñano, B. (1998). Seasonal evolution of suspended particles around a large coal-fired power station: particulate levels and sources. *Atmospheric Environment*, 32(11), 1963-1978.
- Querol, X., Alastuey, A., Rodriguez, S., Plana, F., Ruiz, C. R., Cots, N., . . . Puig, O. (2001). PM10 and PM2.5 source apportionment in the Barcelona Metropolitan area, Catalonia, Spain. *Atmospheric Environment*, 35(36), 6407-6419. doi:[https://doi.org/10.1016/S1352-2310\(01\)00361-2](https://doi.org/10.1016/S1352-2310(01)00361-2)
- Querol, X., Alastuey, A., Ruiz, C. R., Artiñano, B., Hansson, H. C., Harrison, R. M., . . . Schneider, J. (2004). Speciation and origin of PM10 and PM2.5 in selected European cities. *Atmospheric Environment*, 38(38), 6547-6555. doi:<https://doi.org/10.1016/j.atmosenv.2004.08.037>
- R Core Team. (2015). *R: A Language and Environment for Statistical Computing*. Retrieved from Vienna, Austria:
- Rai, P. K. (2016a). Chapter One - Particulate Matter and Its Size Fractionation. In P. K. Rai (Ed.), *Biomagnetic Monitoring of Particulate Matter* (pp. 1-13): Elsevier.
- Rai, P. K. (2016b). Chapter Two - Adverse Health Impacts of Particulate Matter. In P. K. Rai (Ed.), *Biomagnetic Monitoring of Particulate Matter* (pp. 15-39): Elsevier.
- Riediker, M., Cascio, W. E., Griggs, T. R., Herbst, M. C., Bromberg, P. A., Neas, L., . . . Devlin, R. B. (2004). Particulate Matter Exposure in Cars Is Associated with Cardiovascular Effects in Healthy Young Men. *American Journal of Respiratory and Critical Care Medicine*, 169(8), 934-940. doi:10.1164/rccm.200310-1463OC
- Rob Levy, C. H. (2015). MODIS Atmosphere L2 Aerosol Product. NASA MODIS Adaptive Processing System (Publication no. http://dx.doi.org/10.5067/MODIS/MOD04_L2.006).
- Rodriguez, S., Querol, X., Alastuey, A., Kallos, G., & Kakaliagou, O. (2001). Saharan dust contributions to PM10 and TSP levels in Southern and Eastern Spain. *Atmospheric Environment*, 35(14), 2433-2447.
- Ross, Z., Jerrett, M., Ito, K., Tempalski, B., & Thurston, G. D. (2007). A land use regression for predicting fine particulate matter concentrations in the New York City region. *Atmospheric Environment*, 41(11), 2255-2269. doi:<https://doi.org/10.1016/j.atmosenv.2006.11.012>
- Ryan, P. H., & LeMasters, G. K. (2007). A Review of Land-use Regression Models for Characterizing Intraurban Air Pollution Exposure. *Inhalation Toxicology*, 19(sup1), 127-133. doi:10.1080/08958370701495998
- Sahanavin, N., Prueksasit, T., & Tantrakarnapa, K. (2018). Relationship between PM10 and PM2.5 levels in high-traffic area determined using path analysis and linear regression. *Journal of Environmental Sciences*, 69, 105-114. doi:<https://doi.org/10.1016/j.jes.2017.01.017>
- Saliba, N. A., Atallah, M., & Al-Kadamany, G. (2009). Levels and indoor-outdoor relationships of PM10 and soluble inorganic ions in Beirut, Lebanon. *Atmospheric Research*, 92(1), 131-137. doi:<https://doi.org/10.1016/j.atmosres.2008.09.010>
- Saliba, N. A., El Jam, F., El Tayar, G., Obeid, W., & Roumie, M. (2010). Origin and variability of particulate matter (PM10 and PM2.5) mass concentrations over an Eastern Mediterranean

- city. *Atmospheric Research*, 97(1), 106-114.
doi:<https://doi.org/10.1016/j.atmosres.2010.03.011>
- Saliba, N. A., Moussa, S., Salame, H., & El-Fadel, M. (2006). Variation of selected air quality indicators over the city of Beirut, Lebanon: Assessment of emission sources. *Atmospheric Environment*, 40(18), 3263-3268. doi:<https://doi.org/10.1016/j.atmosenv.2006.01.054>
- Sanchez, M., Ambros, A., Milà, C., Salmon, M., Balakrishnan, K., Sambandam, S., . . . Tonne, C. (2018). Development of land-use regression models for fine particles and black carbon in peri-urban South India. *Science of The Total Environment*, 634, 77-86.
doi:<https://doi.org/10.1016/j.scitotenv.2018.03.308>
- Sangrador, J. L. T., Nuñez, M. C. E., Villarreal, A. B., Cadena, L. H., Jerrett, M., & Romieu, I. (2008). A Land Use Regression Model for Predicting PM_{2.5} in Mexico City. *Epidemiology*, 19(6), S259. doi:10.1097/01.ede.0000340260.45006.b5
- Saraswat, A., Apte, J. S., Kandlikar, M., Brauer, M., Henderson, S. B., & Marshall, J. D. (2013). Spatiotemporal Land Use Regression Models of Fine, Ultrafine, and Black Carbon Particulate Matter in New Delhi, India. *Environmental Science & Technology*, 47(22), 12903-12911. doi:10.1021/es401489h
- Saucy, A., Rössli, M., Künzli, N., Tsai, M.-Y., Sieber, C., Olaniyan, T., . . . de Hoogh, K. (2018). Land Use Regression Modelling of Outdoor NO₂ and PM_{2.5} Concentrations in Three Low Income Areas in the Western Cape Province, South Africa. *International Journal of Environmental Research and Public Health*, 15(7), 1452.
- Shaka', H., & Saliba, N. A. (2004). Concentration measurements and chemical composition of PM_{10-2.5} and PM_{2.5} at a coastal site in Beirut, Lebanon. *Atmospheric Environment*, 38(4), 523-531. doi:10.1016/j.atmosenv.2003.10.009
- Shi, Y., Lau, K. K.-L., & Ng, E. (2016). Developing Street-Level PM_{2.5} and PM₁₀ Land Use Regression Models in High-Density Hong Kong with Urban Morphological Factors. *Environmental Science & Technology*, 50(15), 8178-8187. doi:10.1021/acs.est.6b01807
- Son, Y., Osornio-Vargas, Á. R., O'Neill, M. S., Hystad, P., Texcalac-Sangrador, J. L., Ohman-Strickland, P., . . . Schwander, S. (2018). Land use regression models to assess air pollution exposure in Mexico City using finer spatial and temporal input parameters. *Science of The Total Environment*, 639, 40-48. doi:<https://doi.org/10.1016/j.scitotenv.2018.05.144>
- Tian, L., Qiu, H., Pun, V. C., Lin, H., Ge, E., Chan, J. C., . . . Yu, I. T. (2013). Ambient carbon monoxide associated with reduced risk of hospital admissions for respiratory tract infections. *American Journal of Respiratory and Critical Care Medicine*, 188(10), 1240-1245.
- TSI. (2014). DUSTTRAK™ II AEROSOL MONITOR MODEL 8530/8531/8532/8530EP In TSI (Ed.).
- UNHabitat. (2015). Lebanon - Urban Issues. Retrieved from <https://unhabitat.org/lebanon/lebanon-urban-issues/>
- United Nations Environment Programme. (2014). *UNEP year book 2014: emerging issues in our global environment*. Nairobi, Kenya: UNEP Division of Early Warning and Assessment.
- Vanos, J. K., Hebborn, C., & Cakmak, S. (2014). Risk assessment for cardiovascular and respiratory mortality due to air pollution and synoptic meteorology in 10 Canadian cities. *Environmental Pollution*, 185, 322-332. doi:10.1016/j.envpol.2013.11.007
- Vienneau, D., de Hoogh, K., Beelen, R., Fischer, P., Hoek, G., & Briggs, D. (2010). Comparison of land-use regression models between Great Britain and the Netherlands. *Atmospheric Environment*, 44(5), 688-696. doi:10.1016/j.atmosenv.2009.11.016
- Violante, F. S., Barbieri, A., Curti, S., Sanguinetti, G., Graziosi, F., & Mattioli, S. (2006). Urban atmospheric pollution: Personal exposure versus fixed monitoring station measurements.

- Chemosphere*, 64(10), 1722-1729.
doi:<https://doi.org/10.1016/j.chemosphere.2006.01.011>
- Wang, M., Beelen, R., Bellander, T., Birk, M., Cesaroni, G., Cirach, M., . . . Brunekreef, B. (2014). Performance of Multi-City Land Use Regression Models for Nitrogen Dioxide and Fine Particles. *Environmental Health Perspectives*, 122(8), 843-849. doi:10.1289/ehp.1307271
- Wang, X., Chow, J. C., Kohl, S. D., Yatavelli, L. N. R., Percy, K. E., Legge, A. H., & Watson, J. G. (2015). Wind erosion potential for fugitive dust sources in the Athabasca Oil Sands Region. *Aeolian Research*, 18, 121-134. doi:<https://doi.org/10.1016/j.aeolia.2015.07.004>
- Wang, X., Watson, J. G., Chow, J. C., Gronstal, S., & Kohl, S. D. (2012). An Efficient Multipollutant System for Measuring Real-World Emissions from Stationary and Mobile Sources. *Aerosol and Air Quality Research*, 12(2), 145-160.
- Weichenthal, S., Van Ryswyk, K., Goldstein, A., Shekarrizfard, M., & Hatzopoulou, M. (2016). Characterizing the spatial distribution of ambient ultrafine particles in Toronto, Canada: A land use regression model. *Environmental Pollution*, 208, 241-248.
doi:<https://doi.org/10.1016/j.envpol.2015.04.011>
- WHO. (2005). *WHO Air quality guidelines for particulate matter, ozone, nitrogen dioxide and sulfur dioxide, Global update*. Retrieved from
- Wilson, J. G., Kingham, S., Pearce, J., & Sturman, A. P. (2005). A review of intraurban variations in particulate air pollution: Implications for epidemiological research. *Atmospheric Environment*, 39(34), 6444-6462. doi:<https://doi.org/10.1016/j.atmosenv.2005.07.030>
- Wolf, K., Cyrus, J., Harciníková, T., Gu, J., Kusch, T., Hampel, R., . . . Peters, A. (2017). Land use regression modeling of ultrafine particles, ozone, nitrogen oxides and markers of particulate matter pollution in Augsburg, Germany. *Science of The Total Environment*, 579, 1531-1540. doi:10.1016/j.scitotenv.2016.11.160
- Wright, G. R., Jewczyk, S., Onrot, J., Tomlinson, P., & Shephard, R. J. (1975). Carbon Monoxide in the Urban Atmosphere. *Archives of Environmental Health: An International Journal*, 30(3), 123-129. doi:10.1080/00039896.1975.10666660
- Yang, S., Wu, H., Chen, J., Lin, X., & Lu, T. (2018). Optimization of PM2.5 Estimation Using Landscape Pattern Information and Land Use Regression Model in Zhejiang, China. *Atmosphere*, 9(2), 47. doi:10.3390/atmos9020047
- Zhang, Z., Wang, J., Hart, J. E., Laden, F., Zhao, C., Li, T., . . . Chen, K. (2018). National scale spatiotemporal land-use regression model for PM2.5, PM10 and NO2 concentration in China. *Atmospheric Environment*, 192, 48-54.
doi:<https://doi.org/10.1016/j.atmosenv.2018.08.046>
- Zou, B., Luo, Y., Wan, N., Zheng, Z., Sternberg, T., & Liao, Y. (2015). Performance comparison of LUR and OK in PM2.5 concentration mapping: a multidimensional perspective. *Scientific Reports*, 5, 8698. doi:10.1038/srep08698

